M.Sc. Economic Geology Research Report

An investigation into the mineralogy and processing characteristics of the Elsburg reefs at South Deep Gold Mine, South Africa

***M.Sc. Candidate*:**

Viwe Notole (Student No.: 1964355)

***Research project supervisors*:**

Prof. Glen Nwaila

Dr. Julie E. Bourdeau

School of Geosciences, University of the Witwatersrand

November 2022

Declaration

I Viwe Notole, declare that this research report titled "*An investigation into the mineralogy and processing characteristics of the Elsburg reefs at South Deep Gold Mine, South Africa*" is my work, save for that which has been properly acknowledged. This research is being submitted in partial fulfilment of the University of the Witwatersrand's Master of Science (M.Sc.) degree. This report has never been submitted for any other University's degree.

Candidate signature : 

Date signed : 11 November 2022

ABSTRACT

Gold ores of the Witwatersrand Supergroup in South Africa are known to be amenable to metallurgical recovery through the process of cyanidation. However, the continuous decline in gold ore grade, increased environmental liability caused by residual cyanide in tailings and an increase in the complexity of ore composition calls for an alternative processing route. This is important to ensure that low-grade ore recovery is profitable while producing environmentally benign waste residue. Process mineralogy provides a systematic approach for the practical application of mineralogical knowledge, aiding ore characterisation and predictive behaviour, thus optimising how ores can best be mined, blended and processed. This study used mineralogical data and environmentally friendly leach reagent (i.e., glycine) to diagnose and predict processing characteristics of the composite Elsburg reefs at South Deep Gold Mine, South Africa. The mineralogy of these reefs is dominated by quartz and sulphide minerals, with pyrite, arsenopyrite, chalcopyrite and pyrrhotite being the common sulphides. More than 85% of gold in these reefs is locked or hosted in pyrite and quartz. The geochemistry shows high concentrations of siderophile (e.g., Cu, Ni and Co) and chalcophile (i.e., Cu and Zn) elements that can form stable complexes with glycine. A moderate to strong correlation of these elements (Cu, Co, Ni, Zn, etc.) with gold is conformable with the sulphide minerals-gold association. The poor liberation characteristics of Elsburg reefs ore and its geochemistry negatively influence gold recovery using glycine leaching. Sequential or multi-stage leaching is best to process ore with moderate to high Cu concentration and unliberated gold. The outcomes of this study demonstrate that Elsburg reefs gold ore responds well to sequential glycine leaching, with gold recoveries up to 95%, depending on which method or conditions are used. At low glycine dosage (e.g., 300 ppm), leaching duration of 50 hours, and ambient temperature (~23°C), bottle roll leaching of the Elsburg reefs yield low gold recovery (i.e., 30%), while at higher glycine dosage (e.g., 1500 ppm) and same leaching conditions (duration and temperature), a higher gold recovery (i.e., 41%) is attainable. Sequential leaching at a higher concentration of glycine (1500 ppm) with a leaching duration of 101 hours, yield cumulative gold recovery of up to 86%. Furthermore, at higher glycine concentration (1500 ppm) and elevated temperature (i.e., 40°C), Elsburg reefs yield considerably higher gold recovery (95%). The leaching solution was recharged at different time intervals from the beginning to the end of the leaching process. The increase in glycine was complemented by an increase in oxidant concentration (potassium permanganate). The ratio of potassium permanganate to glycine was kept at 2:1 (potassium permanganate: glycine).

ACKNOWLEDGEMENTS

A very special thank you goes to my supervisors, Prof. Glen Nwaila and Dr. Julie E. Bourdeau, for their excellent contribution from proposal preparation to research report completion. I appreciate their enormous knowledge and skills in a variety of fields (such as mineralogy, geochemistry, geometallurgy, and writing skills, among other things) as well as their support in the preparation of this report. I would like to express my gratitude to Dr. Steven E. Zhang for sharing his data visualization expertise.

I would like to thank Prof. Paul Nex for connecting me with the greatest supervisors. I would like to express my appreciation to everyone in the machine learning and geometallurgy research group for their continued encouragement and support. Mr. Louis Mudalahothe and Mr. Sam Tshabalala from the School of Geosciences (technician team) are acknowledged for their support in sample participation and thin section preparation for both microscopy and TIMA analysis. I would like to express my appreciation to those who assisted me in calibrating the full-section microscope in the microscope laboratory. I would like to express my sincere gratitude to Dr. Nonkuselo Madlakana for her assistance with TIMA analysis. Thank you to everyone from the School of Geoscience and the School of Chemical and Metallurgical Engineering who contributed or supported me on my M.Sc. journey.

Most importantly, I extend my heartfelt gratitude to my family for their continued support, and encouragement. For funding my M.Sc. program, I am grateful to the Upstream Training Trust (UTT) and the Council for Geoscience (CGS) Bursaries. Thank you to South Deep Gold Mine for providing me with ore samples. Finally, yet importantly, I would like to express my deepest gratitude to God for providing me with the strength to make it this far!

Table of Contents

Table of Figures

List of Tables

Abbreviations and acronyms

Ccp	: Chalcopyrite
Chl	: Chlorite
EC	: Elsburg Conglomerate
ECBA	: EC Basal Band
ECB	: EC Bottom Band
ECM	: EC Middle Band
ECT	: EC Top Band
DO	: Dissolved oxygen
GCS	: Glycine cyanide synergistic
g/t	: Grams per metric tonnes
MAC	: Modderfontein A Conglomerate

MIB	: Modderfontein Intermediate Bottom Band
MIT	: Modderfontein Intermediate Top Band
MBB	: Modderfontein B Bottom Band
mg/l	: Milligrams per liter
VCR	: Ventersdorp Contact Reef
LOI `	: Loss on ignition
Po	: Pyrrhotite
Py	: Pyrite
TIMA	: TESCAN Integrated Mineral Analyzer
Wt.%	: Weight percentage
XRD	: X-ray Diffraction
XRF	: X-ray Fluorescence

Chemical formulas

$Ca(OH)_2$	: Calcium hydroxide
CN^-	: Cyanide
Cu	: Copper
Fe	: Iron
Fe^{2+}	: Ferrous iron
Fe^{3+}	: Ferric iron
$C_2H_5NO_2$	: Glycine
$C_2H_4NO_2^-$	: Glycinate
$C_2H_6NO_2^+$	: Glycinium
H^+	: Hydrogen ions
H_2	: Molecular hydrogen
K^+	: Potassium ion

KCN : Potassium Cyanide

$KMnO_4$: Potassium permanganate

MnO_4^- : Permanganate ion

Na^+ : Sodium ion

NaCN : Sodium Cyanide

Pb : Lead

S : Sulphur

S^{2-} : Sulphide ion

SO_2 : Sulphur dioxide

SO_4^{2-} : Sulphate ion

Mineral names and formulas

Almandine : $Fe_3Al_2Si_3O_{12}$

Arsenopyrite : FeAsS

Biotite : $K(Mg, Fe_3^{2+}) (Al, Fe^{3+}) Si_3O_{10} (OH, F)_2$

Chalcopyrite : $CuFeS_2$

Chlorite : $(Mg,Fe)3(Si,Al)_4O_{10}(OH)_2(Mg,Fe)_3(OH)_6$

Cobaltite : CoAsS

Electrum : Au± (Ag, Hg)

Fe oxides / hydroxides : $FeO - Fe_2O_3$

Galena : PbS

Gersdorffite : NiAsS

Gold : Au

K-Feldspar : $KAlSi_3O_8$

Muscovite : $KAl_2(AlSi_3O_{10}) (OH)_2$

Monazite : $(Ce, La, Th)PO_4$

Pyrite	: FeS_2
Pyrope	: $Mg_3Al_2Si_3O_{12}$
Pyrrhotite	: $Fe_{1-x}S$
Quartz	: SiO_2
Rutile-Ilmenite	: TiO_2 - $FeTiO_3$
Schorl	: $NaFe_3^{2+}Al_6(Si_6O_{18})(BO_3)_3(OH)_3(OH)$
Uraniferous Minerals	: $\pm UO_2$(Ce, La, Y, Yh) PO_4
Zircon	: $ZrSiO_4$

Glossary

Area%: refers to 2D measurement rather than a 3D volumetric measurement used to quantify minerals based on surface areas.

Average Grain Size: The average intercept length in x-direction of a certain mineral type.

Average Particle Size: Regardless of mineral type, the average particle size is determined by the average intercept length in the x-direction across the particle.

Band: sometimes referred to as a "bed" in this study, is a thin mineralised stratum of a rock (conglomerate horizon) material in a reef.

Free surface: refers to liberated gold grains in this study.

GlyCat: is a gold extraction process that uses tank leaching with glycine as the main reagent in a cyanide-starved solution.

Glyleach: is a hydrometallurgical process that leaches gold, copper, nickel, cobalt, and zinc from free-milling, refractory and complex ores, in an environmentally friendly manner.

Glycine: is the most basic amino acid and can be purchased in large quantities. Its unique characteristics can provide significant benefits over traditional lixiviants (i.e. cyanide).

Grain: A single-mineral grain. The terms 'grain' and 'particle' are synonymous in the context of a liberated grain.

Liberated: A particle that contains more than 70% of the mineral of interest and amenable in glycine leaching is deemed "liberated" in this study. The defined limit may differ based on the mineral or the

treatment technique. Gold just needs to come into contact with the leach media and hence be exposed once.

Locked: When a mineral of interest has less than 30% exposure, it is considered locked in this study. locking refers to a mineral of interest that is enclosed into the host mineral.

Mineral association percentage: The proportion of all gangue mineral pixels linked with the mineral of interest expressed in percentage.

Mineral of Interest: This is the same thing as a 'sort-category'. The dataset will be sorted according to the feature 'particle contains gold' if the goal is to discover the liberation characteristics of gold, for example.

Particle: A particle is made up of many grains. A particle is a fragment of rock or ore whose size is determined by crushing and milling conditions as well as the size class to which it belongs.

Recharging: in the context of this study, refers to rejuvenating the leaching solution by adding glycine, potassium permanganate and lime to reach target pH value and re-use the solution in sequential leaching.

Sequential leaching: simply means multi-stage leaching, where leaching reagents (glycine, potassium permanganate and Calcium hydroxide) are added into the solution in different time intervals. This is done to ensure that the concentration of leaching reagents remains constant during the leaching process and that gold recovery is maximized.

Ternary+ particle: simply refers to multi-mineral boundaries. When two or more phases are associated with the mineral of interest (whether enclosed or attached).

CHAPTER 1: INTRODUCTION

This chapter outlines the background, problem statement, scope (i.e., aim, hypothesis, objectives and key questions) and the structure of this study.

1.1 Background

Gold (chemical symbol: Au) is the most inert, malleable and ductile metal in the periodic table (Yannopoulos, 1991; Schmidbaur et al., *2005*). It is typically found in its pure native form or as electrum (alloyed with elements such as silver and mercury; Adams, 2005; Habashi, 2008). Gold is usually associated with sulphides, silicates, oxides and carbonate minerals in Witwatersrand Supergroup, however gold mineral association can vary depending on the nature of the ore deposit (Goodall, 2005*;* Coetzee et al., 2011; Helmy and Zoheir, 2015). Most gold deposits in South Africa are concentrated in the Witwatersrand Basin, with a few other deposits in the Barberton greenstone belt (Robb and Meyer, 1995; Kirk et al., 2003; Dirks et al., 2013). Gold is one of the most sought-after natural resources worldwide (Kinzley, 2018). South Africa alone contributed approximately 6.8% (191 metric tonnes) of global gold production in 2011 (Nwaila, 2014). Gold production, demand, and flow statistics and information from around the world shows that South Africa contributed about 4.66%, 4.47%, 4.21%, 3.56%, 3.18%, 3.17% and 3.33% in 2015, 2016, 2017, 2018, 2019 and 2020, respectively (USGS, 2020, 2021; Summaries, 2020). This shows an undeniable declining trend in gold production. Despite South Africa's historical contribution to global and national economies, it is confronted with problems of high-energy costs, safety, civil unrest and increasingly inaccessible resources, to name a few (Neingo and Tholana, 2016). Globally, gold mining companies are faced with various challenges, such as mining and processing low-grade ores with complex mineral associations, and increasing environmental concerns and regulations (Sánchez and Hartlieb, 2020).

Due to growing operational expenses and diminishing capital investment, South Africa's mining industry has suffered a decline in production, exploration investment and employment in recent years (Cole and Broadhurst, 2021). These challenges are causing South Africa to lose its competitiveness in the global gold mining industry (Neingo and Tholana, 2016). South Africa was the largest gold producer before the Witwatersrand Basin exceeded its maturity in the mid to late 1970s (Hartnady, 2009). South Africa’s gold production has since been overtaken by China, Australia, Russia and the USA. The decrease in gold production in South Africa is mainly due to increasing mining depths and declining ore grade (Fig. 1; Little, 2016). Ore grade in Witwatersrand gold fields has decreased by approximately 40% over the last 30 years (Nwaila et al., 2020). According to Little (2016) and Chai et al. (2021), the demand for raw materials, including gold, has continued to increase while the discovery rate of new ore deposits has decreased (Fig. 1).

The Witwatersrand Supergroup is located in the central part of the Kaapvaal Craton and was deposited during the Archaean eon with age ranging from ~2.99 to 2.79 Ga, depending on the stratigraphic unit (Robb and Meyer, 1995; Onstott et al., 2006; Dankert and Hein, 2010; Zeh and Gerdes, 2012). For example, the West Rand Group age ranges between 2.99 – 2.91 Ga while the overlying Central Rand Group age ranges between 2.90 – 2.79 Ga (Kositcin and Krapez, 2004). In Section 2.1 of this thesis, the distinctive clastic sedimentary supergroup geological setting, stratigraphy, and structures are reviewed. This basin has produced >53,000 metric tonnes of gold and accounts for "more than one-third of all gold ever produced on Earth" (Tucker and Viljoen, 2016). Gold in the Witwatersrand Basin was discovered in 1886. Since then, most of the gold mined has come from conglomerate beds, informally referred to as 'reefs', which are generally poorly exposed in outcrops but have been well documented over the years of mining (Phillips and Law, 2000; Frimmel et al., 2005; Hatch and Chalmers, 2013; Tucker and Viljoen, 2016).

Several studies have reported that there has been a continuous decline in precious metals ore grades, not only in Witwatersrand gold mining companies but globally; this is the case because the higher-grade surficial deposits are partially mined out (Fig. 1; Dominguez and Valero, 2013; Neingo and Tholana, 2016; Little, 2016). The depletion of high-grade ore deposits is an indication that there is a need for innovation in mining, including the development of new mineral processing and recovery strategies that are less expensive and more environmentally friendly (Spooren et al., 2020). Gold has been processed for over a century using cyanidation introduced by McArthur and Forrester in 1887 (Eugene and Mujumdar, 2009). Gold extraction using the cyanidation process was first used at the Robinson Mine, then within the Witwatersrand Basin goldfields, and is still the principal extraction process for gold today (Durand, 2012). There are still areas that are yet to be explored for mineral resources within Witwatersrand Basin. However, most of these mineral resources are found at increasing depths (>3 - 4 km; Nwaila et al., 2013), making extraction and processing challenges. Extracting these resources will require modernized mining and processing techniques and/or techno-economic processes in order to be mined effectively.

The South Deep Gold Mine, owned by Gold Fields Ltd., is one of the deepest gold (> 3 km) mines within the Witwatersrand Basin. This mine is situated near Westonaria town in the Province of Gauteng (South Africa). It mainly exploits the Mondeor Conglomerate Formation in the Central Rand Group (Witwatersrand Supergroup), formally called the 'Upper Elsburg reefs' and hereon used in this thesis. (Manzi et al., 2012, 2013; Osburn et al., 2014). Furthermore, the Upper Elsburg reefs are characterized by the Waterpan Member (Upper Elsburg Individuals) and the Modderfontein Member (Upper Elsburg Massives) (Joughin et al., 2005; Osburn et al., 2014). The Waterpan and Modderfontein Members are formed by numerous auriferous conglomerate bands (see Section 2.2).

Mines typically lack a comprehensive understanding of the mineralogical assemblage that constitutes their ores. Thus, they cannot integrate this data to understand their effects on gold processing and recovery. Furthermore, the continual use of cyanidation is known to have harmful effects on human health and the broader environment (Patil and Kulkarni, 2014; Akcil et al., 2015). This research project investigates the mineralogical assemblage and use of glycine leaching as an alternative to cyanidation to predict the processing behaviour of low-grade gold ores from the Elsburg reefs at South Deep Gold Mine. The Elsburg reefs has not always been economically viable to mine because of sulphide minerals (e.g., pyrite types) found in its gold ores. Such sulphide minerals from the Elsburg reefs ores are typically reactive and thus consume lots of chemicals (i.e., glycine, cyanide and oxygen) during the leaching process.

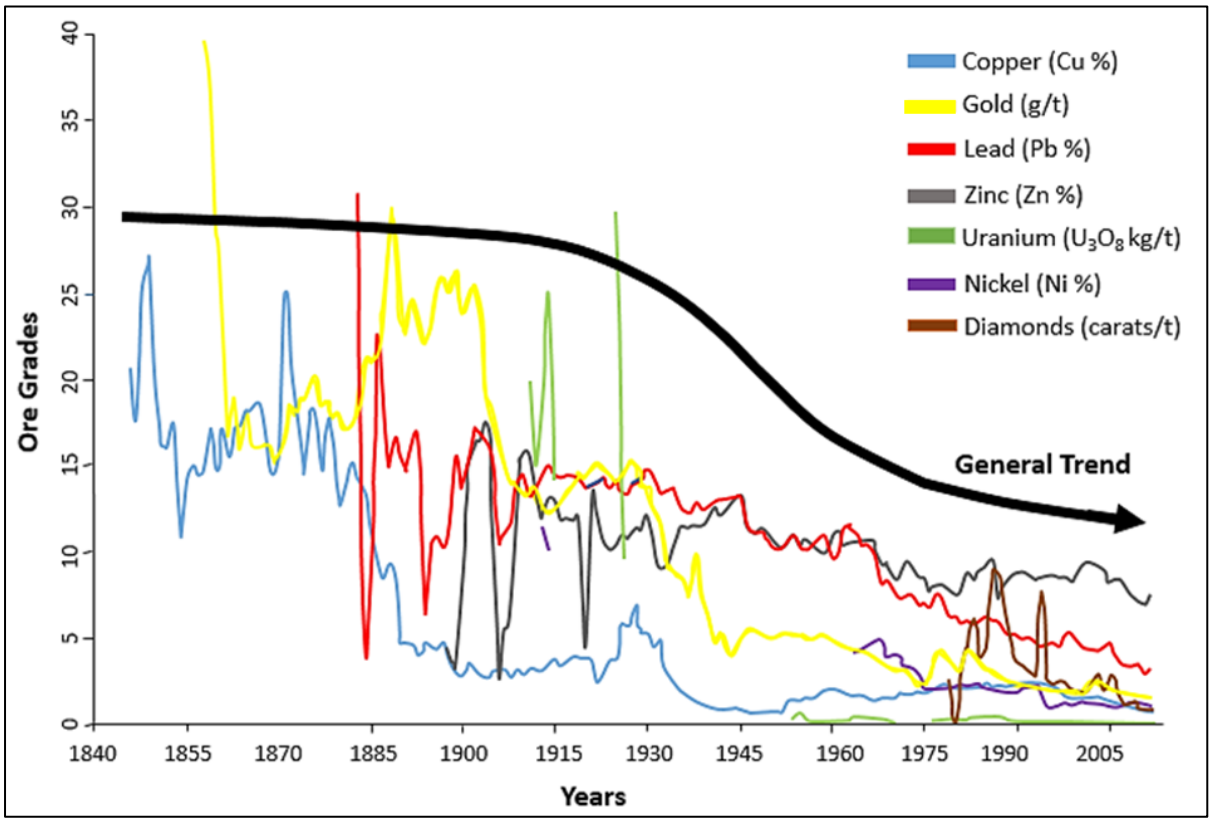

Figure 1: Fluctuation of metal ore grades over the years (modified after Little, 2016).

1.2 Problem statement

Gold extraction using cyanidation is a well-understood and efficient process that many gold mines rely on. However, cyanidation has adverse health and environmental impacts and is not a sustainable method to use indefinitely (Trapp et al., 2003; Eisler and Wiemeyer, 2004; Azcue, 2012). Previous studies have demonstrated that amino acids (such as glycine, histidine and alanine) can be used as an alternative reagent to cyanide in dissolving and recovering gold from ores (Eksteen and Oraby, 2015; Altinkaya et al., 2020). Recent research has demonstrated that gold can be extracted from ores using glycine as the

main reagent in a process that is less expensive, non-toxic, and capable of matching recoveries of cyanidation (Altinkaya, 2021; Oraby et al., 2021). The glycine extraction process has slower reaction kinetics than cyanidation; therefore, it requires a longer extraction time (Eksteen and Oraby, 2015; Dry, 2016). The Witwatersrand Supergroup low-grade ores necessitate an understanding of the mineralogical assemblage to know how the ores can be processed, and new innovative mining and processing techniques that are efficient, environmentally friendly and cost-effective.

1.3 Research scope

1.3.1 Aim

The mineralogical assemblage (petrography and chemistry) influences the Elsburg reefs gold ores liberation characteristics and ultimately affects gold recovery. Therefore, the overarching aim of this study is to investigate the mineralogical assemblage and the use of glycine leaching to predict the processing behaviour of the low-grade Elsburg reefs gold ores such as those found at South Deep Gold Mine in South Africa.

1.3.2 Hypothesis

It is hypothesized that by knowing the mineralogical assemblage (petrography and chemistry) of the Elsburg reefs gold ores, their liberation characteristics can be known. Therefore, this makes it possible to optimise parameter conditions of the glycine system. Thus, optimising parameter conditions of the glycine system will possibly result in relatively higher gold recoveries from low-grade ores.

1.3.3 Objectives of this study

In order to fulfil the aim and hypothesis of this study, the objectives to be addressed are:

- To investigate the modal mineralogy, petrography, mineralogical composition (chemistry), liberation characteristics and association of gold with gangue minerals using an optical microscope and Tescan integrated mineral analyser (TIMA).
- To investigate the influence that the mineralogical assemblage and ore geochemistry has on the recovery of gold. This is achieved by using TIMA and X-Ray Fluorescence (XRF), respectively.
- To examine the efficiency of glycine as an alternative, environmentally friendly reagent, for the recovery of gold. This is accomplished using glycine as the principal reagent in a bottle roll experimental leaching process.

1.3.4 Research key questions

To fulfil the aim of this study, I will attempt to answer the following questions:

- What are the mineralogical assemblages and chemical compositions of the Elsburg reefs (Elsburg conglomerate top [ECT] band and Modderfontein intermediate top [MIT] band), and what liberation characteristics do they have?
- How does the mineralogical assemblage and ore geochemistry affect the recovery of gold?
- How efficient is glycine as opposed to cyanide for the recovery of gold?

1.4 Structure of the research

This report is divided into seven chapters as outlined in Fig. 2 below.

CHAPTER 1: INTRODUCTION

- This chapter provides background, scope and key questions of this study.

CHAPTER 2: GEOLOGICAL OVERVIEW OF WITWATERSRAND BASIN

- This chapter provides a brief overview in Witwatersrand Basin geology, geology of Reefss that are mined at South Deep Gold mine and outline proposed models for Witwatersrand gold deposition.

CHAPTER 3: OVERVIEW OF GOLD AND BACKGROUND OF GOLD PROCESSING METHODS

- This chapter reviews work/studies related to this project to address the knowledge gap in glycene leaching as a potential alternative processing method to cyanidation. Overall, this chapter focuses on the physical and chemical properties of gold, its uses and the deposits, as well as the beneficiation and geometallurgy of gold deposits, especially regarding previous studies on recovery of gold using glycine.

CHAPTER 4 : METHODS AND MATERIALS

- This chapter gives the methodology (analytical/experimental work) carried out in this study to achieve the research obejctives previously stipulated. This chapter is subdivided into two sections: (1) Section 4.1, providing details about bulk ore sampling from South Deep Gold Mine, and (2) Section 4.2 describing analytical methods used for mineralogy and geochemistry, as well as the experimental methods used in this study.

CHAPTER 5: RESULTS

- Chapter 4 presents results on mineralogical charactrization (modal mineralogy, mineral association, liberation and mineral locking), and gold extraction using glycine and potassium permanganate.

CHAPTER 6: DISCUSSION

- This chapter discusses the results attained using microscope, TIMA, XRF and their implications on bottle roll leaching. Most importantly, discusses the effectiveness of glycine on gold leaching.

CHAPTER 7: CONCLUSION

- Conclusions of this reaseah endeavour are presented here. Recommendations for future research/studies are also given.

Figure 2: Structure of this research report.

CHAPTER 2: GEOLOGY OF THE WITWATERSRAND BASIN

This section gives a summary of the Witwatersrand Basin (South Africa). Specifically, the stratigraphic succession, geological framework and age. The mineralogical assemblage of the basin is briefly explored in the last part of this chapter.

2.1 Overview of the regional geology

The oldest rocks belonging to the Witwatersrand Basin consists of the 3086 ± 3 to 3074 ± 6 Ma Dominion Group rocks (Armstrong et al., 1991; Robb et al., 1992). This group consists of a thin basal siliciclastic unit and a bimodal volcanic sequence, altogether reaching a thickness of 2,250 metres (Frimmel and Nwaila, 2020). The Witwatersrand Supergroup overlies the Dominion Group and is divided into West Rand (2.99 – 2.91 Ga) and Central Rand Groups (2.90 – 2.79 Ga) (Kositcin and Krapez, 2004; Minter, 2006; Gumsley et al., 2018; Frimmel and Nwaila, 2020). The Witwatersrand Supergroup dates back to the Mesoarchean (2.99 – 2.79 Ga; Kositcin and Krapez, 2004; Smith et al., 2013) and forms part of the Kaapvaal Craton of Southern Africa (Fig. 3A and B).

The West Rand Group is 5,150 metres thick (Minter, 2006; Frimmel and Nwaila, 2020) and is made up of the Hospital, Government and Jeppestown subgroups (Nwaila, 2017). The Hospital Hill Subgroup is composed of quartzites and shales, with minor conglomerate beds restricted to the upper part of the subgroup (Frimmel, 2019). The Hospital Hill Subgroup is 2,225 metres thick (McCarthy, 2006; Manzi et al., 2013) and is overlain by the interbedded quartzite, shale, with minor conglomerates and diamictite beds of the 750 metres thick Government Subgroup. The Jeppestown Subgroup is the youngest subgroup of the West Rand Group, which consists of interbedded quartzite and shale with minor conglomerate beds, as well as a volcanic unit of basaltic andesite (Crown Formation). A basaltic andesite (Crown Formation) volcanic unit (2914 ± 8 Ma; Armstrong et al., 1991) can be found at the top of the Jeppestown Subgroup. Shale beds and iron formations are from a deeper marine origin; whereas quartzite beds originate from a shallow marine origin (Eriksson et al., 1981; de la Winter and Brink, 1991; Smith et al., 2013). The diamictite beds are overlain by iron formations. There is consistent evidence that sediments from the West Rand Group were transported from the north or northeast of the West Rand Group (Frimmel and Minter, 2002; Stoddard, 2015).

The Central Rand Group attains a thickness of 2,880 metres and has an age of 2790 ± 8 Ma (Gumsley et al., 2018). The Central Rand is divided into Johannesburg and Turffontein subgroups (Fig. 3C). According to Catuneanu (2001), this group consists of fluvial to fluvio-deltaic sandstones and conglomerates separated by erosional unconformities. These conglomerate units result from hinterland uplift and contain abundant gold and uranium, especially along the edges of the basin where paleocurrent entry points have been identified (Frimmel, 2019; Ormond, 2019; Nwaila et al., 2021).

The Ventersdorp Supergroup volcanics (approximately 3 km thick) were deposited on top of Central Rand Group, in turn followed by deposition of the Transvaal Supergroup sediments (approximately 15 km thick; Burger and Coertze, 1975; Poujol et al., 2005). Transvaal sedimentation ceased with the Rooiberg Group bimodal volcanism, dated at 2061 ± 2 Ma (Walraven, 1997) and the Bushveld Igneous Complex emplacement, dated at 2055.91 ± 0.26 Ma (Zeh et al., 2015) north of the Witwatersrand Basin. The Vredefort impact in 2023 Ma (Frimmel and Hallbauer, 1999) formed a 90 km wide dome-like structure, fractures and thrust faults, which allowed fluid circulation. The fluid circulation could be the result of transportation (over a short distance) and the re-deposition of gold within the basin. There are several goldfields in the northern edges of the Witwatersrand Basin, one of which is the West Rand goldfields (Tucker and Viljoen, 2016).

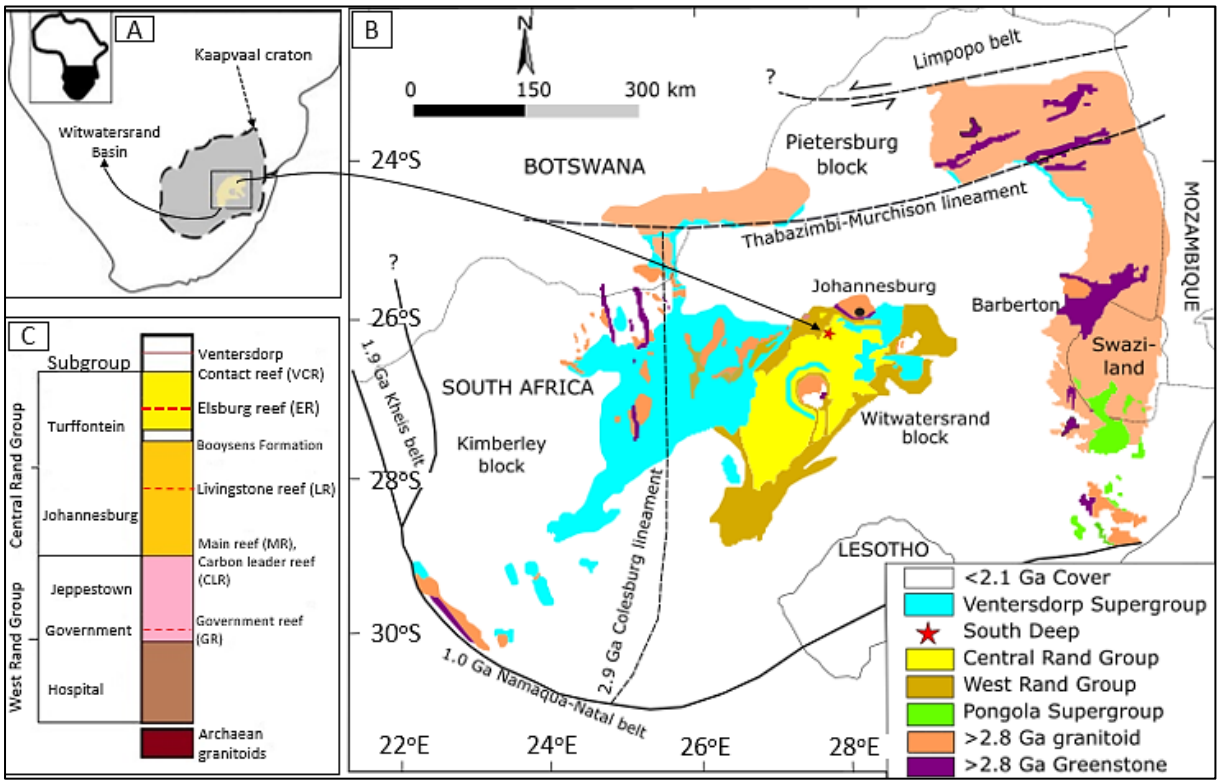

Figure 3: (A) Map showing the locality of the Kaapvaal Craton and Witwatersrand Basin in southern Africa (modified after Nwaila et al., 2021). (B) Simplified map of the Kaapvaal Craton showing the locality of the Witwatersrand Supergroup (i.e., West Rand Group and Central Rand Group; modified after Frimmel, 2005). (C) Simplified stratigraphic column of the Witwatersrand Supergroup (i.e., West Rand Group and Central Rand Group; modified after Nwaila et al., 2021).

2.2 Elsburg reefs (ER) at the South Deep Gold Mine

The South Deep Gold Mine is located ~45 km southwest of Johannesburg, near the town of Westonaria. In the South Deep Gold mine, the principal gold reefs that are exploited include the Ventersdorp Contact Reef (VCR) and the underlying Elsburg reefs at the base of the Mondeor Formation (Manzi et al., 2013;

Tucker et al., 2016; Mngadi et al., 2019). The Mondeor Formation is the Witwatersrand Supergroup topmost Formation and is typically located south of Johannesburg, within the Turffontein Subgroup of the Central Rand group (Eriksson and McClung, 2021). The Mondeor Formation is characterized by erosion resistant, well-developed conglomerates and medium to coarse-grained quartzites (Shivambu, 2016). It is overlain by Ventersdorp volcanics of the Ventersdorp Supergroup (Taylor and Anderson, 2018).

The Elsburg reefs are characterized by a succession of thin conglomerate beds separated from the VCR by a barren quartzite layer (Fig. 4; Osburn et al., 2014). The amount of gold and uranium in each conglomerate bed varies significantly. The Elsburg reefs are enriched with detrital gold that is mainly associated with detrital pyrite and exhibits a positive correlation with coarse conglomerate units (Drennan and Robb, 2006; Nwaila et al., 2013).

The Upper Elsburg reefs are part of an easterly divergent clastic wedge, sub-cropping the VCR in a north-northeast trending direction and underlies VCR in the southern side. At the eastern boundary of the mine, this wedge has a thickness of approximately 120 - 130 metres (Manzi et al., 2013). South Deep mineral reserves consist of 99% Upper Elsburg Reefs and 1% VCR (Fields, 2011, 2012). The Upper Elsburg Reefs are divided into two Members, the Upper Elsburg individuals (Waterpan Member), and Upper Elsburg massives (Modderfontein Member; Osburn et al., 2014, Mutobvu, 2019). There are four Upper Elsburg individuals or Elsburg conglomerate (EC) clusters that are vertically separated by conglomeratic zones and immature quartz wackes. The bands in the Elsburg reefs (Elsburg conglomerate) unit from bottom to top are as follows, the: 1) EC basal band (ECBA), 2) EC bottom band (ECB), 3) EC middle band (ECM), and 4) EC top band (ECT) (Fig. 4; Fields, 2012; Manzi et al., 2013; Mngadi et al., 2019). The ED (well-defined quartz wacke) unit separates the Elsburg conglomerate (EC) unit from the overlying Upper Elsburg massives (Modderfontein Member; Osburn et al., 2014). There are four conglomeratic package (bands or beds) that form the Upper Elsburg massive reefs (Fig. 4). From bottom to top, they are the: 1) Modderfontein A conglomerate (MAC), 2) Modderfontein intermediate bottom band (MIB), 3) Modderfontein intermediate top band (MIT), and 4) Modderfontein B bottom band (MBB) (Fields, 2012; Osburn et al., 2014; Mutobvu, 2019).

The VCR forms a single reef horizon above Turffontein Subgroup footwall (Fig. 3C, Nwaila et al., 2021). The VCR is characterized by a diverse mineralogical assemblage, variable gold grades and structural complexities caused by rapid dip and thickness changes (Frimmel, 2005). In the VCR, there is a great difference between the footwall and hanging wall lithology. Gold in VCR is mainly associated with euhedral pyrite, chlorite and different generations of quartz crystals (Nwaila et al., 2013). In the Elsburg reefs, Frimmel and Gartz (1997) found that rounded gold grains are typically absent from the matrix, and as a result, gold found in gangue minerals appears as sophisticated intergrowths, micro-veinlets and micro-inclusions.

In this report, the conglomerate bands of interest are indicated by red stars, namely: 1) Elsburg conglomerate top band (ECT), and 2) Modderfontein intermediate top band (MIT). Gold in the conglomerate bands generally occurs together with pyrite, quartz and pyrobitumen on degradational surfaces (Drennan and Robb, 2006; Manzi et al., 2013; Fuchs et al., 2016; Frimmel, 2019).

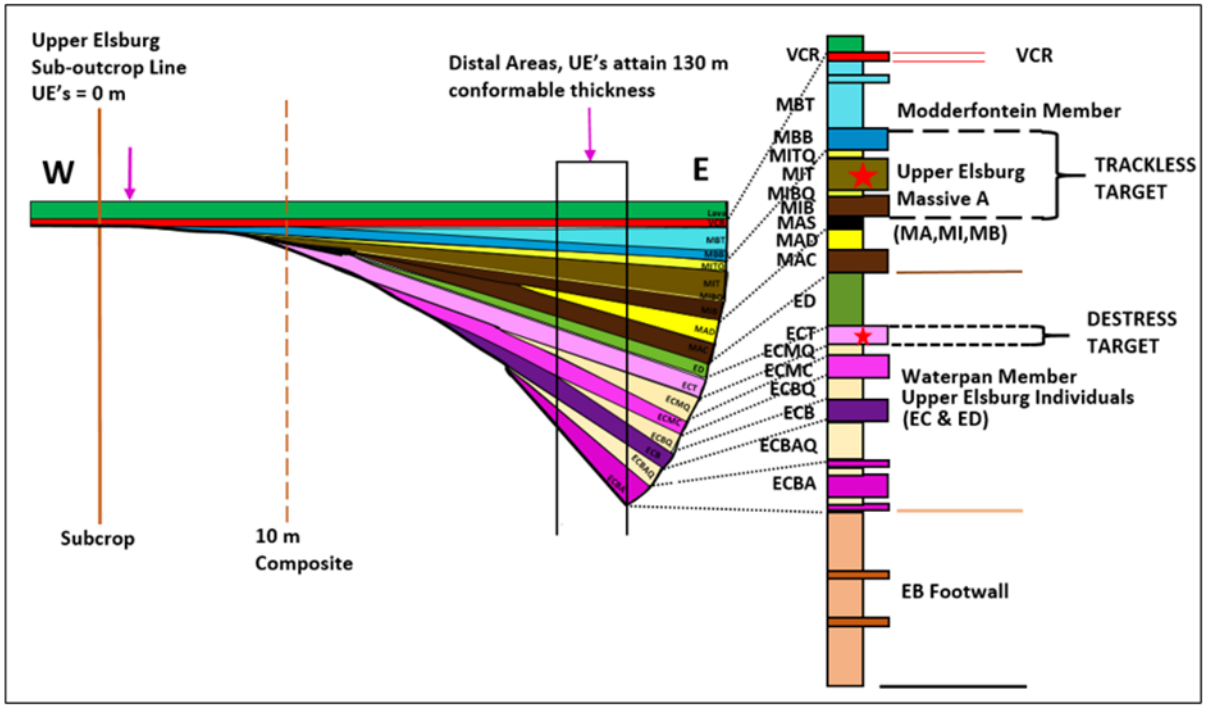

Figure 4: Schematic section through the Elsburg reefs packages (bands or beds) and VCR at the South Deep Gold Mine (Osburn et al., 2014).

2.3 Gold in the Witwatersrand Basin

The Witwatersrand Supergroup is one of the world's largest gold producer provinces (Gartz and Frimmel, 1999; Frimmel, 2005). Historically, gold production and gold grade from the Witwatersrand Supergroup ores was high, with an annual production of over 950 tonnes of gold in 1965 (Hartnady, 2009), at an average grade of > 5.2 – 15 g/t, depending on goldfield (Tucker et al., 2016). However, since the mid to late 1970's ore extracted from Witwatersrand Basin decreased because of increasing mine depths and the easily accessible ore have increasingly become low-grade. The Witwatersrand Basin has a current resource estimate of 44,000 metric tonnes of gold (Frimmel, 2014). Gold ores in Witwatersrand Basin are categorized into three main categories (i.e., free milling, refractory and complex ores). The Witwatersrand Supergroup gold ore deposits are known to have free-milling and refractory components or characteristics, depending on which reef is exploited (Nwaila et al., 2020).

The Witwatersrand gold-type deposits are commonly associated with Archean to Paleoproterozoic cratons (Frimmel, 2014). These deposits form in tectonic settings such as continental rifts, passive

margins and synorogenic foreland basins (Frimmel, 2014). The formation or emplacement of Witwatersrand gold-type deposits is a highly discussed issue in economic geology (Davidson, 1965). Many genetic models or theories have been proposed. Some of the most notable models include the: 1) palaeoplacers (Mellor, 1916), 2) hydrothermal (Barnicoat et al., 1997), 3) modified palaeoplacers (Robb and Meyer, 1991), 4) magmatic (Graton, 1930), 5) sedimentary–exhalative (Hutchinson and Viljoen, 1987), 6) metamorphic (Phillips and Myers, 1989), 7) impact-related (Reimold, 1994), 8) syngenetic microbial mediated (Mossman et al., 1999), and 9) H_2 degassing of Earth's core (Walshe et al., 2004) models. However, the leading models in explaining the origin of Witwatersrand gold include the: 1) palaeoplacer, 2) hydrothermal, and 3) a blend of the previous two models, referred to as the modified palaeoplacer model.

The palaeoplacer model proposes that gold is of a detrital origin, originating from the erosion of the Archean-aged granite-greenstone rocks located north-west from the Witwatersrand Basin (Minter, 1978; Frimmel and Minter, 2002; Frimmel et al., 2005). A number of Archaean-aged lode gold deposits are found in all of Kaapvaal Craton's greenstone belts. Furthermore, the source of the detrital gold was inferred by comparing the $\delta^{18}O$ distributions in quartz pebbles and quartz sands (Vennemann et al., 1995). Additionally, the detrital origin of gold and pyrite grains in the Witwatersrand Basin is supported by both rhenium (Re)–osmium (Os) isotopic ratios ranging between 14 to 87 (Kirk et al., 2001). Some gold grains display a distinct water-laid character. Round gold nuggets were deposited as a heavy mineral concentrates on small cross-bed foresets (Minter, 1993).

The hydrothermal model states that much of the gold as well as secondary pyrite of the Witwatersrand Basin crystallized from hydrothermal fluids that infiltrated barren conglomerates long after the deposition of host rocks/sediments (Plant et al., 2018). The source of Witwatersrand gold is therefore within or beneath the Witwatersrand Basin itself, and thus gold was introduced to its current position after sedimentation (Phillips and Powell, 2011, 2015). Gold was transported as bisulphide complexes in hot hydrothermal fluids channelled through porous beds or along bedding-parallel thrust faults in brittle rocks (Fuchs, 2016). Gold was then precipitated when hydrothermal fluids encountered carbon or iron oxides; while the associated pyrite crystals were themselves derived from the sulphidation of iron oxides during gold precipitation (Phillips and Law, 2000). Therefore, gold, uraninite, pyrite and hydrocarbons are all cogenetic in Witwatersrand Supergroup (Barnicoat et al., 1997).

The modified palaeoplacer model suggests that gold was derived from the north-west from the erosion of the Archean-aged granite-greenstone rocks that bound the Witwatersrand Basin (Frimmel, 2008). The gold grains were mobilised into alluvial fans at the time of sedimentation (Muntean et al., 2004), and concentrated by continuous re-deposition and settling (reworking) of gravels by streams, waves and wind during basin uplift (Pretorius, 1991; Robb and Meyer, 1991; Frimmel and Minter, 2002). Gold

was further remobilized (centimetre to metre scale) by the infiltration of hydrothermal fluids after burial, allowing recrystallization of gold into fine fractures (Hayward et al., 2005).

There are two distinct forms of pyrites typically found in the Witwatersrand Supergroup (for instance, in Elsburg reefs): detrital (coarsely crystalline pyrite, planar-laminated pyrite) and authigenic (sub-rounded pyrite) (da Costa et al., 2020). According to Hayward et al. (2005), the Elsburg reefs gold's composition is remarkably similar to that of Barberton gold, hence the modified placer model is the favoured explanation for how the Elsburg reefs gold deposit formed in this study.

CHAPTER 3: OVERVIEW OF GOLD AND BACKGROUND OF GOLD PROCESSING METHODS

3.1 Gold properties and uses

Gold is a soft, dense, inert, yellow-coloured element with an atomic number (P) of 79 in the periodic table. It typically occurs in veins and alluvial deposits and is almost always associated with pyrite or quartz. It is the most malleable and ductile of metals (Carne, 1912). The metal can be found in native form or associated with other elements such as silver and copper (Valero et al., 2011). It is important to know whether the type of gold that is being processed is native gold (easily processed) or is an alloy. Gold that occurs with other metals (e.g., Cu, Ag, etc.) is not easy to process because other metals will compete with gold during dissolution or leaching process. Gold crystallizes in cubic form. However, crystals are usually found as irregular plates or grains (sometimes called 'nuggets') due to its malleability. Gold's thermal and electrical conductivity is high (Mason et al., 2020). The only naturally occurring gold isotope is ^{197}Au. Nevertheless, 19 artificially produced isotopes range from ^{185}Au to ^{203}Au (Yannopoulos, 1991; Ahamed, 2018). These radioactive isotopes have half-lives that range from a few seconds to 199 days. Many gold alloys and pure gold are non-magnetic (Ahmad et al., 2017). Alloys of gold with manganese have some magnetic properties, and gold alloys containing iron, nickel, or cobalt are ferro-magnetic. Hansen and Anderko (1958) describe the equilibria of many binary gold alloys. Except for selenic acid, simple weak acids such as acetic acid (CH_3CO_2H) and formic acid (HCO_2H) do not dissolve gold. The hydrometallurgical technique known as cyanidation is often used to dissolve and extract gold from ores (Section 3.4). In addition, hydrochloric acid can also dissolve gold in the presence of oxidants (such as nitric acid, oxygen, cupric or ferric ions and permanganate). Aqua regia is a combination of hydrochloric and nitric acids that vigorously attack gold. See the following reaction (i):

$$Au + 4HCI + HN0_3 \rightarrow H[AuCI_4] + 2H_20 + NO \quad \text{(i)}$$

Gold is one of the most valuable metals obtained from the Earth (Kamunda et al., 2016). A variety of its unique gold characteristics (electric conductivity, malleability, etc.) contributes to its usefulness. Gold is a fascinating metal with a unique place in our hearts and is mainly used in jewellery (50%), electronics (37%), official coins (8%) and (5%) other uses (Summaries, 2019; USGS, 2020). For many years, gold has been used to create decorative artefacts and jewellery (Corti, 2001). The majority of newly mined or recycled gold is used in jewellery production such as rings (Fritz et al., 2020). Jewellery manufacturing consumes about 78% of all gold produced each year. Pure gold is far too delicate to withstand the forces that many jewellery products endure (Butterman and Amey, 2005; USGS, 2020). Gold can be rendered more durable by alloying it with other metals like copper, silver and platinum. Gold alloys are less valuable per unit of weight than pure gold. The gold proportion of these alloys is

indicated by a trade standard known as ‘karatage’ (Kaspin, 2013). Twenty-four-karat gold is pure gold, 18-karat gold is a 75% gold alloy and 12-karat gold is a 50% gold alloy (Bovin, 1976). High-karat jewellery is generally softer and more tarnish-resistant. The hue of manufactured items varies as gold is alloyed with other metals.

Gold is also commonly used in the electronics industry. Solid-state electrical devices operate at extremely low voltages and currents, which can be rapidly disrupted by corrosion or tarnish at the contact points (Dini, 2021). Gold is the most efficient conductor for carrying minimal currents while being corrosion-free. Gold-plated electronics are extremely durable. The conventional desktop or laptop computer contains gold in numerous places such as micro-processor and memory chips.

3.2 Gold ore deposits

There are many different types of gold deposits, and they occur in different geological settings (Robert et al., 1997; Zhou et al., 2004; Rowe and Zhou, 2007). Intrusion related gold deposits are iron oxide-copper-gold, epithermal, porphyry, skarn and are categorized as magmatic-hydrothermal deposits (Nguimatsia et al., 2017). Hydrothermal gold deposits are characterized as orogenic, volcanogenic massive sulphide deposits and Carlin-type (Zhu et al., 2011). Placer gold deposits are classified as sedimentary gold deposits (Peng et al., 2017; Sillitoe et al., 2020). The Mesoarchean was the most significant period in terms of gold deposit formation (Frimmel, 2008; Heinrich, 2015).

All geologic characteristics of an ore deposit such as mineralogical, textural, structural and compositional features that record both the deposit's original deposition and any later deformation, alteration, or modification are considered geologic drivers of geometallurgy (Hoal and Frenzel, 2022). Geometallurgy is a cross discipline approach combining geology, metallurgy and mine planning that aims to improve fundamental understanding of resource economics and viability (Dunham and Vann, 2007). These characteristics, when combined, describe the current state of the rocks, which is what a mining operation will have to contend with. Geometallurgy should start from the exploration process, when the observations are taken in the field, on the drilling stage and/or in the laboratory to acquire/build deposit database. Early indications of continuity on geochemical correlations, and mineralogical assemblages can assist in finding out how the ore can be processed (Grunsky and de Caritat, 2020; Hoal and Frenzel, 2022). The deposit database includes prospective indicators of ore processing characteristics so that, in addition to deposit knowledge, some understanding of variables that may affect mine planning, beneficiation and extractability can be acquired (Drielsma et al., 2016). Figure 5 depicts some of the correlations between downstream mining processes and geology, mineralogy and other ore properties. Each ore geology characteristic may be significant in some aspects of the ore processing. Understanding these characteristics and their expected implications on production can assist in early detection of mine concerns (Edwards, 2012).

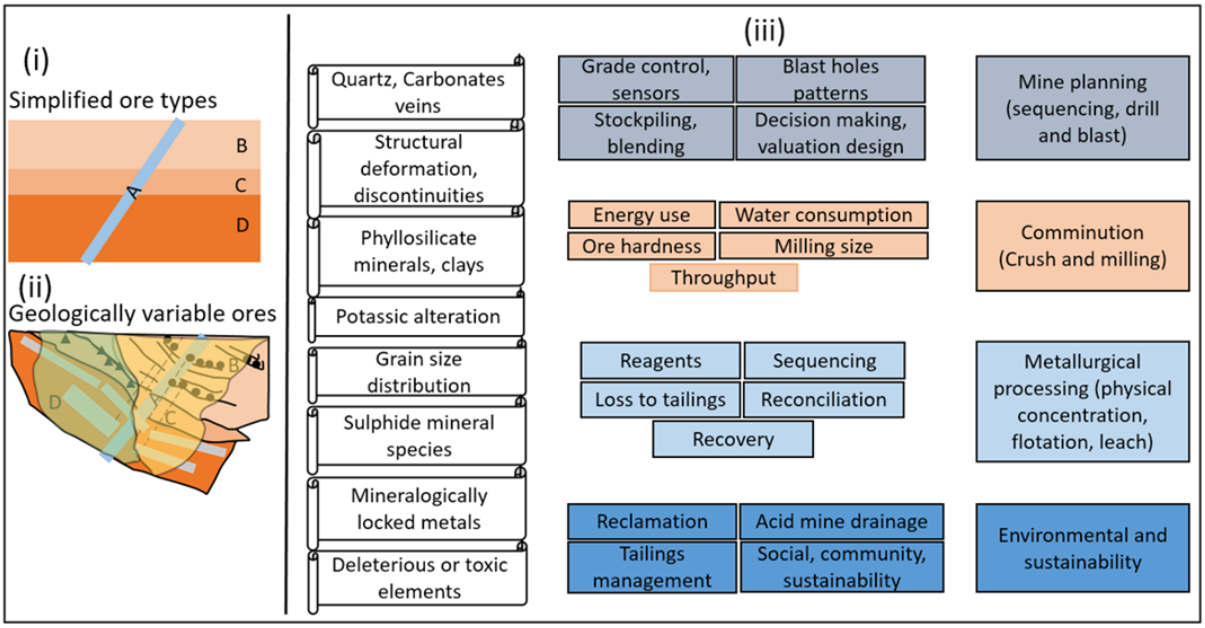

Figure 5: This diagram illustrates how types of ore deposits drive mining operations (modified after Hoal and Frenzel, 2022). Geometallurgy considers geology in a spatial context for better mine operations. The view of an ore deposit from the perspective of a mine operator is based on assumptions of (i) consistent ore types (A, B, C, D), whereas in reality, (ii) the spatial distribution of internal geologic variability (black lines) and alteration overprints (stippled pattern) can have a direct impact on operations. (iii) Some geologic factors affecting operations encompass mineralogical, textural, and structural factors, all of which could lower the mining project's effectiveness and overall profitability.

The source of the Witwatersrand Basin gold deposit has been debated in the past with many researchers favouring modified placer model (Hayward et al., 2005; Muntean et al., 2005; Tucker et al., 2016). Natural concentrations of heavy minerals such as gold, chromite, rutile, native copper, zircon and other gemstones, induced by the force of gravity on moving particles, with streams or rivers as means of transport from the source, form placer deposits (Lifton and Luepke, 1987; Candhi and Sarkar, 2016; Haldar, 2018). Heavy minerals concentrate in riverbed, coastal and lag (residual) gravels, forming ore deposits. Placer gold deposits can be found in any geological setting where gold is associated with hard rock (lobe or vein related deposits; Sillitoe, 2000). Gold in placer deposits can be easily liberated or has already been liberated before being processed; with a diameter ranging from 50 to 100 µm (Zhou et al., 2004; Phillips and Powell, 2011). This type of gold deposit is amenable in conventional cyanidation. The origin of Witwatersrand Basin gold type could possibly be as a result of washed and transported gold bearing rocks from somewhere outside the basin (Minter, 1977) and then remobilised by hydrothermal fluids triggered by regional metamorphism (Phillips and Law, 1994).

3.3 Beneficiation and geometallurgy of gold

Gold ores can be divided into three major metallurgical groups based on their mineralogical association, liberation and texture, and processing behaviour when subjected to conventional cyanidation. The three gold ore types are: (I) free milling, (II) refractory, and (III) complex ores (Fig. 6). The mineralogy, texture, and liberation characteristics of gold ores influence gold processing and recovery. Thus, gold ores are classified into different types according to their mineralogical features and the mineral processing behaviour (Zhou et al., 2004; Nwaila et al., 2014). These ores require different processing procedures to recover economical acceptable gold percentage from the ore.

Free-milling ores (discrete gold particles dispersed throughout the boundaries of the host assemblages) can be defined as ore that contains more than 90% of gold that is recoverable by conventional cyanide leaching (Ahtiainen, 2020), given that 80% of sample particles can pass a 75 µm mesh (Zhou et al., 2004). The main types of free-milling ores include palaeoplacers, quartz vein gold ores, silver-rich ores and oxidized ores. Gold is unliberated in palaeoplacer ores, therefore crushing and grinding are required to extract enough gold via hydrometallurgical methods such as cyanidation. Gold in quartz veins is found mainly in the fault zone of rock fractures and is usually deposited by hydrothermal fluids passing through the fault or fractured zone (Tripp and Vearncombe, 2004).

The ore is categorized as refractory if the gold recovery is economically unfeasible or insufficient when subjected to conventional cyanide leaching. Refractory ore (gold incorporated into host minerals) requires the usage of more reagents and/or additional complex pre-treatment processes to recover an acceptable amount of gold (Ahtiainen, 2020). Epithermal vein deposits and sulphidic gold deposits are good examples of refractory ores. Gold is extensively dispersed and locked up in sulphide minerals such as pyrite and arsenopyrite in the form of micro or sub-micro particles in sulphidic refractory gold ores and is often recovered by flotation with these sulphide minerals (Kononova et al., 2001; Drif et al., 2018; Wang et al., 2019). The fundamental mineralogical characteristics of gold ores, particularly the manner of existence and association with gold, as well as the presence of carbonaceous materials, might contribute to ore refractoriness (Celep et al., 2009).

To recover gold from complex gold ores effectively and economically, high concentrations of reagents such oxygen and cyanide must be used. Other metals such as copper, silver, antimony and arsenic may dissolve from sulphide and sulphide-arsenide minerals during gold cyanide leaching, depleting the free-cyanide and oxygen concentration in the solution and ultimately reduce gold recovery.

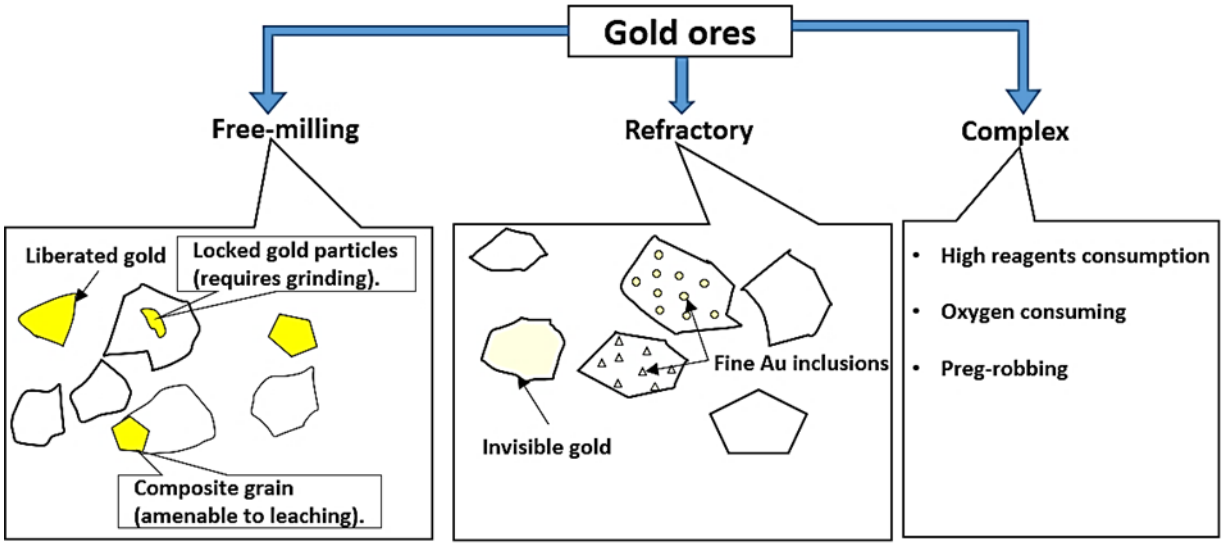

Figure 6: Schematic diagram showing different types of ores (modified after Altinkaya, 2021).

3.4 Gold Cyanidation

Gold recovered from Witwatersrand Supergroup ore deposits using the cyanide processes referred to as cyanidation (Fig. 7). This gold processing method was developed in the early 19st century and first introduced by McArthur and Forrester in 1887 (Fleming, 1992; Hilson and Monhemius, 2006; Nwaila, 2014). Cyanide is a chemical compound in which a carbon atom is triple-bonded to a nitrogen atom ($C\equiv N^-$), and is used as a principal reagent to extract gold from ore. Cyanide (CN^-) is a predominant reagent used for gold extraction because of its remarkable effectiveness for gold dissolution with high reaction rates and high gold recovery (Hilson and Monhemius, 2006; Akcil et al., 2015), strong complex formation with gold, and technical ease of the leaching process (Altinkaya et al., 2020). Sodium cyanide (NaCN) and potassium cyanide (KCN) are regarded as the most used compounds as sources of cyanide in hydrometallurgical gold extraction. These compounds dissolve easily in water. As demonstrated in Eq. 1, NaCN dissolves to produce a metal cation (Na^+) and free cyanide ions (CN^-). The formation of HCN and OH^- ions by the interaction of cyanide ions with water (Eq. 2) increases the solution's pH. At high pH, the dissolved cyanide exists as free cyanide. In the case of cyanide leaching, oxygen can oxidize hydrogen cyanide and free cyanide to form cyanate (CNO^-), which may cause unwanted reactions (Eqs. 3 and 4). The cyanate does not dissolve gold; instead, it lowers the concentration of free-cyanide, thus reducing the reaction rate between cyanide and gold (Marsden and House, 1992).

The mineralogy and presence of specific major (e.g., Fe) and/or trace elements such as copper (Cu), nickel (Ni), zinc (Zn) etc., of the ore have a considerable influence in gold cyanidation. These elements form complexes with leaching reagent (e.g., $Cu(CN)_2^-$, $Cu(CN)_3^{2-}$ and $Cu(CN)_4^{3-}$), consume it, and result in low gold recoveries (Jiang et al., 2001; Sayiner and Acarkan, 2014). The leaching parameters such as pH and temperature as well as the concentration of free-cyanide available in leaching solution

influences gold dissolution as well as recovery of gold in alkaline solution. The pH range between 9.5 and 11 is effective for cyanide leaching. Gold is extracted from pulverized ores using alkaline cyanide solution via the following reaction(s) (Eqs. 5 to 8):

$NaCN \leftrightarrow Na^{+} + CN^{-}$ *Eq.1*

$CN^{-}+H_2O \leftrightarrow HCN+OH^{-}$ *Eq.2*

$4HCN+3O_2 \leftrightarrow 4CNO^{-} +2H_2O$ *Eq.3*

$3CN^{-} +2O_2+H_2O \leftrightarrow 3CNO^{-} + 2OH^{-}$ *Eq.4*

$2Au + 4NaCN+O_2+2H_2O \rightarrow 2Au\,(CN)_2^{-} + 2NaOH + H_2O_2$ *Eq.5*

$2Au + 4CN^{-} + H_2O_2 = 2Au\,(CN)_2^{-} +2OH^{-}$ *Eq.6*

$4Au + 8CN^{-} + O_2 + 2H_2O \rightarrow 4Au(CN_2)^{-} + 4OH^{-}$ *Eq.7*

$4Au+8NaCN^{-}+O_2+2H_2O \rightarrow 4NaAu\,(CN)_2 + 4NaOH$ *Eq.8*

The anionic species of gold ($AuCN_2^{-}$) is adsorbed on activated carbon. In order to recover metallic gold, these adsorbents are incinerated at high temperatures to desorb gold (Inoue et al., 2019).

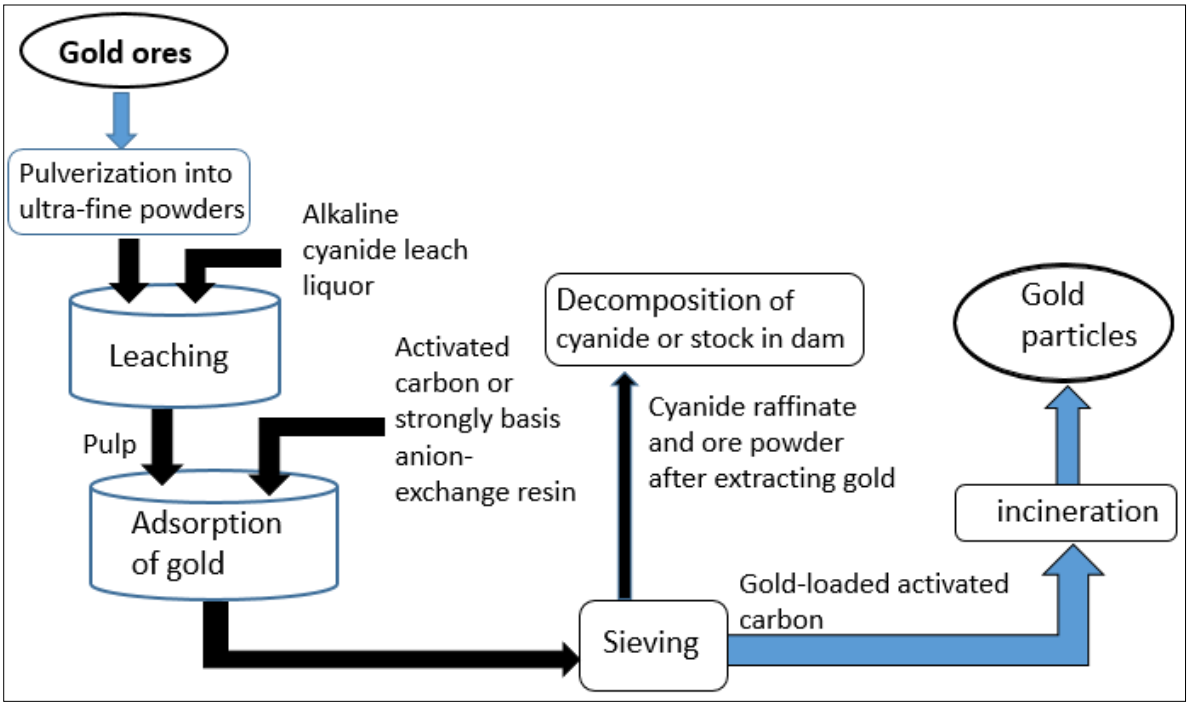

Figure 7: Process flow diagram for using alkaline cyanide solutions to recover gold from gold ore (modified after Inoue et al., 2019).

Disadvantages of cyanidation:

- Presents challenges in terms of the environment, health and safety. Substantial cyanide toxicity in cyanide leaching process can cause severe environmental problems such as the killing of wildlife

(including micro-organisms). It consequently requires environmental protection and incur safety costs.

- In the presence of refractory minerals, carbonaceous matter and copper-bearing gold ores, slow leaching kinetics and excessive cyanide consumption can be seen, elevating processing costs (Altinkaya et al., 2020).

New leaching reagents (such as glycine, thiosulfate, thiocyanate, etc.) have been proposed in response to these problems because it is evident that a fit-for-purpose strategy is required, as there is no panacea lixiviant that is equally acceptable for all mineralogical and geochemical characteristics of every ore. Glycine is the most promising reagent and is investigated in this report.

3.5 Glycine background information

Glycine is a chemically stable amino acid having the formula: NH_2CH_2COOH (Korobushkina et al., 1974; Bogdanovskaya et al., 1986; Holtom et al., 2005). Amino acids are organic compounds containing both a carboxyl group (-COOH) and an amino group ($-NH_2$) bonded to the same carbon atom in α-position (Trabocchi et al., 2005). A side group (R) is a property of a certain amino acid that defines its properties. The hydrogen atoms make up the side chain of glycine, the most minor alpha-amino acid (Ustunol, 2015; Fig. 8).

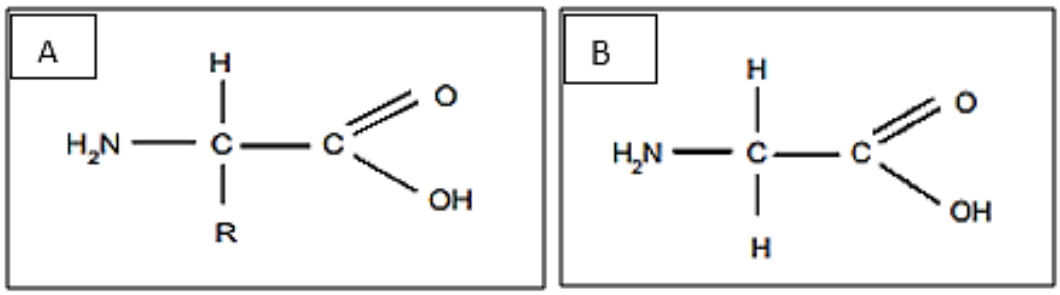

Figure 8: Basic structure of amino acid and general structure of glycine are shown in A and B, respectively.

In nature, glycine is an amphoteric organic compound. In aqueous solution, an amphoteric compound can behave as either an acid (proton donor) or a base (proton acceptor) depending on the pH of the solution (Bordes and Holmberg, 2015). It forms cationic glycinium ion ($^+H_3NCH_2COOH$) in acidic solutions (pH < 2.35), the neutral zwitterion ($^+H_3NCH_2COO^-$; pH of 2.35 to 9.78), and the anionic glycinate ion ($H_2NCH_2COO^-$) in alkaline solutions (pH > 9.78), demarcated by two pKa values at 2.34 and 9.78 (Aksu and Doyle, 2001; Tanda et al., 2017; Eksteen et al., 2018). Glycine is stable over a wide Eh-pH range in alkaline conditions (amino acids; Fig. 9), just like cyanide (Aylmore, 2016; Tanda et al., 2017; Altinkaya et al., 2020; Altinkaya, 2021). Glycine forms stable complexes with trace elements and/or transition metals such as copper, for example copper (II) glycinate (Ly et al., 2016). Therefore,

mineralogy and presence of certain elements in the ore will affect gold dissolution in glycine alkaline media.

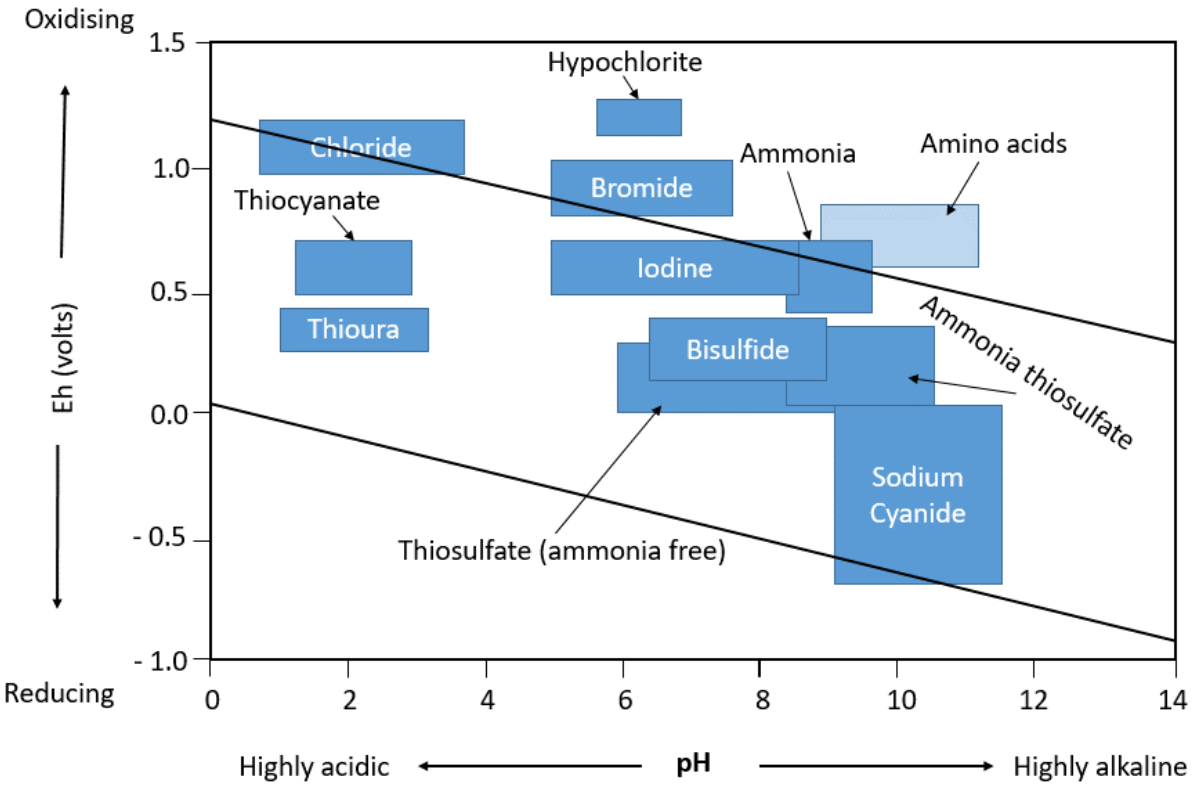

Figure 9: Eh-pH diagram of gold reagents and their performing zone (Modified after Aylmore, 2016).

Glycine is characterised as follows (Wade, 2013; Tanda et al., 2017):

- In its purest form, it is a colourless, odourless, sweet-tasting crystalline substance.
- It is water soluble (250g/L at 25°C), has a density of 1.607 kg/t, molar mass of 75.07 mg/L, forms both acids and alkalis, but is not soluble in organic solvents (0.038 g/100 mL) (Fleck and Petrosyan, 2014, Oraby and Eksteen, 2015).
- Can be decomposed by specific microorganisms.
- The melting point of glycine is high ~262°C and the disintegration threshold is 292°C (Huang et al., 2013, Tanda et al., 2017).
- The bonding of two hydrogen atoms with alpha carbon renders glycine optically inactive (Tanda et al., 2017).
- It is much more stable (as a glycinate anion) as compared to cyanide or thiosulfate anions (Oraby and Eksteen, 2015).

Glycine is a favourable amino acid for gold leaching as it produces glycinate ions in alkaline solution. According to Aylmore (2016), glycinate forms a stable complex with oxidized gold and aurous gold [Au (I)]. The gold-glycinate [$Au(NH_2NCH_2COO)_2^-$] complex has a stability constant of 18, which is

higher than that of other gold ligand complexes such as $Au(SO_3)_2^{3-}$, $Au(SCN)_2^-$, $AuBr_2^-$ and $AuCl_2^-$ (Aylmore, 2016). Eksteen and Oraby (2015a, 2015b, 2014), Oraby et al. (2019a), Oraby and Eksteen (2014); Eksteen et al. (2017); Tanda et al. (2017); Eksteen et al. (2018) studied and recognized glycine as a primary lixiviant in gold and other precious metal leaching. They discovered that among the amino acids (e.g., histidine and alanine), a single amino acid (glycine) has the maximum gold dissolution, and they recommended its use because of its low cost and high availability.

3.6 Previous studies on recovery of Au using glycine

Several experimental works (examples below) have been conducted over the years using glycine (and other reagents) in attempt to find a lixiviant that will be as effective as cyanide in the gold leaching processes. Glycine has a number of advantages compared to other method that have been proposed in the past and minor disadvantages. Information on glycine is available in publications by Oraby and Eksteen (2015), Tanda et al. (2017) and Altinkaya et al. (2020), among others. This section will be summarized using three publications: (A) using a synergistic reagent mixture of glycine and cyanide to extract gold from gold-copper ores and concentrates (Oraby et al., 2017); (B) gold extraction from the ore using cyanide-free glycine solution (Altinkaya et al., 2020); (C) in the presence of permanganate, gold is leached from oxide ores in alkaline glycine solutions (Oraby et al., 2020).

3.6.1 Using a synergistic reagent mixture of glycine and cyanide to extract gold from gold-copper oxide ores and concentrates:

The existence or availability of copper minerals has a negative impact on gold extraction from gold-copper ores and concentrates unless a sufficient cyanide solution is added to retain a CN:Cu molar ratio of 4:1 (Jiang et al., 2001). In addition to decreased gold recovery, additional expenditures are required to either extract the copper, or to eventually eliminate cyanide and weak acid dissociable (WAD) cyanide species in the final tail solutions (Sceresini, 2005). Figure 10A reveals that gold extraction was only 5% at 300 ppm concentration of sodium cyanide, which corresponds to a CN:Cu molar ratio of 1:1. It is widely established that to increase gold recovery and limit copper adsorption on activated carbon in Au-Cu ores, cyanide should be applied at a CN:Cu molar ratio of 4:1 (Souza et al., 2014; Oraby et al., 2017 and Deng et al., 2019). Gold extraction has been considerably improved in the presence of glycine, at a CN:Cu molar ratio of 1:1. Gold extraction by the glycine cyanide synergistic (GCS) technique is 70.1% at comparable cyanide dosages, compared to 5% by cyanidation solely. Gold extraction only reaches ~47.9% at cyanide concentration of 1000 ppm (CN:Cu molar ratio 3.2:1). Gold extraction rose from 29.2% to 38.9% when glycine dosage of 2 g/L was added at the same concentration as cyanide (450 ppm NaCN; Fig. 10B). The cyanide was only added in a 1.3:1 molar ratio to the copper available in the ore, and gold extraction was only 31.0% at 800 ppm NaCN (Fig. 10C). Gold extraction increased up to 99.5% when glycine is added to a comparable amount as cyanide (800 ppm). This data

suggests that processing gold-copper deposits with the glycine cyanide synergistic (GCS) process offers at the very least four economic benefits or advantages: (I) minimal cyanide consumption; (II) good metal recovery; (III) negligible or no free-cyanide during leaching; and (IV) the cupric glycinate complex contains the majority of the copper in the leachate (Oraby et al., 2017).

Glycine has been discovered to boost gold extraction from gold-copper ore deposits when it is added to a starved cyanide leaching solution. For gold leaching in a starved cyanide solution, glycine is a more powerful oxidant and stabilizes the cupric ion in the solution (Oraby and Eksteen, 2015b). Figure 10D illustrates the effects of adding glycine at a preserved cyanide dosage of 800 ppm as NaCN on the extraction of gold, silver and copper from a gold-copper ore deposits. The maximum gold extraction was achieved with a glycine concentration of 5 g/L. The same gold extraction is accomplished using 2 g/L, 5 g/L and 10 g/L glycine over a 48-hour period (Fig. 10D).

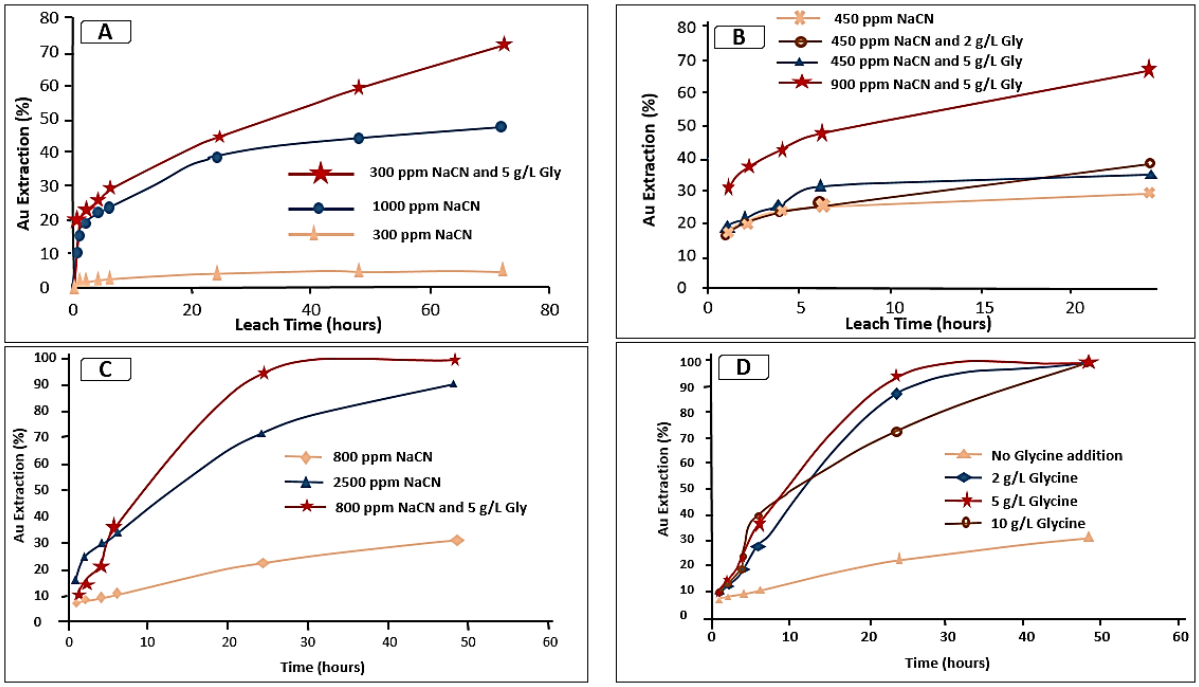

Figure 10: From A to D, the leaching conditions are as follows: solid content = 50%, grind = 100% passing 75 µm, pH value = 11.0, and room temperature. (A) The GCS and traditional cyanidation techniques were used to recover gold from gold-copper oxides. (B) GCS and conventional cyanidation procedures were used to recover gold from gold-copper sulphides. (C) GCS and standard cyanidation techniques were used to dissolve gold from gold-copper ore deposits. (D) Effectiveness of glycine (Gly) concentrations on gold extraction from gold-copper concentrates using the GCS technique with 800 ppm NaCN and the leaching conditions described above (modified after Oraby et al., 2017).

3.6.2 Gold extraction from the epithermal ore deposit using cyanide-free glycine solution:

The application of hydrogen peroxide (H_2O_2) as an alternative oxidizing reagent to oxygen for gold dissolution from a mixture of silver-gold materials in alkaline glycine solutions was introduced by Oraby and Eksteen (2015a, b), and Eksteen and Oraby (2015). They discovered that increasing the concentrations of glycine (0.025 to 1 M), pH (5.8 to 12.8), temperature (23 to 75°C), or hydrogen peroxide (0 to 2%) improved gold solubility. Furthermore, Eksteen and Oraby (2015a) reported that when a catalyst is added to the system, gold dissolution increases significantly, whereas pyrite has a detrimental influence on gold extraction. Gold dissolution reaction by alkaline glycine solution in the presence of peroxide can be illustrated by the equation below (Eq. 9; Altinkaya et al., 2020):

$$2Au + 4NH_2CH_2COOH + 2OH^- + H_2O \rightarrow 2Au\,(NH_2CH_2\,COO)_2^- + 4H_2O \qquad \textit{Eq. 9}$$

The impact of temperature, pH, and glycine concentration on gold extraction using the glycine leaching method is illustrated in Fig. 11. Gold dissolution is marginally affected by glycine concentrations (0.5-2 M) in the initial leaching process (Fig. 11A). At elevated glycine concentration (2 M), gold concentration of 0.55 mg/L was observed, while the lowest gold concentration of 0.4 mg/L was found with a 0.5 M glycine dosage (Altinkaya et al., 2020). However, in terms of the kinetics of gold dissolution, temperature is clearly critical. At room temperature, gold dissolves almost linearly (Fig. 11B), reaching 0.3 mg/L of gold after 24 hours, while at 60°C, it reached the maximum of 0.55 mg/L of gold within 24 hours. Dissolution of gold is also dependent on pH. The dissolution of gold at pH 10 is very small, and the amount of gold dissolved at pH 11 is 0.4 mg/L, with even more at pH 12 (Fig. 11C).

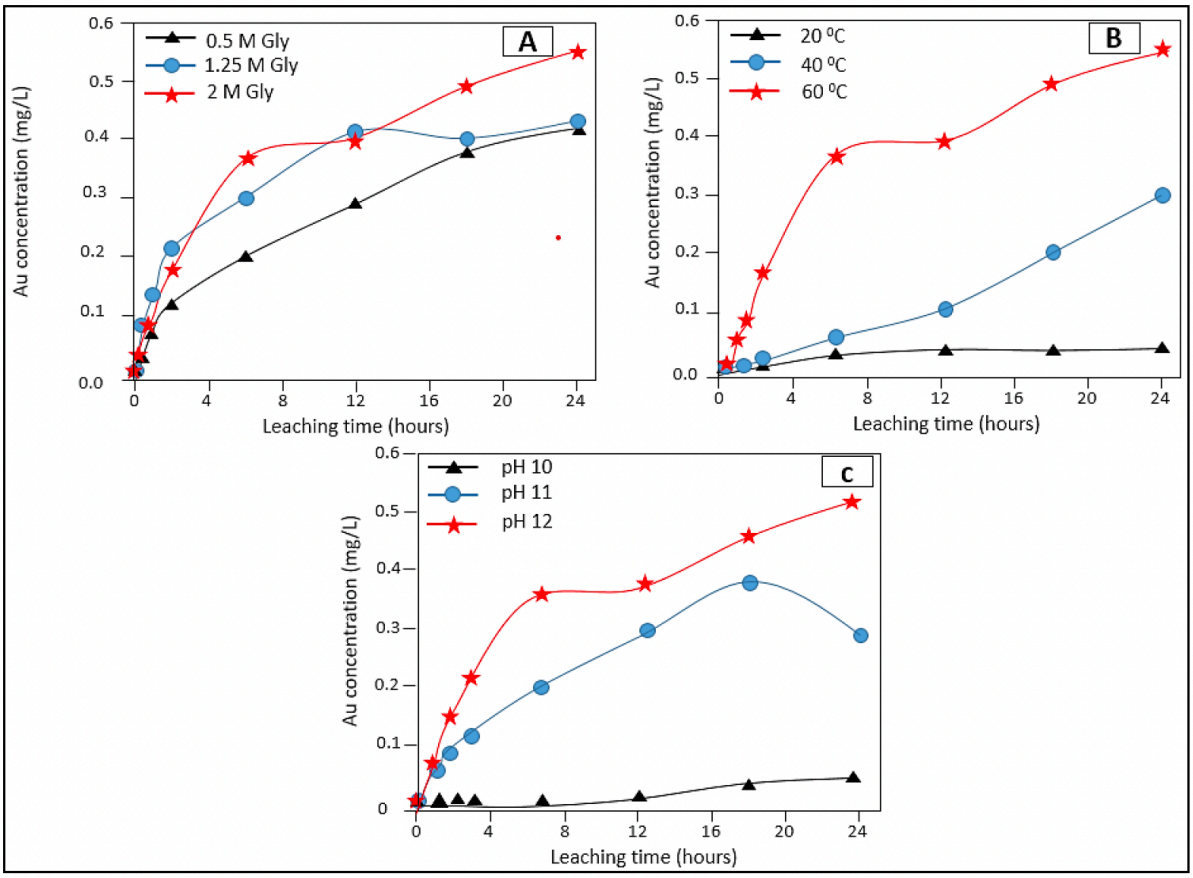

Figure 11: Effects of glycine concentration, temperature, as well as pH on gold dissolution. Highest gold recoveries are observed when leaching parameters remain fixed at 2 M glycine (Gly), 60°C, pH = 12, O_2 feed: 1 L/min; after Altinkaya et al., 2020.

3.6.3 Using alkaline glycine media and potassium permanganate to recover gold from oxide ores:

Glycine is most effective for tank leaching with a cyanide-starved process called GlyCat, where cyanide serves as a catalyser (Oraby et al., 2017). The toxic cyanide problem is not entirely solved by this process. Carbon adsorption, resin adsorption and sulphide precipitation are effective ways to recover gold (Deng et al., 2020). In a recent study by Oraby et al. (2020), diluted glycine and conventional bottle roll aeration technique were applied. Eq.10 shows the reaction between gold and glycine.

In similar conditions, glycine has significantly slower leaching rates than cyanide. In order to rectify this, the temperature of the system can be raised up to ~ 60°C or a catalyst can be added. Oraby et al. (2020) used permanganate (MnO_4^-) as a strong oxidant to oxidise gold ore. Manganite is formed in the presence of oxygen by the reaction of manganese dioxide and manganese ore with potassium hydroxide as detailed in Eq. 11. In the presence of an alkaline solution, manganite is electrolytically oxidized to potassium permanganate Eq. 12. In order to ensure the presence of sufficient free-glycine in the system

for gold complexation, it is essential to add glycine to permanganate at more than a stoichiometric ratio for effective leaching (Eq. 13). Nitrogen is produced by oxidizing ammonia by-products with permanganate (Eq. 14) and CO_2 is produced by oxidizing oxalate (Eq. 15).

$$4Au + 8NH_2CH_2COOH + 4NaOH + O_2 \rightarrow 4Na[Au(NH_2CH_2COO)_2] + 6H_2O \quad Eq.10$$

$$2MnO_2 + 4KOH + O_2 \rightarrow 2K_2MnO_4 + 2H_2O \quad Eq.11$$

$$2K_2MnO_4 + 2H_2O \rightarrow 2KMnO_4 + 2KOH + H_2 \quad Eq.12$$

Glycine oxidation:

$$2MnO_4^- + 2(NH_2CH_2COO)^- + \frac{1}{2}O_2 \rightarrow 2MnO_2 + 2C_2O_4^{-2} + 2NH_3(aq) + H_2O \quad Eq.13$$

Ammonia oxidation:

$$2MnO_4^- + 2NH_3(aq) \rightarrow 2MnO_2 + N_2 + 2OH^- + 2H_2O \quad Eq.14$$

Oxalate oxidation:

$$C_2O_4^{-2} \rightarrow 2CO_2 + 2e^- \quad Eq.15$$

Oxygen reduction:

$$O_2 + 2H_2O + 4e^- \rightarrow 4OH^- \quad Eq.16$$

The results of glycine and permanganate reactions, when oxygen is present, as well as its effect on gold leaching, are summarized in Fig. 12A. Results from Oraby et al. (2020) have been outlined with regard to the impact of pH, glycine and permanganate concentration of the solution, as well as the type of oxidant or catalyst used.

Effect of glycine concentration (Fig. 12B): A variation in glycine concentration affected gold recovery at pH 10.5 in the presence of potassium permanganate at 1.0 g/L. After 4 hours of leaching, the gold dissolution rate is proportional to the glycine concentration. A high concentration of glycine may necessitate solution recycling from an economic perspective. Altinkaya et al. (2020) utilized high concentrations of glycine ~93.75 g/L and enhanced temperatures up to 60°C in contrast to the procedure and results by Oraby et al. (2020). The use of permanganate in combination with glycine reduces the processing intensity significantly and is cost effective.

Effect of permanganate concentration (Fig. 12C): It is interesting to note that although the leaching rate is quicker at the beginning when using 2 g/L permanganate, total gold recovery is higher when using only 1 g/L permanganate. After 48 h, gold recovery increases to 76.4% using 1 g/L permanganate, while it decreases to 67.9% when using 2 g/L. As a result of the oxidation of glycine by excess permanganate,

gold concentrations decreased with higher concentrations of permanganate (Insausti et al., 1992; Oraby et al., 2020). In order to compensate for the loss of glycine due to oxidation, the concentration of glycine can be increased in order to increase the total amount of available free glycine in the system.

Effect of pH: The recovery of gold at various pH values is illustrated in Fig. 12D. It can be seen that gold leaching rate is slower at pH 9.5; however, recovery is slightly higher after 48 hours than pH 10.5 and 11.5. Such findings indicate that using less lime and/or caustic may be viable, as well as allowing the use of lower-quality water, which can act as a buffer at alkaline pH, owing to magnesium presence in salty waters. In terms of gold recovery as well as reagent consumption, leaching at 9.5 pH is more efficient. When gold is leached at 6.5 pH, it dissolves very poorly. The amount of gold extracted after 48 hours at pH 6.5 was 10%. At pH 6.5, gold recovery levels are lower due to the fact that glycine in zwitterion state does not leach gold as efficient as anionic glycinate does at pH 9.5.

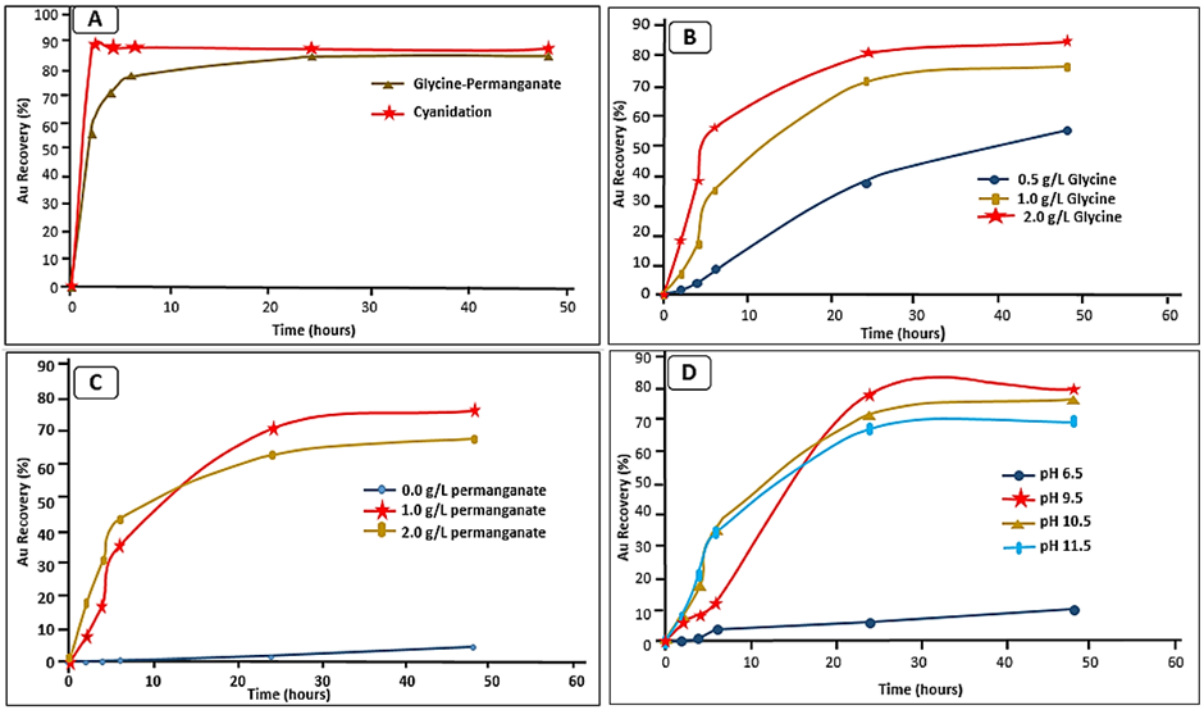

Figure 12: Graphs illustrating the effects of different leaching parameters (modified after Oraby et al., 2020). (A) Gold extraction from gold oxide ore using cyanidation and glycine-permanganate; leach conditions: glycine dosage = 2 g/L, solid content = 30%, milling or grind = 100% passing 75 µm, pH = 10.5, and permanganate = 2.0 g/L at room temperature. (B) Glycine concentration effects on gold recovery from gold oxide ore using the Glyleach technique. (C) Permanganate concentration effects on glycine-based gold recovery from gold oxide ore. (D) Effect of different pH values on gold recovery from gold oxide ore deposits using glycine as the primary reagent. Conditions of leaching from B to D: solid content = 30%, grind = 100% passing 75 µm, pH = 10.5, glycine dosage = 1.0 g/L, and permanganate = 1.0 g/L at room temperature.

Effect of oxidant type (Fig. 13): Several oxidants were used to study the gold dissolution, including peroxide, chlorate, ferricyanide and potassium permanganate, among others (Fig. 13). The permanganate is the most effective, as is immediately evident in Fig. 13. A slight improvement in gold extraction rate was observed when ferricyanide was added; however, it is likely that this is only good for heap or in-situ leaching. Other oxidants (chlorate and ferricyanide) show poor leaching recoveries. Researchers have looked into hydrogen peroxide and discovered that considerable leaching recovery occurred at temperatures above 40°C (Eksteen and Oraby, 2015). As a result, potassium permanganate is by far the most effective oxidant in stirred tank leaching at room temperature. Permanganate outperforms the other oxidants because it produces MnO_2 in a colloidal state, which functions as an extra oxidant during leaching and is a more potent oxidant in alkaline solution (Pratesa et al., 2019; Oraby et al., 2020).

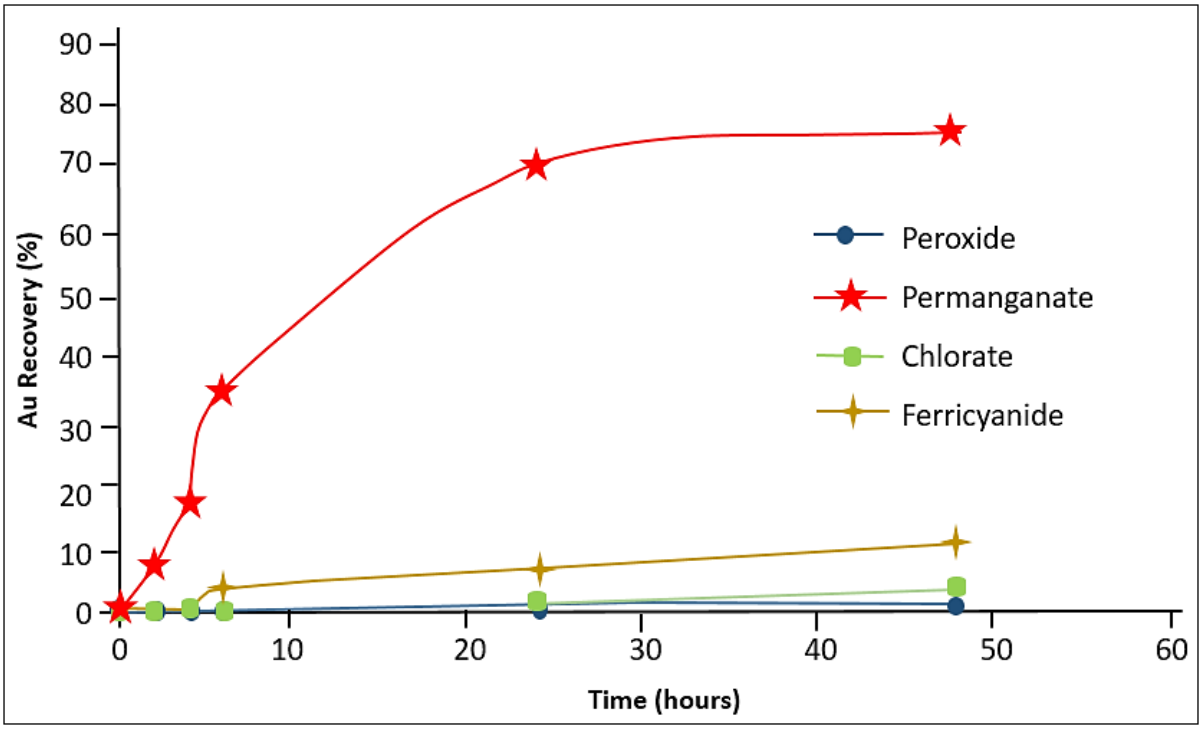

Figure 13: Effects of oxidants on gold leaching from gold oxide ore deposits with glycine as the major reagent under leach conditions of solid contents = 30%, grind = 100% passing 75 µm, pH = 10.5, glycine dosage = 1.0 g/L, oxidant dosage = 1.0 g/L and at room temperature (modified after Oraby et al., 2020).

Table 1 summarizes the differences between the publications by Altinkaya et al. (2020) and Oraby et al. (2020). Oxide gold ores are essentially the same in both cases. The alternatives for glycine leaching in the presence and exclusion of a catalytic oxidant have been illustrated by these two cyanide-free glycine-leaching techniques. To determine which approach is most appropriate for a given ore, the

techno-economics (economic performance) of the overall process, including downstream processing, reagent recycling and recovery must be considered.

Table 1: A comparative gold leaching conditions without the use of cyanide by Altinkaya et al. (2020) vs. Oraby et al. (2020). [g/L] = concentration and $D_{\%}$ = percentage of ore particles size passing certain screening sieve size.

Leach parameter	**Altinkaya et al. (2020)**	**Oraby et al. (2020)**
Temperature (°C)	60	Ambient (~23)
Oxygenation (L/min)	1	None, only air ingress through lid
Optimal Glycine [g/L]	93.75	2
Optimal pH	12	10.5
Agitation (rpm)	900 (overhead agitation)	100 (bottle roll)
% Solids	10	30
Gold ore grade (g/t)	5.4	3.74
Grind (μm)	D_{80} = 86	D_{100} =75
Oxidant/catalyst addition (g/t)	None	$KMnO_4$ (1 g/t)
Recovery (%)	90	85
Leach duration (h)	24	48

3.7 Advantages and disadvantages of glycine

3.7.1 Advantages:

- Glycine is a standard commercial lixiviant with properties that make it ideal for precious metal extraction: it is water-soluble, re-usable, stable, non-volatile and non-toxic.
- Glycine is environmentally friendly and very safe to work with, in addition to the processing advantages; it is recycled as part of hydrothermal processing, resulting in cheap operating costs and no specific disposal concerns (Wang et al., 2019).
- Glycine has high selectivity, forms stable complexes with copper, gold, nickel, cobalt, zinc, during leaching in alkaline conditions, but not with iron, magnesium or manganese (Eksteen et al., 2017; Huang et al., 2017).
- A mixed glycine-cyanide (with CN^- acting as catalyst/oxidant) solution can successfully leach out gold from ore deposits. The amount of cyanide to be used is a quarter of what is needed in traditional cyanidation. The resultant solution will therefore contain substantially less weak acid dissociable (WAD) cyanide, lowering or eliminating the expense of detox. A different oxidant/catalyst should be used to overcome the cyanide environmental problem anyway.

- Under Glyleach conditions, most typical gangue minerals do not respond or react (Oraby et al., 2019; Eksteen et al., 2020).

3.7.2 Disadvantages:

- The significant disadvantages of glycine leaching over conventional cyanidation is that gold dissolves slowly in Glyleach and low gold recoveries have been observed. However, the leaching rates using glycine may be improved by either adding catalysis or by increasing temperature up to 60°C. The addition of a catalyst or the use of a higher temperature offers some benefits, including: (I) increased gold leaching rates, and (II) the introduction of a cyanide-free leaching method. At room temperature, adding potassium permanganate as a catalyst can assist to achieve high leaching rate and improved gold recovery.
- Application of a catalyst and higher temperatures (~60°C) will increase gold ore processing costs.

CHAPTER 4: MATERIALS AND METHODOLOGY

This chapter presents the analytical/experimental work carried out in this study and is subdivided into two sections. Section 3.1 provides details about bulk ore sampling from South Deep Gold Mine, which is situated ~45 km southwest of Johannesburg near Westonaria Town. Section 3.2 describes analytical methods used for mineralogical and geochemical results as well as the glycine leaching experimental methods used in this study (Fig. 14).

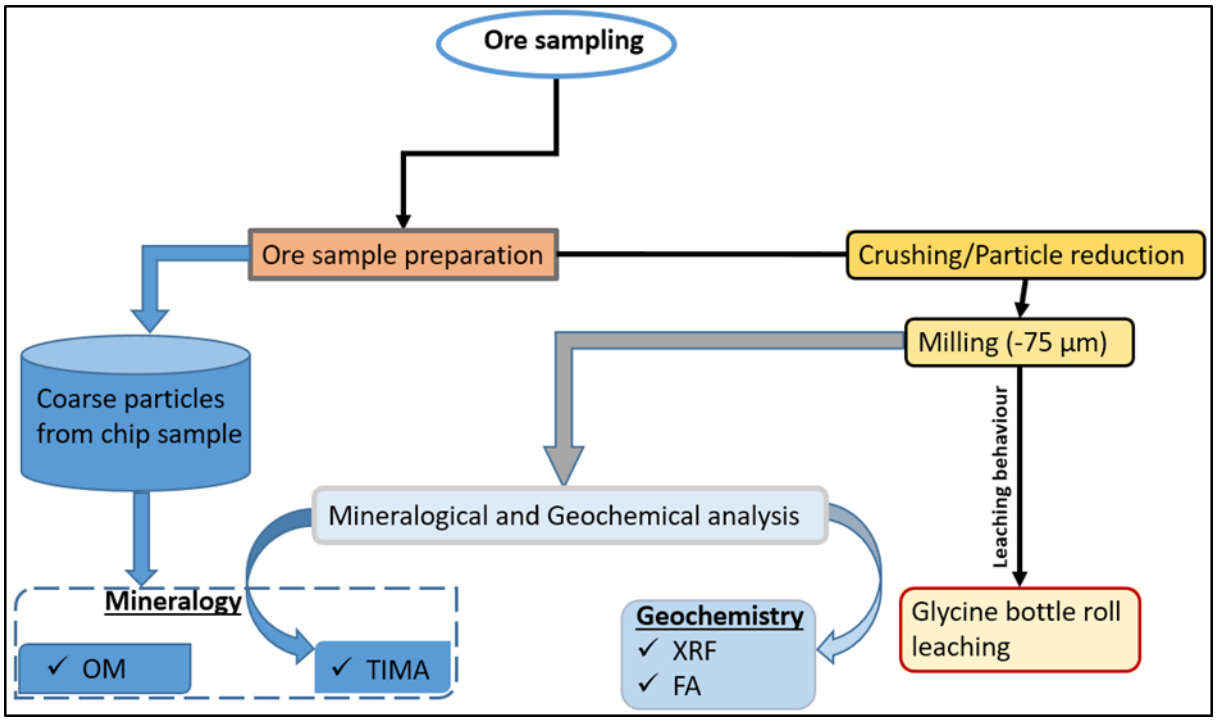

Figure 14: Schematic flowchart showing geological/geometallurgical, mineralogical, geochemical and processing approach of the Elsburg reefs (Modderfontein Intermediate Top [MIT] and Elsburg Conglomerate Top [ECT]) gold ore deposits. Abbreviations: OM = Optical microscopy; TIMA = TESCAN Integrated Mineral Analyser; XRF = X-ray fluorescence; and FA = fire assay.

4.1 Sample collection and preparation

Sampling took place underground at the South Deep Gold Mine, where the Elsburg reefs are exposed. Approximately 40 kg of bulk (high-grade: ~20 kg, and low-grade: ~20 kg) gold-bearing ore samples were collected from two conglomerate beds which are part of the Elsburg Reefs package. High-grade samples were taken from the Modderfontein Intermediate Top Band (MIT), and low-grade samples were taken from the Elsburg Conglomerates Top Band (ECT; Fig. 15). Samples from both MIT and ECT were prepared for thin sections, and the remaining portion of the samples were crushed and milled (comminution in subsection 3.1.2) into smaller particles (~75 µm) in preparation of bottle roll leaching experiments.

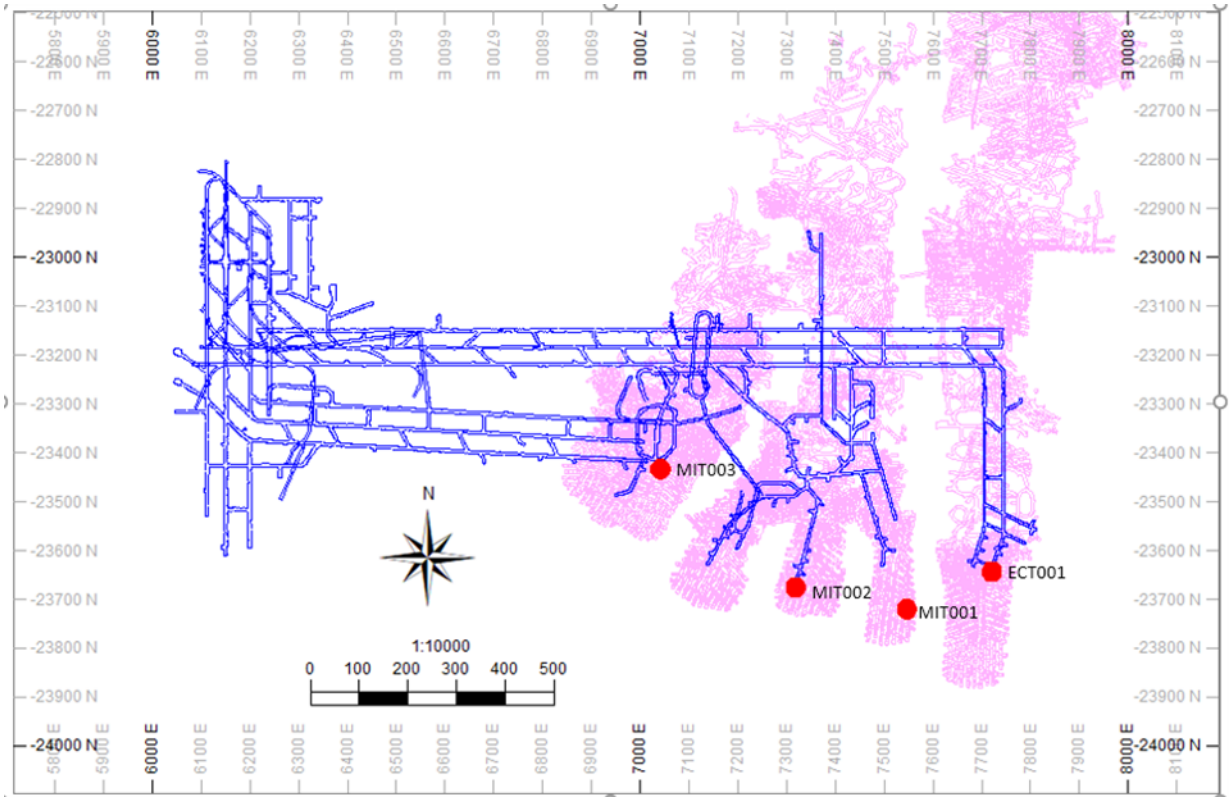

Figure 15: Underground mine plan from South Deep Gold Mine showing sampling locations. Map constructed using micromine from mining data provided by South Deep Gold Mine. ECT001 is a low-grade ore (< 2 g/t Au) and MIT001 to MIT003 are moderate to high-grade with average of ~14 g/t Au.

4.1.1 Thin section preparation

The run-of-mine samples from the MIT and ECT bands, Elsburg reefs, were carefully selected for thin section preparation (see Appendix I for examples). Six of the grab samples from the mine were used to cut acceptable size slabs for mounting (four from MIT and two from ECT). Each rock slab is labelled, and the other side is lapped level and smooth on a cast iron lap. Epoxy is used to adhere a glass slide to the slab's lapped face. Using a thin section saw, the slab was cut-off close to the glass slide. A thin section grinder is used to reduce the thickness even more. The segment is lapped on a glass plate with 600 grit carborundum to reach a final thickness of 30 microns. Prior to polishing, a fine grinding with 1000 grit was done. The segment is held in a holder and polished with nylon cloth and diamond paste on a polishing machine until a satisfactory finish is produced for microscopy or TIMA examinations. This was done at the University of the Witwatersrand's School of Geoscience.

4.1.2 Comminution

Comminution is the breaking, crushing, and/or milling of rock or mineral particles to reduce their size in attempt to liberate valuable minerals from gangue minerals. In this study, comminution was

conducted in School of Geosciences at the University of the Witwatersrand, utilizing a steel jaw crusher to break ore samples into 2 cm particles. The jaw-crushing machine was cleaned using acetone acid and dried between samples to avoid cross-contamination. The gravel-sized particles were then pulverized using a milling machine. For this study, the ore was pulverized to the point where 80% of the particles could pass through 75 μm sieving screens.

4.2 Analytical techniques

Different analytical methods were used to gain a better understanding of mineralogy, geochemistry and geometallurgical aspects of the ore, as shown in Fig. 14.

4.2.1 Mineral analysis

Two mineralogical characterisation instruments were used, namely the: 1) optical microscope, and 2) Tescan Integrated Mineral Analyser (TIMA). Analysis using both instruments were carried out at the School of Geosciences, University of the Witwatersrand.

Mineral identification and characterisation using an Olympus BX-41 petrographic microscope was done to establish the mineralogical composition and textural characteristics of the samples taken from the Elsburg reefs. The same samples analysed using a petrographic microscope were also analysed using TIMA to confirm mineral phases identified under the microscope. TIMA was used to establish modal mineralogy, gold liberation and association with gangue minerals as well as textural characteristics of mineral phases. The thin sections were coated with carbon before analyses were done. Using the VEGA3 SEM analyser and the VEGA3 X64 TESCAN TIMA 2.4.0, the samples were subjected to energy-dispersive X-ray spectroscopy (EDS). The TIMA machine was calibrated for acquisition measurements as follows: pixel spacing of one μm, a minimum-maximum brightness of 10 to 100%, used dot mapping for X-ray mapping resolution, dot spacing of 9 μm, X-ray counts of 1000 and imaging speed of 4 μm were used. Data processing was conducted thereafter acquiring TIMA readings.

4.2.2 Lithogeochemistry

Ten pulverized ore samples (from blended bulk sample) were analysed for their chemistry using X-ray fluorescence (XRF). XRF was used to determine both major and minor elements as well as select trace elements. All XRF analyses were performed at the Earth Lab, University of the Witwatersrand.

For major element oxide determination, samples were fused using the Johnson Matthey Spectral flux 105 at 1000°C. Samples weighed 0.35 grams, and flux weighed 2.0 grams. Samples were then analysed using a Panalytical Axios X-Ray Spectrometer. Operating conditions were 50 kV and 50 mA. Raw data were corrected using in-house software. Standard calibrations include synthetic oxide mixtures and international standard rocks (i.e., BCR-2, NIM-P, NIM-D, W-2, NIM-S, GSP-2, NIM-N, NIM-G,

PCC1, BHVO2, AGV2 and G2 DTS1; see Appendix II for standard values), as well as in-house controls. Precision is taken as 1% for elements in the abundance of greater than 5% by weight and 5% for elements in abundance less than 5% by weight.

Trace elements were determined using pressed pellets created by a Moviol solution binder and pressing machine. Samples were analysed for elements: Sc, V, Cr, Co, Ni, Cu, Zn, Ga, Rb, Sr, Y, Zr, Nb, Mo, Ba, Pb, Th and U. The instrument used is the Philips PW2404 x-ray spectrometer. Calibration was carried out using USGS (USA) and NIM (South Africa) reference materials. Precision was determined based on counting times and is taken as 5% for elements in abundance greater than 100 ppm and 10% for elements in abundance between 10 and 100 ppm.

4.2.3 Bottle roll gold leaching experimental methods

Hydrometallurgical techniques are well suited for processing complex and low-grade ores because of process flexibility, relatively low capital cost and potential selectivity they pose (Syed, 2012). Since the introduction of cyanide leaching in the late 19th century, hydrometallurgical processes have dominated the treatment of gold ores. The processing of gold, as a general flowsheet, consists of leaching, solution purification and recovery (Fig. 16). The ore's components (usually precious metals such as gold, silver and copper) can be dissolved into a solution using diverse chemicals such as water, acids, alkaline solutions and salts in a solid-liquid mass and/or heat transfer process called leaching. Various gold leaching processes (heap or dump leaching, in-situ leaching, vat leaching, reactor leaching and intense cyanidation) are used to extract gold from low-grade ores, depending on the mine's geographical, geological, metallurgical, mineralogical and environmental conditions (Marsden and House, 2006; Altinkaya, 2021). The type of leaching used in this study is tank (bottle roll) leaching.

Figure 16: Simplified flowsheet for gold processing.

For this study, bottle roll experiments were conducted using Elsburg reefs gold ores (i.e., blended MIT and ECT beds). Ore blending was done to get a uniform gold grade and a representative sample of the Elsburg reefs. Glycine was used as the principal reagent and potassium permanganate as an oxidant at ambient laboratory conditions. These experiments were carried out at the hydrometallurgy laboratory based at the University of the Witwatersrand. Six experimental runs (using blended bulk ore) have been performed in different leaching conditions (glycine and $KMnO_4$ concentrations, leaching time, recharging, temperature and pH values). The slurry (mixture of pulverized ore and water) was monitored for dissolved oxygen (DO), glycine (NH_2-CH_2-COOH), $Ca(OH)_2$ and gold contents at different time intervals for each experiment. To determine the amount of gold leached after a certain

period of time, a small (~50 mL) portion of the sample was taken at different time intervals per experiment. In all experiments, the pH was regulated using $Ca(OH)_2$ to the target pH and the bottles were rolled at 35 revolutions per minute (rpm). The summary of experimental parameters used in each experiment are shown in Table 2.

Experiments 1 and 2 were performed using 20% solids and 80% distilled water mixed in a 2-litre beaker to form a slurry. The pH adjustment was made using a pH meter and lime $Ca(OH)_2$ to make sure that the initial pH value was kept as close as possible to 10.50. The slurry was transferred into the three 5 litre bottle rollers, which were then placed in an agitator for an hour. The initial pH value was recorded after an hour to be 10.56. Different dosages of glycine and potassium permanganate were used in each bottle. Specifically, in bottle roll one, two and three, glycine dosages of 300 ppm, 1000 ppm and 1500 ppm were used, respectively. The ratio of glycine to potassium permanganate is 1:2 in each bottle. All three bottles were placed on a roller to roll for 35 hours under experiment 1 and 50 hours under experiment 2. Experiment 1 was recharged two times, while experiment 2 was recharged three times with a solution that has the same concentration of glycine, $KMnO_4$ and pH as when leaching started. Leaching residue sample preparation was achieved by setting up the filter press and ensuring that the filter paper was placed correctly. A clean cylinder was placed underneath the filter press to collect the filtrate or leachate. The bottle was taken from the roller, swirled sample/slurry carefully and poured into the filter press cylinder. Filter press pressure was increased to separate leachate from solid residues. The sample was then dried in an oven for 24 hours before measuring the weight and/or performing further analyses.

Experiments 3 and 4 were performed to determine the effects of slurry density on gold leaching by using a very high glycine dosage without recharging and recycling the leaching solution. Experiment 3 was performed using 20% solids and 80% distilled water, while experiment 4 used 30% solids and 70% distilled to make a slurry. Both experiments 3 and 4 were carried out at room temperature, using 4500 ppm glycine and 9000 ppm potassium permanganate, and initial pH values of ~10.56. No recharging was performed for the entire duration of leaching, which corresponds to 48 hours.

Experiment 5 was carried out at room temperature, using 30% solids and 70% liquid, 1500 ppm glycine, 3000 ppm $KMnO_4$ and initial pH values of ~10.5. A small solution sample of ~50 ml was collected from each battle roll to determine the amount of gold dissolved at time intervals of: 0, 11, 17, 23, 29, 41, 52, 64 and 76 hours. During these time intervals, glycine, $KMnO_4$ and $Ca(OH)_2$ were added to the bottle rolls. The experiment was stopped after 101 hours. The solid residues were dried in an oven for 24 hours, and then its mass was recorded. Leachate and residue samples were submitted to a commercial laboratory for gold grade analysis.

Experiment 6 was performed in a glycine ($C_2H_5NO_2$) media using a 5 litre jacketed beaker reactor under elevated temperature with a leaching time of 48 hours. Samples consisted of a 30% solid and 70% liquid

ratio. The temperature was set between 35°C and 45°C, and a glycine concentration of 1500 ppm was used. A pitched blade impeller was used to agitate the solution at a constant speed of 800 rpm. Solution sample was taken in time intervals of: 0, 12, 20, 28, 36 and 44 hours, to determine concentrations of dissolved gold and glycine. $KMnO_4$ and $Ca(OH)_2$ were also added during these time intervals to increase free glycine in solution and strengthen gold-glycine complexing ability.

In all experiments, residue samples were dried in an oven at 60°C for at least 24 hours and the residue mass was recorded before taking the samples for gold grade determination. Gold fire assay (FA) was used to determine gold concentrations or grade (g/t) for solid head feed and residue samples. Atomic Absorption Spectrometry (AAS) was used to analyse gold in leachate or filtrate. All gold leaching analyses in both residues and filtrate were done by a commercial laboratory (Super Laboratory services). In a Super Laboratory services unpublished report, QAQC-Chips35 (2021) reference materials with a gold grade of 1.560 g/t were used to test the accuracy of gold grade results. An assayed value of 1.520 g/t Au was attained. The upper limit of 1.720 g/t and lower limit of 1.400 g/t, with a standard deviation of 0.16 g/t, are acceptable, according to the Super Laboratory services unpublished report. Therefore, gold grade results with standard deviation ≤ 0.16 g/t are considered accurate in this study. Leaching recoveries were calculated using equation 1 for all experiments except for experiment 6, where equation 2 was used.

$$\text{Recovery}(\%) = \frac{\text{head grade}\left(\frac{\text{g}}{\text{t}}\right)\times\text{head mass(g)} - \text{residue grade}\left(\frac{\text{g}}{\text{t}}\right)\times\text{residue mass(g)}}{\text{head grade}\left(\frac{\text{g}}{\text{t}}\right)\times\text{head mass(g)}} \times 100 \quad (1)$$

$$\text{Recovery}\ (\%) = \frac{\text{head grade}\ \left(\frac{\text{g}}{\text{t}}\right)\times - \text{residue grade}\ \left(\frac{\text{g}}{\text{t}}\right)}{\text{head grade}\ \left(\frac{\text{g}}{\text{t}}\right)} \times 100 \quad (2)$$

where head grade is the grade of pulverized ore before leaching, head mass corresponds to the initial mass of ore used for leaching, residue grade is grade of solids after leaching, and residue mass is mass of dry solids after leaching.

Table 2: Summary of experimental work. Ore used was pulverized to particle size = ~80% passing 75 µm, feed grade = 5.33 g/t and RT = room temperature.

Experimental ID	Time (hrs)	Recharge #	Temperature (°C)	Glycine concentrations
Experiment 1	34	2	RT	300 to 1500 ppm
Experiment 2	50	3	RT	300 to 1500 ppm
Experiments 3 and 4	48	-	RT	4500 ppm
Experiment 5	101	8	RT	1500 ppm
Experiment 6	48	5	35 – 40°C	1500 ppm

CHAPTER 5: RESULTS

This section focusses on mineralogical characterisation (mineral assemblage, modal quantities and the morphologies of different minerals, especially pyrite), mineral association, liberation and locking of gold by gangue minerals. Most importantly, this chapter also presents the results from bottle roll leaching using glycine and potassium permanganate as major reagents.

5.1 Mineralogical characterisation

The Elsburg reefs (Modderfontein Intermediate Top (MIT) and Elsburg Conglomerate Top (ECT) bands) gold ores were studied using two distinct mineralogical characterization techniques, namely: optical microscopy and the Tescan integrated mineral analyser (TIMA). The functions of both approaches are complementary. That is, the optical microscopy depicts mineral phases and textural characteristics (photographs shown in Fig. 17) and TIMA provides mineral phases in details (Fig. 18), quantitative modal mineralogy (Table 3), association and locking and/or liberation analysis. Microphotographs taken using an optical microscope (reflected light) are shown in Fig. 18, and the mineral association with gold as well as minerals locking gold are presented in Fig. 19 and 20, respectively.

Table 3: Estimated mineralogical composition and mineral quantification of the Modderfontein Intermediate Top (MIT) and Elsburg Conglomerate Top (ECT) gold ore samples as determined by TIMA. Results are given in mass %.

Minerals	MIT	ECT
Gold	< 0.01	<0.01
Pyrite	14.64	8.93
Arsenopyrite	0.34	<0.01
Pyrrhotite	0.33	0.3
Chalcopyrite	0.03	<0.01
Other Sulphides	0.07	<0.01
Quartz	72.61	84.48
Chlorite	3.67	1.42
Zircon	1.72	0.85
Mica	3.31	1.97
Apatite	0.03	0.04
Rutile	0.02	0.04
Fe Oxides/Hydroxides	0.09	0.07

Chromite	0.04	<0.01
Monazite	0.03	<0.01
Uraniferous minerals	<0.01	<0.01
Almandine	0.94	0.65
Others	2.07	1.19

The main constituents of the auriferous Elsburg reefs ore corresponds to matrix-supported conglomerates defined by sub-angular to sub-rounded grains of quartz (0.1 – 5 mm) with minor pyrite grains (Fig. 17). Pyrite is the dominant sulphide mineral in the studied ore. The type of pyrite associated with Elsburg reefs is detrital pyrite and appears as euhedral grains with rounded edges (Fig. 17A and B). Grain size of the pyrites range between < 50 μm and 2 mm. Pyrrhotite and chalcopyrite occur in fractures in and around pyrite crystals (Fig. 17C), indicating the effect of hydrothermal fluids after the deposition of pyrite. The ECT bed of the Elsburg reefs consists of sub-rounded porous pyrites with irregular shaped gold at the edges of the pyrite grains (Fig.17A). All visible gold is associated with quartz and pyrite in the ECT bed, with a few gold crystals also found in the fractures of pyrite grains. In the MIT bed, sub-rounded gold grains are associated with both quartz, pyrite and arsenic-bearing mineral such as gersdorffite (Figs. 17B and 18B). Some gold is found as inclusions within detrital pyrite grains (Fig. 17C(i)) with chalcopyrite filling gaps between the pyrite grains (Fig. 17C(ii)). Most of the invisible gold in Elsburg reefs is believed to be associated with arsenopyrite, as seen in Fig. 18B, as well as Au-tellurides.

The matrix of the conglomerate is made up of authigenic/metamorphic quartz, muscovite, biotite, chlorite and other arsenic-rich minerals such as gersdorffite. The detrital heavy-mineral assemblage includes: rutile, zircon, chromite, Fe–oxides (hematite/magnetite) and different Cu–(Fe) sulphides such as chalcopyrite and pyrrhotite. Typical secondary mineral phases (either authigenic, metamorphic and/or hydrothermal) include: muscovite, biotite, chloritoid and/or chlorite, with minor rutile, pyrite, gold and other uranium-bearing minerals (Fig. 18). In some cases, discrete grains of irregular-shaped gold are visible in the multi-mineral boundaries of the meta-conglomerate and in the edges of sulphide minerals (i.e., pyrite and pyrrhotite).

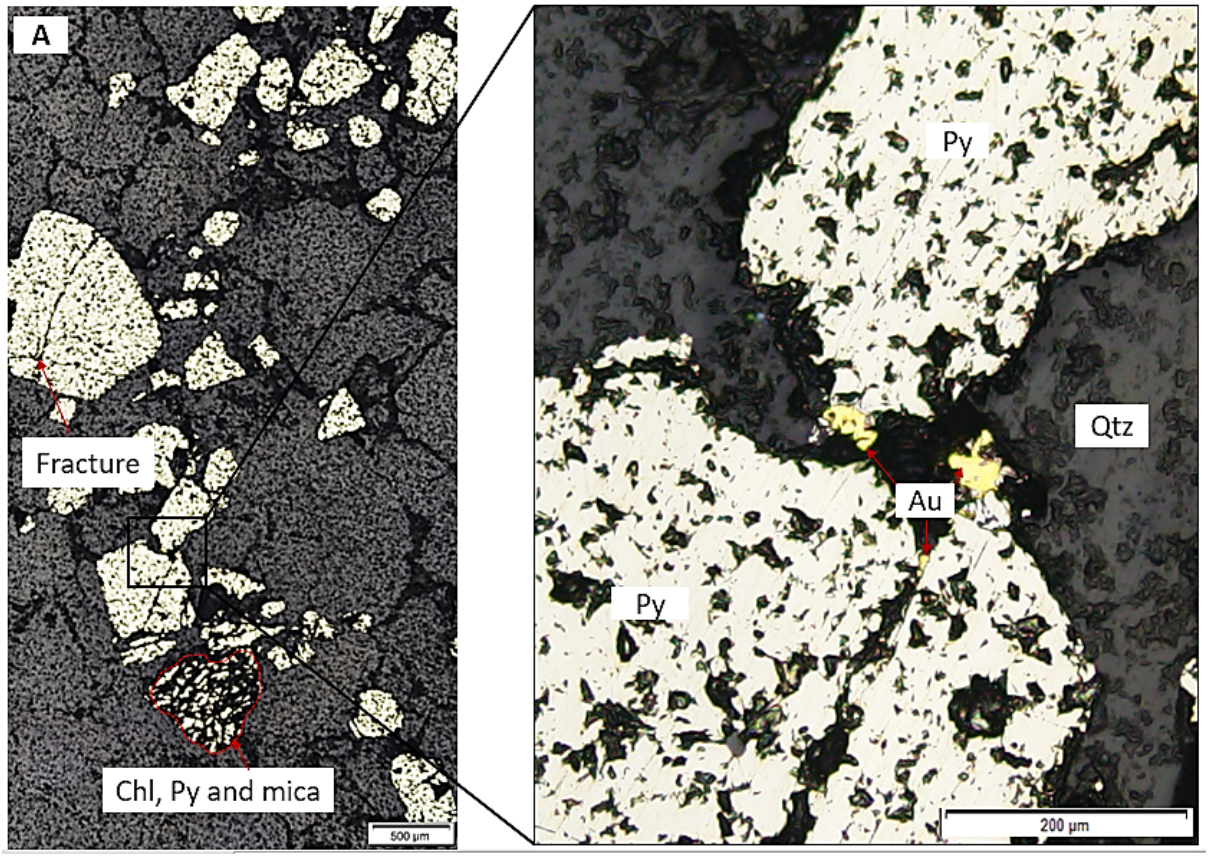
A
Fracture
Chl, Py and mica
500 µm
Py
Qtz
Au
Py
200 µm

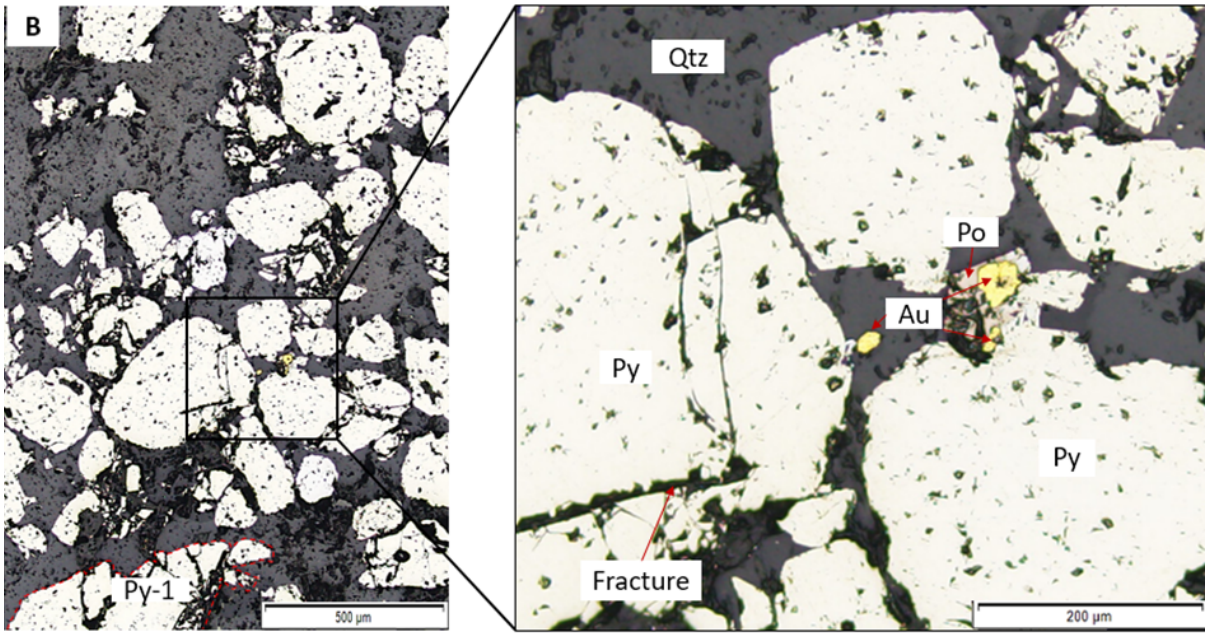
B
Py-1
500 µm
Qtz
Po
Au
Py
Py
Fracture
200 µm

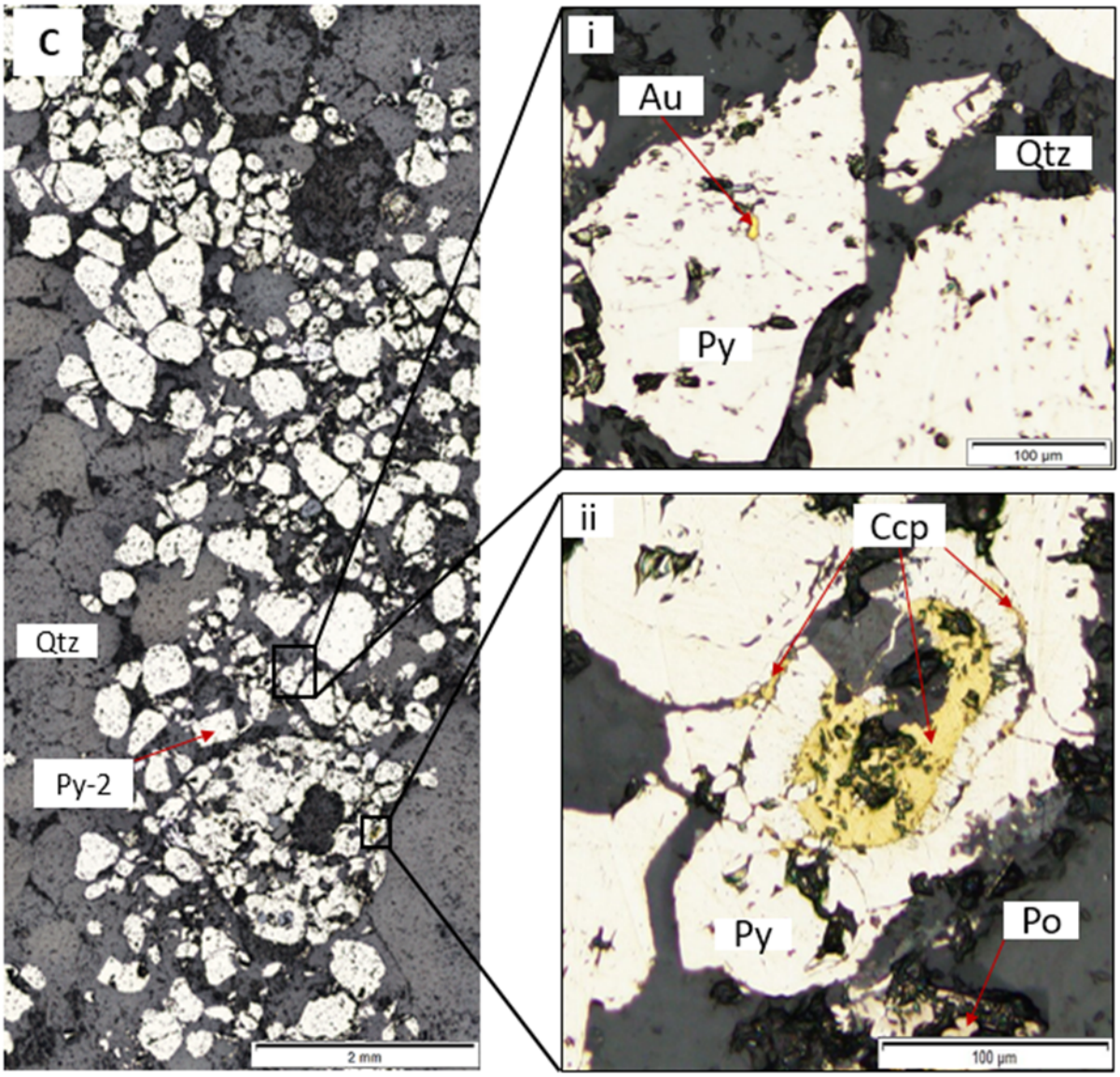

Figure 17: Reflected light photomicrographs of Elsburg reefs ore showing quartz (Qtz), pyrite (Py) and pyrrhotite (Po) as major host minerals for gold (Au). Elsburg Conglomerate Top (ECT) bed with subhedral porous and inclusion-rich pyrite is shown in A. Irregular shaped gold is also found at the edges and fractures of the pyrite grains. In B, Modderfontein Intermediate Top (MIT) bed with subhedral pyrite, pyrrhotite and quartz associated with gold. C: Mineralisation from MIT bed. C(i) an inclusion of gold hosted in subhedral porous pyrite. C(ii) Chalcopyrite (Ccp) filling gaps between pyrite grains. Py–1 = fractured pyrite and Py-2 = euhedral pyrite.

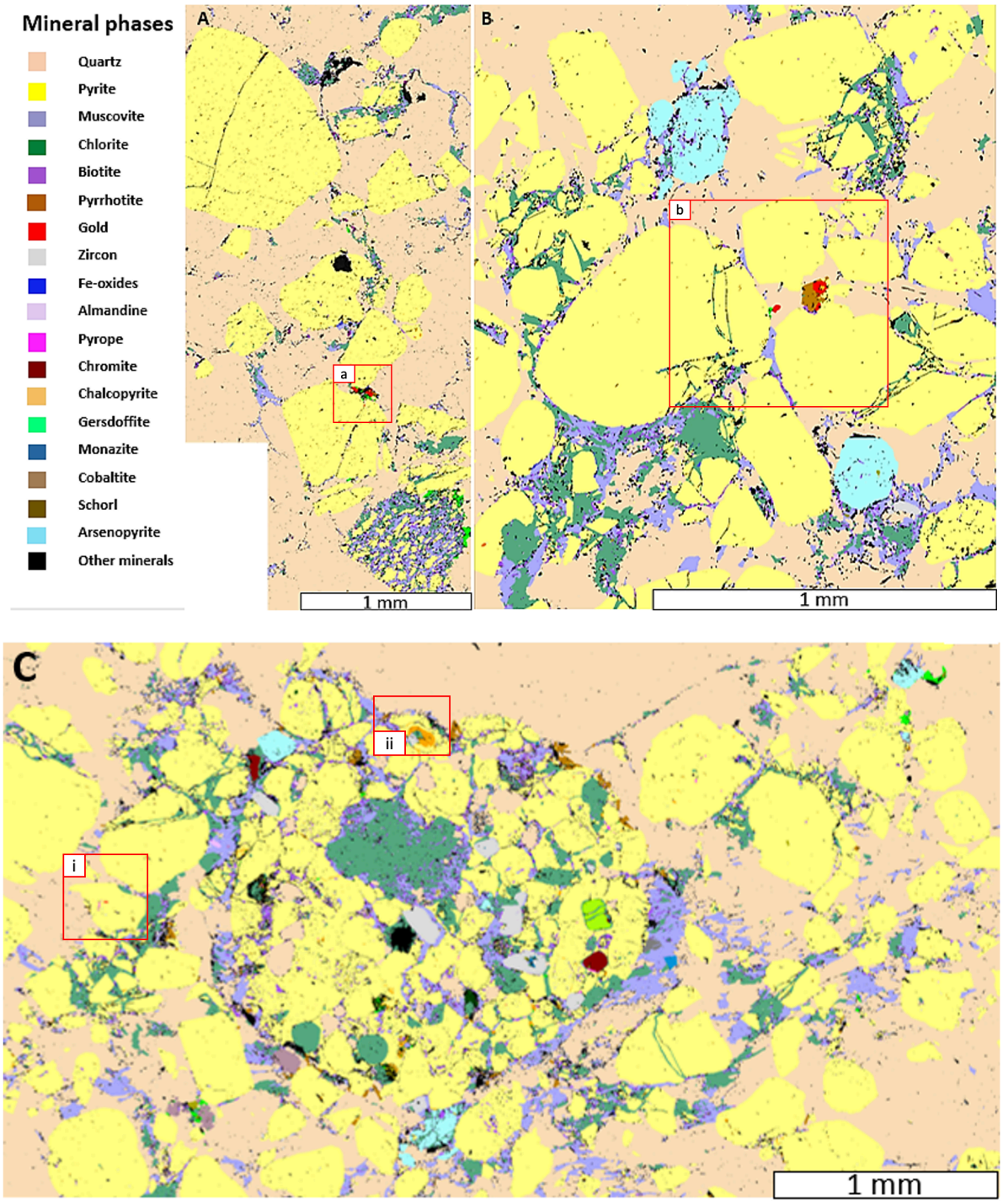

Figure 18: Mineral phases of the Elsburg reefs, specifically the Elsburg Conglomerate Top (ECT) and Modderfontein Intermediate Top (MIT) beds, as determined via TIMA. Both ore portion of the conglomerate beds are dominated by subangular to subrounded quartz and pyrite grains. (A): ECT bed showing subrounded pyrite and quartz grains with mica, chlorite and gold. (B) MIT bed showing sub-rounded pyrite, arsenopyrite, chlorite and gold (at the edges of pyrite, pyrrhotite and quartz). (C) MIT bed showing chalcopyrite, pyrrhotite, chromite, chlorite and mica minerals. Porous pyrite grains host

gold and invisible gold is hosted in arsenopyrite. The small red squares are comparable to zoomed portions of Fig. 17A, B and C.

5.1.1 Mineral associations with gold

Leaching investigations require a thorough understanding of gold association with other mineral phases or gangue minerals, as these minerals can react with leaching reagents, slowing the leaching rate and resulting in low recoveries (Petersen, 2016; Tanda et al., 2017). TIMA is used to determine the mineralogical relationships with gold. Electrum (i.e., weishanite [$(Au, Ag)_3Hg_2$]) and native gold are the most common forms of gold found in Elsburg reefs. There are a lot of variations in gold mineral associations because analysed thin sections were made from different grab samples (i.e., ECT and MIT) and specific portions of thin sections (i.e., ECT 1 from ECT_FTS; MIT_7W_1 and MIT_7W_2 from MIT_FTS). According to TIMA, most of the gold (>56 wt.%) is associated with sulphide minerals (i.e., pyrite, pyrrhotite, chalcopyrite, gersdorffite, and minor galena, cobaltite and sphalerite), quartz (24 wt.%), and other minerals (> 20 wt.%) such as such as chlorite, zircon, columbite, wolframite and almandine (Fig. 19). The weigh percentages (wt.%) were averaged.

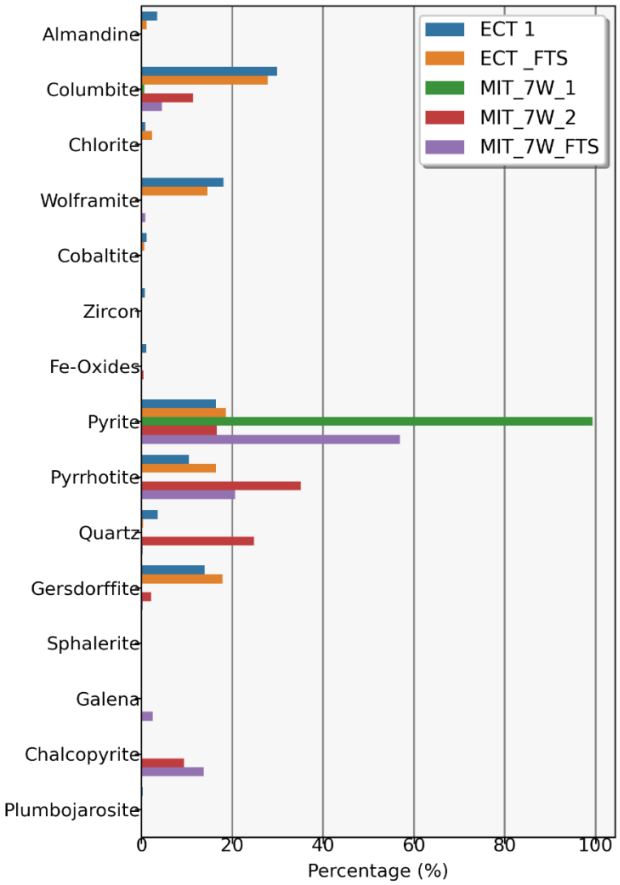

Figure 19: Mineralogical association of gold with other mineral phases from the Modderfontein Intermediate Top (MIT) and Elsburg Conglomerate Top (ECT) beds as measured using TIMA. ECT 1

is a selected portion of a thin section (ECT_FTS); MIT_7W_1 and MIT_7W_2 are selected small portions of thin section (MIT_7W_FTS). In MIT_7W_1, gold is associated with pyrite and columbite only. FTS = full thin section. ECT_1 and FTS comes from ECT001 and all MIT_7W samples are coming from MIT003.

5.1.2 Liberation and locking of gold

The most essential mineral characterization variable in gold leaching is liberation and/or locking of gold in gangue minerals. To dissolve gold, a grain must be fully or partially exposed to a leaching reagent such as glycine. In this study, the term "free surface" refers to gold that has been emancipated from its host material or associated with matrix. According to TIMA, the majority of gold in the Elsburg reefs is enclosed in sulphide minerals (largely pyrite), quartz and other minor minerals. The results indicate that around 62% of gold is locked in quartz, nearly 30% of gold is locked in pyrite, and the remaining 8% gold is confined to various groups of minerals (see ECT_FTS in Fig. 20). Thus, there is no liberated god. In the MIT bed, more gold is trapped in sulphide minerals (i.e., pyrite ~57%, pyrrhotite ~ 21% and chalcopyrite ~ 15%), while the rest of the gold (~7%) is locked in different groups of minerals, with only 2% of gold in the free surface, as illustrated in Fig. 20 (MIT_7W_FTS) below. Selected portions of thin sections (i.e., ECT_1, ECT_2, MIT_7W_1 and MIT_7W_2) shows that most of the gold in the samples is enclosed in sulphide minerals and quartz (>80%). Other minerals such as zircon and oxides host very small amounts of gold (<20%). The small percentages (<2%) of gold in free surface suggest that gold in studied ore samples is not liberated.

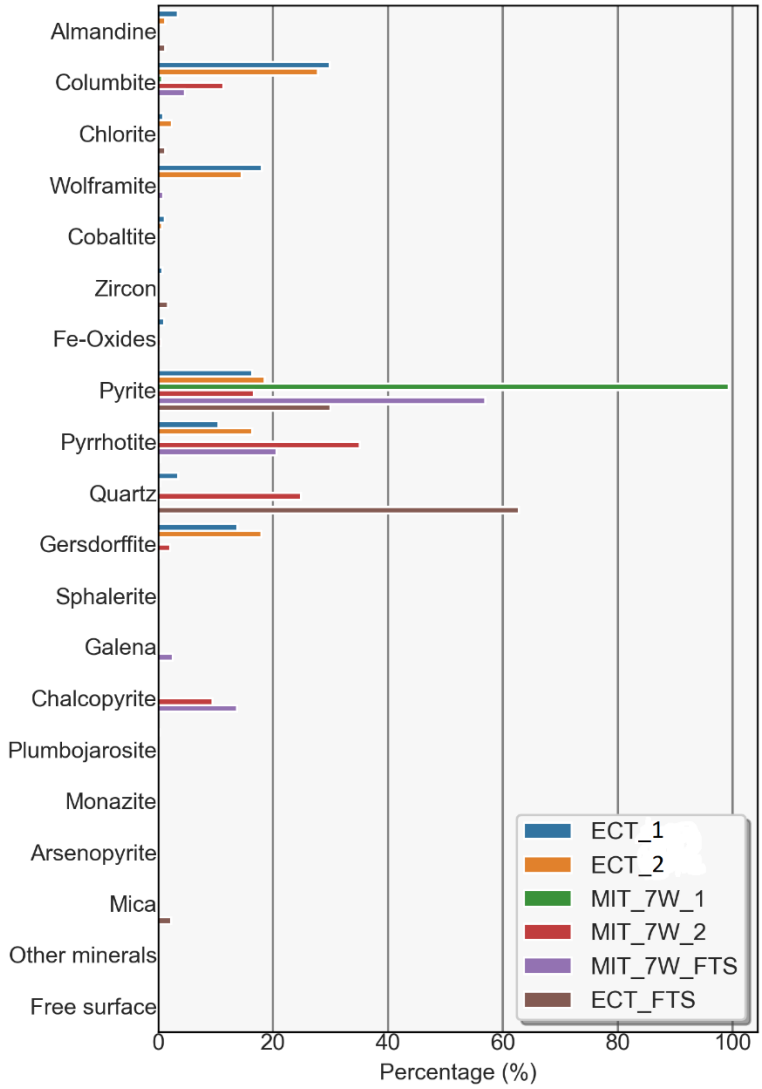

Figure 20: Mineral phases locking gold particles from Modderfontein Intermediate Top (ECT) and Elsburg Conglomerate Top (ECT) bands as determined using TIMA. ECT_1 and ECT_2 are small selected portions of ECT thin section (ECT_FTS); MIT_7W_1 and MIT_7W_2 are selected small portions of MIT thin section (MIT_7W_FTS). In MIT_7W_1, gold is locked in pyrite and columbite only. FTS = full thin section. ECT_1, ECT_2 and ECT_FTS are from ECT001 and all MIT_7W are coming from MIT003.

5.2 Lithogeochemistry

The major element chemical compositions (expressed in oxides) from the Elsburg reefs are presented in Table 4. The rocks (studied ore samples) are very rich in silica, iron and aluminium oxides and depleted in most of other oxides such as sodium, manganese and nickel oxide. Chemical cross-plots give a good indication of geochemical variation between different major oxides (Fig. 21). The compositional variations appear to reflect mineralogical variations within the reefs (between MIT and

ECT beds). Common minerals in this reefs includes quartz, pyrite, mica (muscovite and biotite), chlorite and other minor minerals such as uraniferous minerals and other sulphides. Only the most abundant minerals are reflected in the abundance of major elements, and minor minerals are chiefly reflected in the abundance of trace elements, for example, the high concentrations of Zr, U, Cr, Pb and Zn are due to presence of minerals such as zircon, chromite, uraniferous minerals and sulphide minerals such as galena and sphalerite, respectively.

Table 4: Major elements concentrations of samples from the Elsburg reefs in weight percent (wt.%). MIT01, MIT02 and MIT03 are from blended MIT001, MIT003, and MIT003 beds. MIT04, MIT05 and MIT06 comes from MIT003 bed. ECT01, ECT02, ECT03 and ECT04 are all from ECT001 chip samples (Fig. 15).

wt.%	MIT01	MIT02	MIT03	MIT04	MIT05	MIT06	ECT01	ECT02	ECT03	ECT04
SiO_2	92.46	89.5	90.84	95.29	85.15	90.58	96.43	95.33	96.31	96.24
Al_2O_3	0.81	0.91	1.68	0.78	1.27	1.06	0.64	0.82	0.56	0.58
Fe_2O_3	3.99	5.62	3.78	1.53	8.18	4.83	0.98	1.72	1.71	1.56
MnO	0.01	0.01	0.01	0.01	0.02	0.02	0.01	0.01	0.01	0.01
MgO	0.17	0.05	0.24	0.33	0.23	0.27	0.21	0.12	0.12	0.12
CaO	0.05	0.03	0.05	0.03	0.05	0.04	0.06	0.04	0.04	0.03
Na_2O	0	0.01	0.01	0.02	0.02	0.01	0	0	0	0
K_2O	0.1	0.2	0.38	0.06	0.21	0.16	0.1	0.06	0.04	0.04
TiO_2	0.05	0.05	0.05	0.04	0.05	0.04	0.03	0.03	0.04	0.03
P_2O_5	0.03	0.02	0.02	0.02	0.03	0.02	0.02	0.02	0.02	0.02
Cr_2O_3	0.05	0.02	0.02	0.02	0.03	0.02	0.01	0.01	0.01	0.01
NiO	0.02	0.01	0.01	0	0.02	0.01	0	0.01	0	0

5.2.1 Major Elements

Chemical data for major element oxides from analysed Elsburg reefs samples shows that:

- High SiO_2 content in the ore is due to the presence of silicate minerals (e.g., quartz). All samples have SiO_2 concentrations ranging between 85.15 - 96.31 wt.%, and averages of 90.63 and 96.07 wt.% in the MIT and ECT band, respectively. SiO_2 and Al_2O_3 have a negative correlation (Fig. 21), which reflects high quartz content relative to Al-bearing minerals such as muscovite in Elsburg reefs.
- Samples from the MIT bed have higher Fe_2O_3 content, ranging between 1.53 – 8.18 wt.%, and average of 4.66 wt.%, while samples from the ECT bed have 0.98 – 1.72 wt.% and averaging to 1.49 wt.%. This due to high concentration of Fe–bearing minerals such as hematite/magnetite and

Fe-bearing sulphides such as pyrrhotite and pyrite. Positive correlation between Fe_2O_3 and MgO with Al_2O_3 (Fig. 21) is most likely to be as results of high chlorite concentrations in Elsburg reefs.

- MIT bed samples have a high Al_2O_3 content, averaging to 1.09 wt.%, relative to ECT bed samples which averaging to 0.65 wt.%.
- A good correlation of K_2O and CaO with Al_2O_3 (Fig. 21) is due to presence of mica group minerals and minor feldspars (< 0.01wt.%).
- The correlation between TiO_2 and Al_2O_3 (Fig. 21) is due to the Fe-Ti oxides present in the samples.
- TiO_2, K_2O and CaO also represent major oxides, while Na_2O, MgO, P_2O_5 and MnO_2 occur in minor amounts, at generally less than 0.3 wt.%.
- The relatively high Fe_2O_3, MgO and K_2O contents in Elsburg reefs samples is attributed to the abundance of micas and other Fe-Mg bearing minerals.

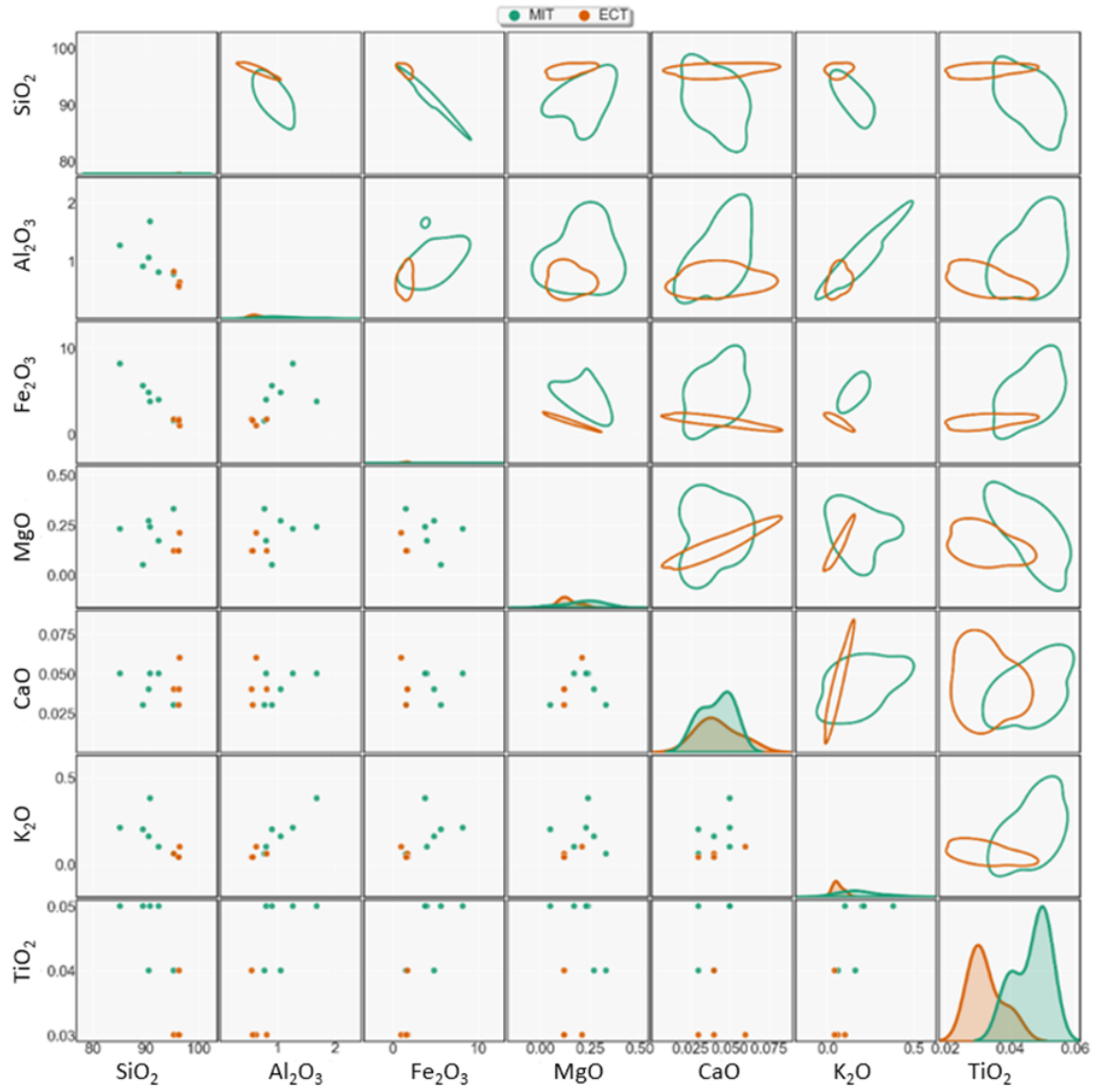

Figure 21: Bivariate plots of major elements oxides of Elsburg reefs samples (Modderfontein Intermediate Top (MIT) and Elsburg Conglomerate Top (ECT) beds) in the Witwatersrand Basin.

5.2.2 Trace Elements

The mineralogical and chemical compositions of clastic sedimentary rocks such as sandstones and conglomerates are the products of numerous variables that include provenance, weathering conditions, transport, diagenesis, climate and tectonism. In geochemical studies, some selected major oxides, especially TiO_2 and trace elements like La, Y, Sc, Cr, Th, Zr and Nb, are sensitive indicators of the source rocks, provenance, paleo-weathering and tectonic setting (McLennan et al., 1980; McLennan, 2001). This is as a result of their relatively low mobility and insolubility during the aforementioned sedimentary and post-sedimentary processes. The entrainment of minerals like zircon and monazite attributes to high concentrations of trace elements like the high field strength elements (HFSE) and light rare earth elements (LREE). Trace elements related with zircon includes Zr and Hf, while monazite is commonly associated with Th and LREE enrichment. The entrainment of some phases from the source is further demonstrated by the trace element pattern or concentrations in Table 5.

Table 5: Trace elements concentrations from samples taken from Elsburg reefs. All elemental concentrations are given in ppm. Dl = below detection limit. MIT04, MIT05 and MIT06 are from the MIT003 bed. ECT01, ECT02, ECT03 and ECT04 are all from ECT001 chip samples (Fig. 15).

PPM	MIT01	MIT02	MIT03	MIT04	MIT05	MIT06	ECT01	ECT02	ECT03	ECT04
Sc	1.39	2.33	1.2	2.29	2.64	3.12	dl	2.22	0.02	1.2
V	4.14	9.82	18.03	5.39	5.56	6.3	6.16	10.12	6.12	2.86
Cr	244.58	133.3	118.41	104.18	237.16	145.78	48.37	79.05	74.51	63.59
Co	61.55	45.89	33.14	19.25	100.91	41.85	4.16	22.62	14.74	12.31
Ni	71.47	44.23	86.37	21.21	89.92	42.46	11.58	30.42	16.98	16.89
Cu	22.37	10.46	14.79	17.77	51.5	21.63	8.83	43.09	7.65	9.63
Zn	99.85	4.88	265.13	7.02	38.43	63	9.71	163.07	33.37	43
Ga	1.69	0.59	0.87	0.17	2.15	1.1	0.64	0.18	0.12	0.92
Rb	3.64	7.6	13.12	dl	6.06	3.82	2.95	1.79	1.04	0.8
Sr	4.16	3.88	2.78	1.13	5.05	2.73	1.99	4.51	2.87	2.75
Y	10.61	6.88	5.86	13.31	16.16	9.78	2.87	6.68	4.73	5.11
Zr	126.92	89.25	47.16	71.09	90.05	61.94	26.87	49.08	34.71	31.47
Nb	4.71	2.49	1.82	1.07	2.68	1.81	0.53	2.37	1.1	1.49
Mo	1.49	0.53	1.73	1.98	2.12	1.57	0.57	1.27	1.2	1.79
Ba	13.38	31.42	74.17	dl	5.56	9.34	4.38	9.11	5.88	3.29
Pb	116.31	17.74	21.18	21.82	390.79	147.36	11.6	138.27	56.45	59.1
Th	17.36	1.78	2.49	7.97	25.85	10.77	2.96	11.39	6.35	5.77
U	166.45	21.18	23.21	45.59	404.19	112.31	3.79	106.87	49.86	46.79

Au	1.07	1.025	0.98	7.825	14.67	43.16	1.98	1.74	1.5	1.62

5.2.2.1 Trace elements distribution:

The results of trace element concentrations and the distribution of the data from the different Elsburg reefs beds (MIT and ECT) are presented in a box and whisker plot (Fig. 22) and correlated using heat map (Fig. 23) and ternary diagrams (Fig. 24), respectively. The statistical distributions and means of trace elements for Elsburg reefs bands are illustrated in Fig. 22, with boxes representing the 25th (lower) and 75th (upper) quartiles/percentiles, and a line crossing through the box symbolizing the data mean or averages. The little dots or circle showing the outliers, while the whiskers illustrate the minimum and maximum data values. The following are trace elements with relatively high concentrations: U (<3.79 - 404.19 ppm), Pb (<11.6 - 390.79 ppm), Cr (<48.37 – 244.58 ppm), Zn (<4.88 -125.13 ppm), Co (<4.16- 100.91 ppm), Ni (<11.58 – 89.92), Cu (<7.65 – 51.5 ppm) and Au (0.98 – 43.16 ppm). The MIT and ECT beds appear to have a highly similar lithochemistry, despite the slight differences in concentrations of certain elements. When compared to the ECT bed, the MIT bed appears to contain higher concentrations of every trace element, including gold. For example, the ECT bed shows moderate to low concentrations of U (<3.79 – 106.87 ppm), Cu (7.65 – 43.08 ppm) and Au (1.5 – 1.98 ppm), whereas the MIT bed has higher concentration ranges of U (21.18- 404.19 ppm), Cu (<10.46 – 51.5 ppm) and Au (0.98 – 43.16 ppm). A complete dataset for this can be seen in Table 5.

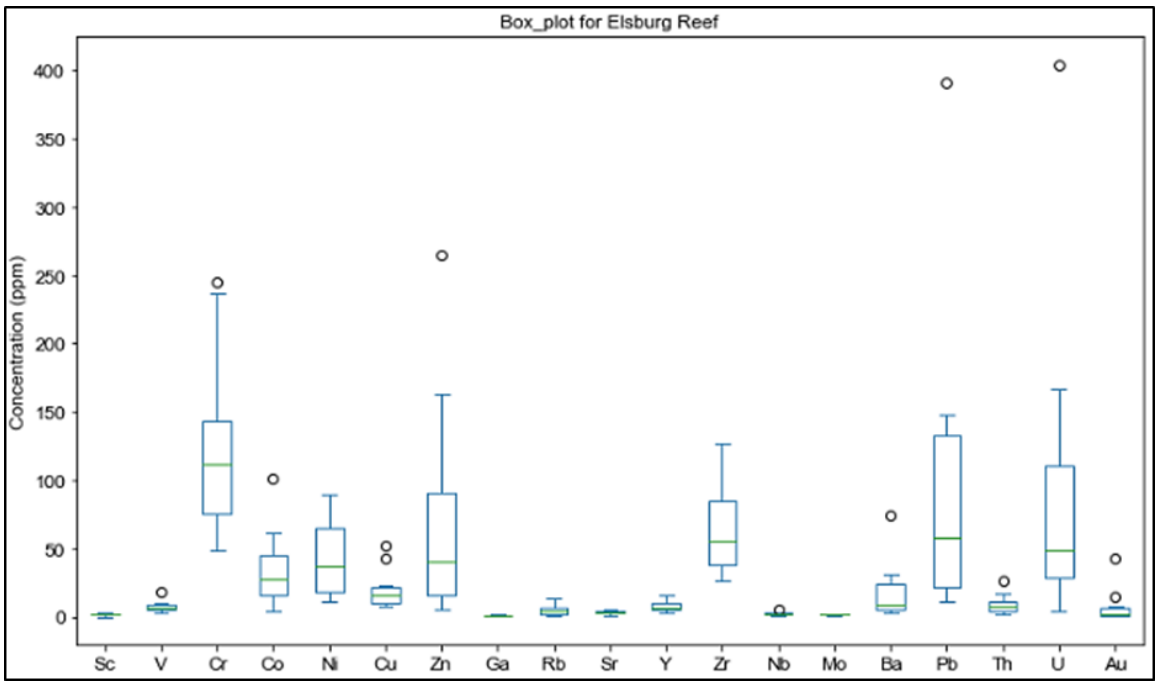

Figure 22: Trace element concentrations plotted as a box and whisker plot for Elsburg reefs ore samples. The 25th to 75th quantiles are delineated by boxes, with whiskers extending to the minimum and maximum. Small circles correspond to outliers.

5.2.2.2 Trace elements correlation with gold:

Trace elements data analysis is important for establishing correlations between elements such as Rb, Sr, K, Mn, and others, which are possibly associated with hydrothermal modifications of host rocks, as well as those (e.g., Au, Cu, Fe, S, As, Ag) involved in the composition of primary and secondary ore minerals in the deposit. Most importantly, these data aid in establishing the relationship between Au and metals (such as Cu, Ni, Zn and others) that influence gold extraction from the ore by leaching. The correlation matrix denotes several well-defined to weak correlations between elements such as Au-Sc, Au-U, Au-Th, Au-Cu, Au-Pb, Au-Co, Au-Ga, Au-Cr, Au-Mo among others (see Elsburg reefs correlation heat map in Fig. 23). Ni and Zr have a reasonable positive relationship with Au. All trace elements have a positive correlation with gold except for Zn, V, Rb, Nb and Ba that show a moderate to poor negative correlation with gold (Fig. 23). Trace elements with high positive correlation coefficient amongst themselves and gold as well as those implicated in the composition of ore minerals and mineral associations in the deposit are given special consideration in the interpretation of results.

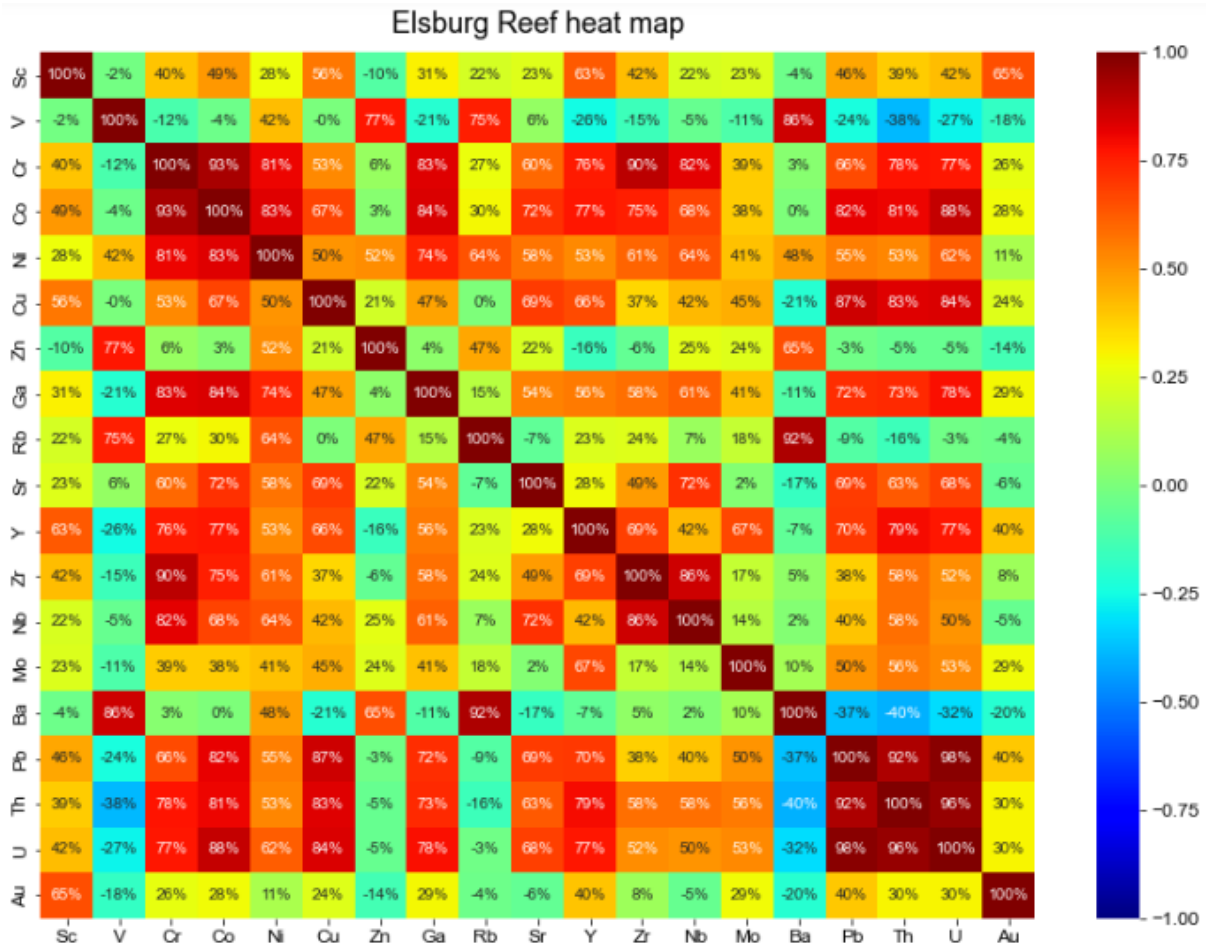

Figure 23: Heat map correlating trace elements with gold.

The geochemical results suggest that the sampled ore has high levels of uranium, thorium, and transition metals like Cu, Ni, Zn, Cr and Co (see Table 5 for specific concentrations). The association between these metals and gold is depicted in the ternary charts below (Fig. 24). It is apparent that gold occurs in conjunction with minerals containing U, Cr and sulphide metals (Cu, Ni, Zn and Co).

The correlation ternary plot (V – Cr – Au; Fig. 24) reveals that Cr and Au have substantial correlations, whereas V and Au have an adverse correlation. In contrast to Th, the relationship between U and Au is quite strong. The correlation between gold and all sulphide metals (Ni, Co, Cu and Zn) is moderate to strong. The negative correlation between V and Au indicates that the samples are non-uniform, with elements occurring independent to one another. Figure 23 depicts the overall correlation characteristic of Au with the rest of the trace elements, whereas Fig. 24 depicts the relationship between Au and some of the transition metals that are thought to be problematic in hydrometallurgical gold extraction. Elsburg reefs ore mineralogy results in a moderate to high correlation coefficients between the elements Au, U, Cu, Ni and Cu as well as a negative correlation of Au with Zn.

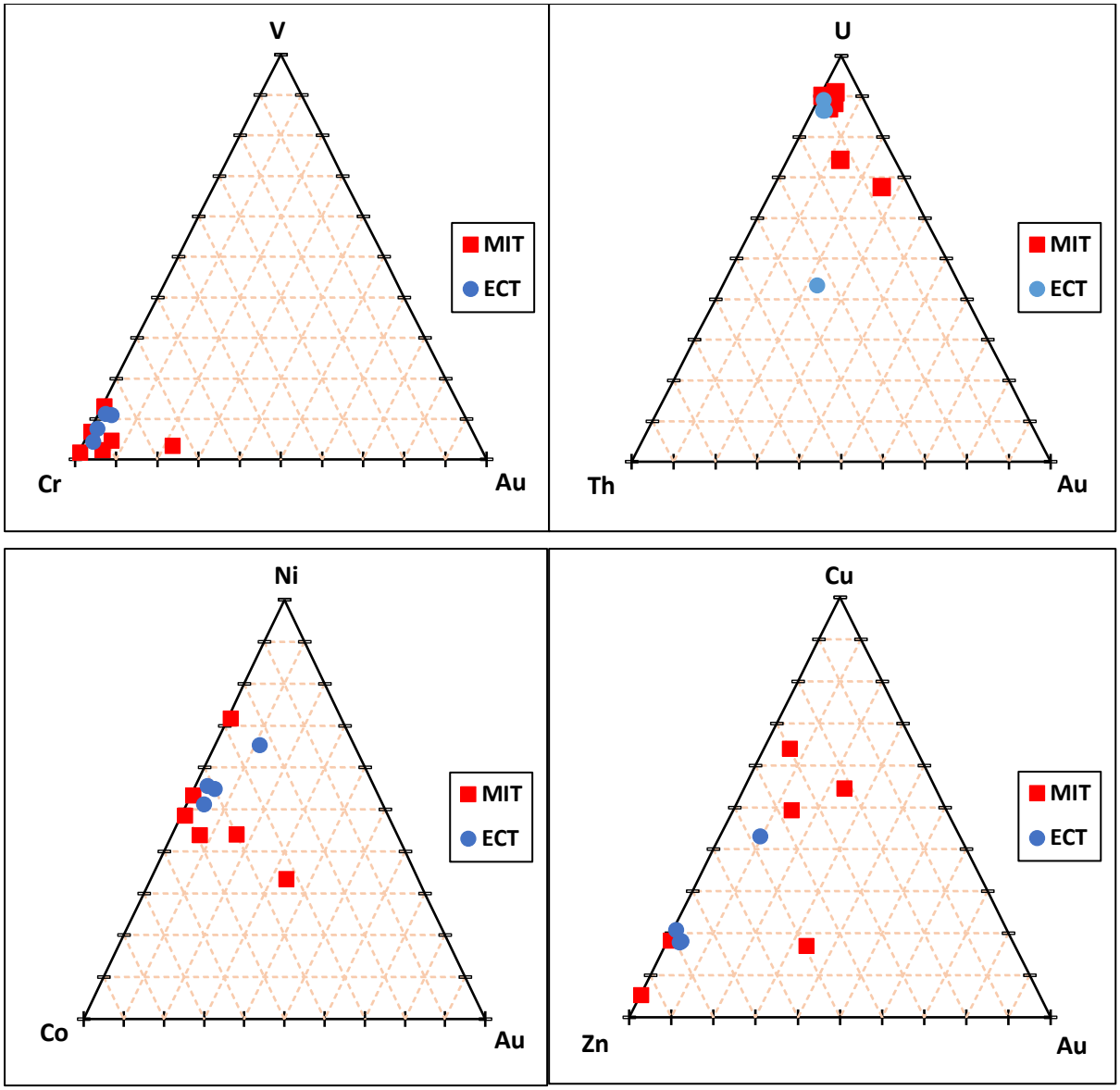

Figure 24: Ternary plots showing correlation between selected trace elements and gold from Modderfontein Intermediate Top (MIT) and Elsburg Conglomerate Top (ECT) bands.

5.3 Gold Glycine leaching experiments

In order to evaluate the processing behaviour of the Elsburg reefs gold ores, six experiments were conducted. To optimise gold recovery from the Elsburg reefs gold ore, bottle roll leaching with glycine as the principal reagent and potassium permanganate as the oxidant was utilized. The effects of glycine concentration, recharge and leaching duration on gold recovery are evaluated in experiments 1 and 2. The findings indicate that by applying 1500 ppm glycine and recharging twice, only up to 35% gold recovery can be accomplished in 34 hours (Fig. 25; BR300 – BR1500A). Figure 25 BR1500B illustrates that using 1500 ppm glycine, charging three times and extending the leaching time to 50 hours can result in a better gold recovery of 41%.

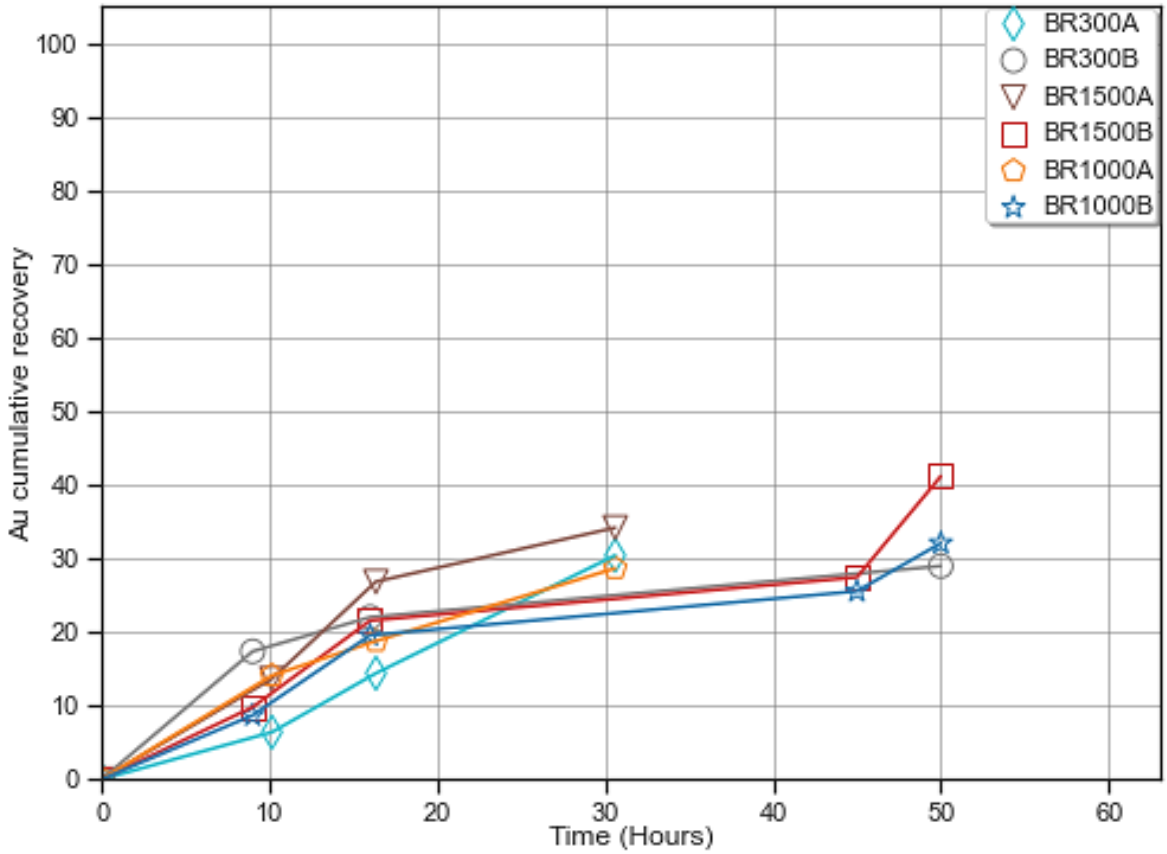

Figure 25: Bottle roll leaching using glycine in Elsburg reefs gold ore from the Witwatersrand Basin. Leaching parameter: 20% solids, 70% distilled water, 300, 1000, and 1500 ppm glycine concentration, potassium permanganate concentration = 2 times glycine concentrations at room temperature. A: Experiment 1 was recharged two times with a leaching duration of 34 hours, while B: Experiment 2 was recharged three times with a leaching duration of 50 hours. BR300A = bottle roll experiment 1 with 300 ppm glycine concentration, BR1000A = bottle roll experiment 1 with 1000 ppm glycine concentration, and BR1500A = bottle roll experiment 1 with 1500 ppm glycine concentration. BR300B = bottle roll experiment 1 with 300 ppm glycine concentration, BR1000B = bottle roll experiment 2 with 1000 ppm glycine concentration, and BR1500B = bottle roll experiment 2 with 1500 ppm glycine concentration.

Experiments 3 and 4 show that using a high glycine concentration (4500 ppm) without recharging can result in poor recovery. In experiments 3 and 4 only 29.68% and 36.58% of gold were dissolved from the ore as shown in Fig. 26; these recoveries are low compared to experiment 2 gold recovery. This emphasizes the significance of recharging and recycling glycine-leaching solutions. A slurry with low density in experiment 3 displays poor gold recovery compared to a higher slurry density in experiment 4 (Fig. 26). This shows that Elsburg reefs ore responds better to gold glycine leaching when 30% solids and 70% liquid are being used.

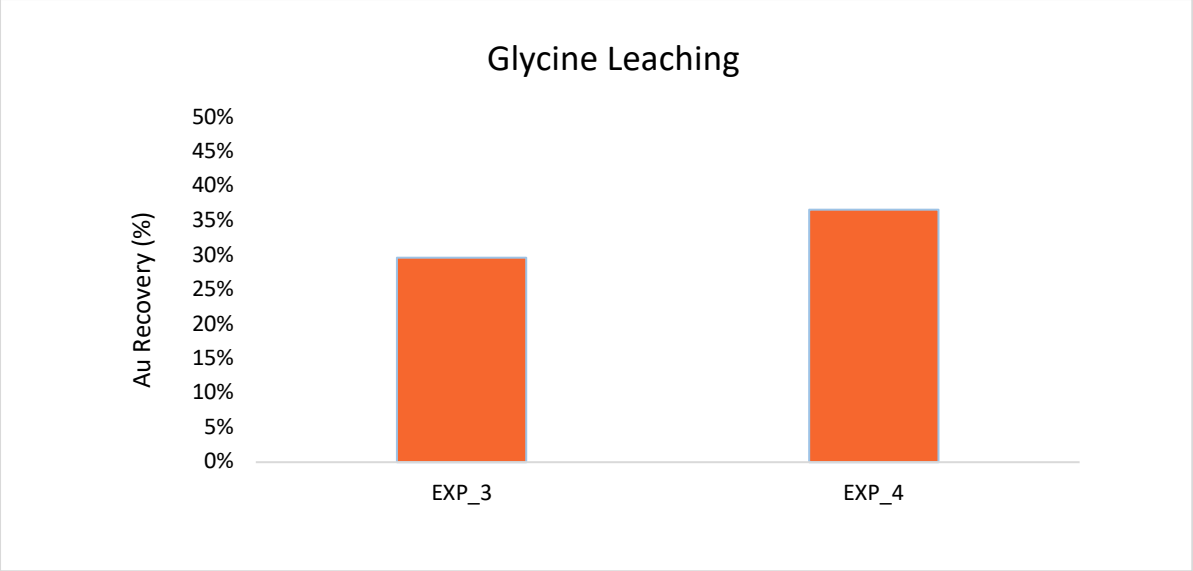

Figure 26: Bar graphs showing gold recoveries between low-density slurry in experiment 3 (EXP_3) and high-density slurry in experiment 4 (EXP_4) under the same leaching conditions (i.e., at 4500 ppm glycine, 9000 ppm $KMnO_4$ and at room temperature).

The most crucial test run in this study is experiment 5. Figure 27 depicts the outcomes of this experiment. The results of the experiment reveal that samples from the Elsburg reefs gold ore responds well to glycine leaching; however, gold recoveries vary depending on temperature, pH and the amount of dissolved oxygen (DO) in the solution. Gold recoveries range from 75 to 86% in the first five sub-experiments (experiments 5-1 to 5-5). Sub-experiment 5-6 is an outlier since it has the lowest gold recovery (58%) of all the experiments (Fig. 27). The exceptional low gold recovery in sub-experiment 5-6 could be due to a slight change in one of the leaching parameters such as glycine dosage, pH and dissolved oxygen.

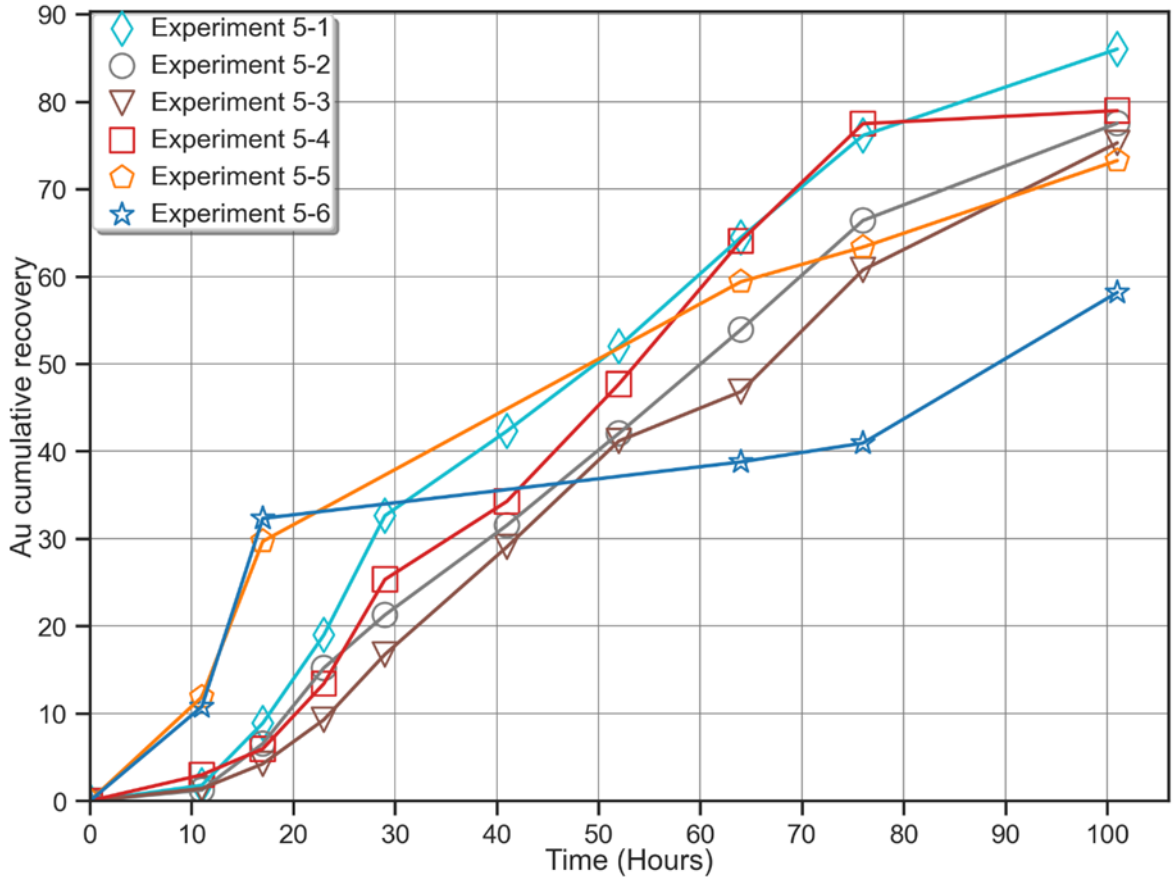

Figure 27: Glycine leaching experiment using Elsburg gold ore samples. Leaching parameters includes 1500 ppm glycine concentration, 3000 ppm $KMnO_4$, initial pH values of 10.55 ± 0.5, final pH of 9.65 ± 0.5, average DO (%) = 57% and DO (mg/l) = 3.801 at room temperature (~19.35°C).

The relationship between cumulative gold recoveries, pH value, dissolved oxygen (mg/l) and temperature (°C) is shown in Fig. 28 below with leaching duration fixed at 101 hours. All these variables are important in glycine leaching for gold recovery. At the beginning of the leaching process, all pH values were set as close to 10.5 as possible. This was done to maintain an alkaline condition of glycine leaching solution and stimulate the glycine-gold reaction in the slurry. The pH of the slurry declines to between 9.0 and 9.4 after ten hours of leaching (Fig. 28), then rises to 9.65 as the slurry is recharged (i.e., calcium hydroxide, potassium permanganate and glycine are added) at different time intervals. The dissolved oxygen levels in the first four studies (sub-experiments 5-1 to 5-4) follow a similar trend, beginning around zero, increasing, and stabilizing at ~4.5 mg/l. Sub-experiments 5-5 and 5-6 shows unstable dissolved oxygen patterns with final average of ~4.0 mg/l. The average dissolved oxygen (mg/l) value in experiment 5-6 is the lowest and fluctuates more than all of the other trials. Consequently, cumulative gold recovery in sub-experiment 5-6 is exceptionally low (58%), and the pattern differs from that of the other experiment trails (Figs. 27 and 28). The reaction rates between

gold and glycine were slow in all of these experiments (sub-experiments 5-1 to 5-6) since they were conducted on cold and rainy days with an average temperature of 19.35°C.

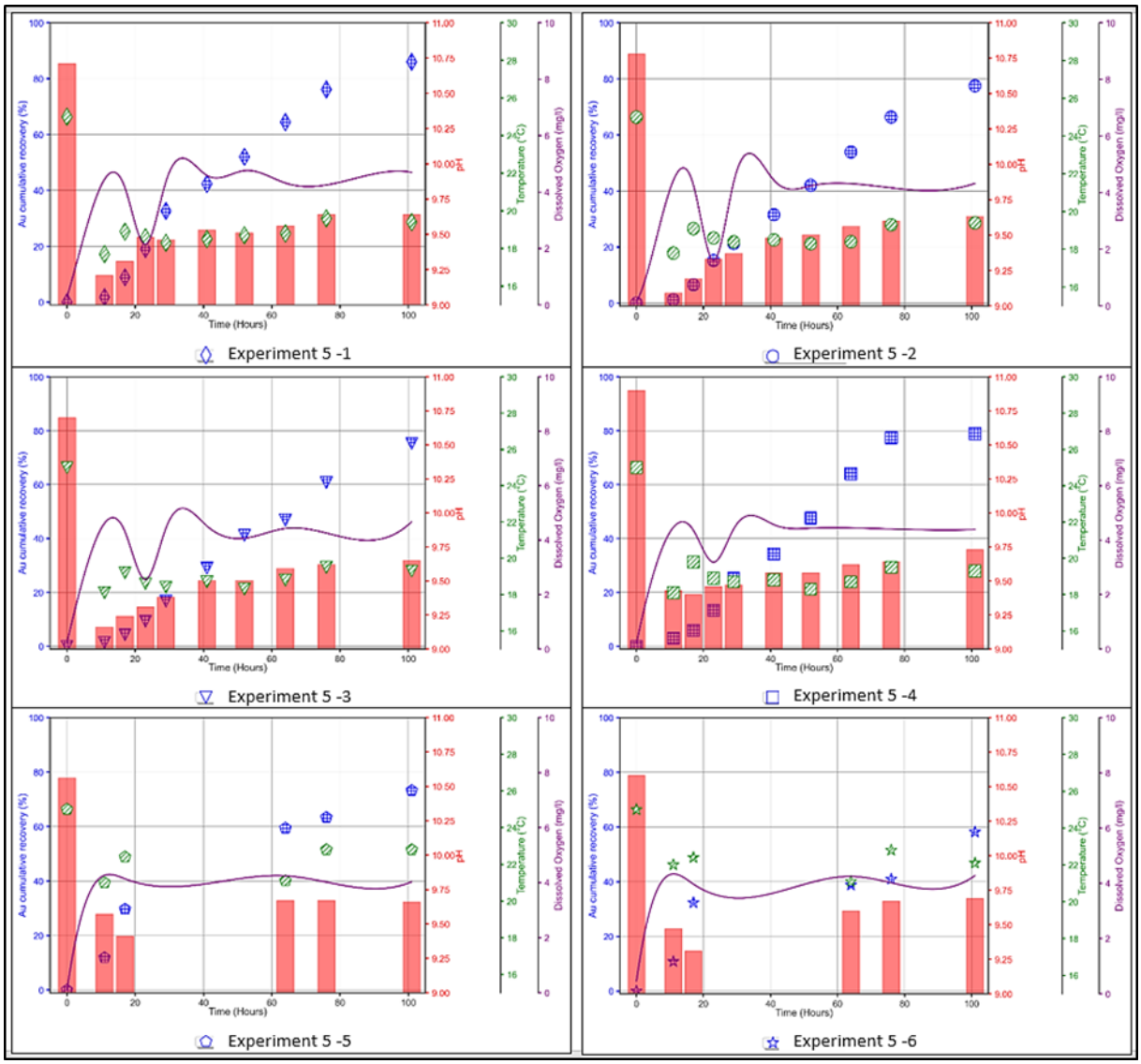

Figure 28: Graphs showing relationship between gold cumulative recoveries (blue) and different leaching parameters (i.e., dissolved oxygen (DO (mg/l), purple line), temperature (°C, green) and pH values, reddish orange).

The data from experiment 5 was used to estimate how long it would take to extract 100% gold from the Witwatersrand (Elsburg reefs) gold ore using glycine leaching at room temperature. The model (Fig. 29) demonstrates that after 220 hours of glycine leaching, 100% gold recovery from Elsburg reefs ore may be accomplished using the same parameters as in experiment 5. (Experimental data; Fig. 29). The upper (red line) and lower (blue line) standard deviations (SD) show that after 180 and 140 hours of leaching, 100% gold recovery is possible.

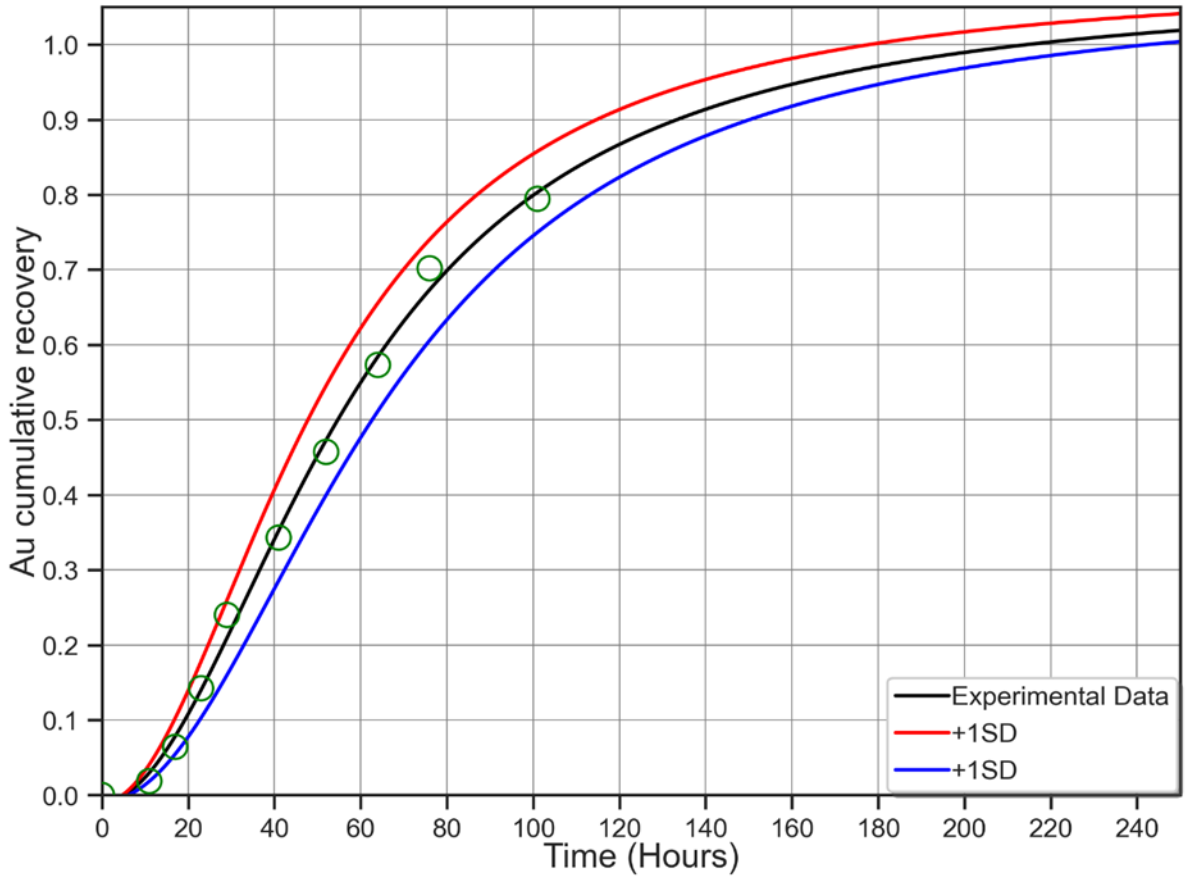

Figure 29: Model suggesting the time at which 100% recovery can be achieved using 1500 ppm glycine concentration at room temperature.

The outcomes of the experimental data presented here suggests that solution recharging and recycling, glycine concentration and leaching time all play a significant role in the extraction of gold from the feed ore through leaching. Experiment 6 has been carried out to see how temperature affects gold dissolution. Figure 30 presents the outcomes of this trial, which reveals that the effect of temperature is more important in terms of gold dissolution kinetics. Temperatures of 35 to 40°C, a glycine concentration of 4500 ppm, and agitation at 800 rpm for 48 hours yields the greatest gold recovery (88 and 95%), with average recoveries of 79.80 and 78.27% for A and B, respectively. This shows how temperature affects gold dissolution in alkaline glycine solution.

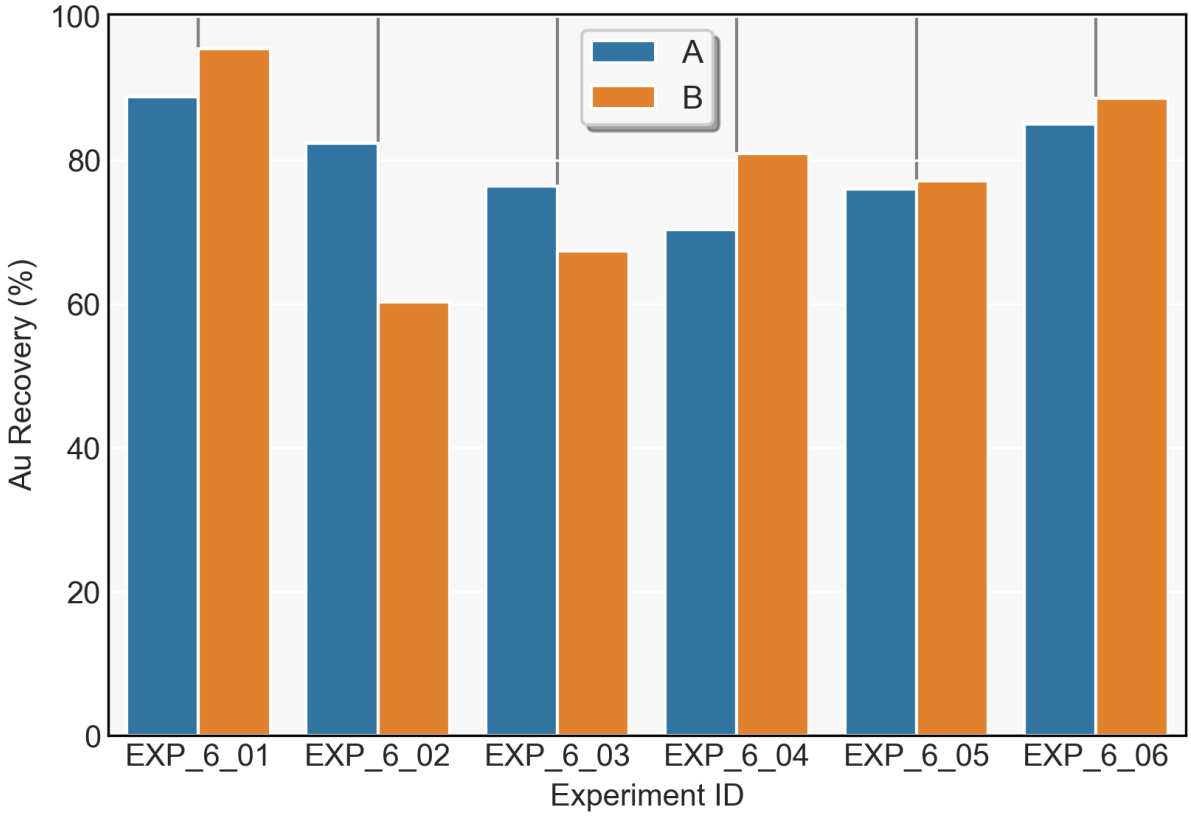

Figure 30: Bar graph showing the gold recoveries from glycine leaching, using 4500 ppm glycine concentration at T = 35 – 45°C and grind to approximately 80% of particles size passing 75 µm sieving screen.

CHAPTER 6: DISCUSSION

The results of the previous chapter's mineralogical characterization, geochemistry and gold extraction using glycine from Elsburg reefs ore are discussed in this chapter.

6.1 A mineralogical perspective on gold extraction in Elsburg reefs

Gold in Witwatersrand Basin is mostly found in interstitial spaces within conglomerate matrixes (Mngoma, 2012; Tucker and Viljoen, 2016; da Costa et al., 2020; Nwaila et al., 2020). This indicates that gold will be located in places that are delicate (i.e., easily breakable) during ore comminution (crushing and milling) and will be conveniently dissolved during glycine leaching. The mineralogical and textural composition of each ore, on the other hand, varies. The gold leaching process is extremely reliant on the mineral properties of a particular reef (Marsden and House, 2006). Pure gold on the edges of pyrite crystals tend to dissolve easy during leaching process as compared to invisible gold that is usually hosted in arsenopyrite. The results using both the optical microscope (Fig. 17) and TIMA (Fig. 18) shows that the Elsburg reef gold ore is dominated by quartz, pyrite, chalcopyrite, pyrrhotite and other sulphide minerals such as galena, heavy minerals such as rutile, zircon, and alteration minerals such as chlorite. Most of the gold in the reef is associated with quartz and sulphide minerals (Fig. 19). In Elsburg reefs, the most typical gold type is electrum gold. Furthermore, visible gold in Elsburg reefs generally occurs at the edges of mineral grains (Fig. 17A), with some small amount of gold being enclosed in host minerals (Fig. 17C). However, TIMA estimated the averaged locked gold in different host minerals to be more than 97% and liberated gold to be less than 3% (Fig. 20).
The Witwatersrand Basin has three different forms of pyrite: 1) porous pyrite, 2) compact pyrite, and 3) hydrothermal pyrite (England et al., 2002; Koglin et al., 2010 and Agangi et al., 2013, Costa et al., 2020). In Elsburg reefs, porous pyrite comes in a variety of grain sizes ranging from 0.1 to 2 mm (Fig. 17). As a result of the remobilization-induced reworking, the morphology of porous pyrite, also defined as ‘concretionary pyrite’, is often subrounded to rounded and inclusion-rich (Fig. 17). Micro-inclusions contain sulphides and mica-group minerals, indicating that concretionary pyrite is syn-sedimentary. Sub-rounded, inclusion-rich porous pyrite was found to be the most prevalent form in this investigation.

Compact detrital pyrite has a gain size similar to porous pyrite, with few to no inclusions and is usually subrounded to rounded in shape (Agangi et al., 2015; da Costa et al., 2020). Attrition during sediment transport is thought to have given the Witwatersrand Basin compact pyrite its roundness. Hydrothermal pyrites were generated through remobilization and re-crystallization of detrital pyrites caused by hydrothermal fluids, and it is euhedral in shape (Fig. 17).

The liberation features of the Elsburg reefs ores demonstrate that most of the gold is locked or hosted in sulphide minerals, silicate minerals (i.e., quartz) and at mineral boundaries (Figs. 17, 18 and 20). In this study, free surface refers to gold that has been released or liberated from its host material. Only a

small proportion of gold grains (less than 3%) were discovered to be affiliated with a free surface. There are three gold liberation types that have been observed in the samples of ore. These liberation types influence gold leaching performance differently (negative leaching influence ranging from low to high), namely: 1) gold grains on the surface of gangue mineral particles are accessible to the leaching solution (Fig. 17 A); 2) gold grains located inside the host mineral grain or in the boundaries of two minerals and linked to the surface by fractures or pores (Fig. 17 B); and 3) gold grains enclosed/locked in the gangue mineral particles and inaccessible to leaching solution until the host mineral is dissolved (Fig. 17 C(i)).

The influence of pyrite on gold leaching is determined by its form, concentration and distribution (Kianinia et al., 2018). Leaching rates are minimally altered when the gold-enriched ore contains less than 20% pyrite (Nwaila et al., 2014). Gold extraction rates are lowered to around 80% when pyrite concentration is greater than 20%, according to kinetic leaching studies (Guo et al., 2004). The shape and concentration of pyrrhotite also has a big impact on gold leaching effects. Pyrrhotite comes in two types, magnetic and non-magnetic pyrrhotite, both of which are troublesome in leaching when compared to pyrite. The oxygen consumer, magnetic pyrrhotite, is well recognized (Becker et al., 2010; Bunkholt and Kleiv, 2015). Oxidation and non-oxidation dissolution investigations of pyrrhotite revealed that oxidative dissolution produces acids whereas non-oxidative dissolution consumes acids (Thomas et al., 2000; Kim et al., 2021). During gold leaching, chalcopyrite ($CuFeS_2$) dissolves fast, generating stable copper which complexes with the leaching reagent. Copper dissolution should be avoided because it uses both leaching reagent (glycine) and oxygen. The negative effect of copper on gold dissolution can be avoided or reduced by adding fresh leaching solution with free glycine (i.e., recharging) to the reactor on a regular basis (Marsden and House, 2006).

The presence of porous inclusion-rich pyrite, pyrrhotite and chalcopyrite in studied ore samples will negatively affect glycine efficiency during leaching, resulting in slower extraction rates and poor gold recoveries. This is the case because sulphide minerals usually contain elements (e.g., Cu, Ni, Co, etc.) that competes with gold in dissolution stage during leaching process and consume lots of leaching chemicals.

6.2 Geochemistry perspective on gold extraction in the Elsburg reefs

The modal mineralogy of the investigated ore has a significant impact on major element oxide concentrations. Figure 21 depicts a graphical illustration of the correlation scatter-plots for selected oxides. High concentrations of SiO_2 confirm that quartz is the most dominant mineral in all samples. Fe_2O_3 is the second highest oxide which corresponds to sulphide minerals (e.g., pyrite, chalcopyrite). The negative correlations between SiO_2 and Fe_2O_3 reflect the heterogeneity of the sample sets, in which the elements (Fe and Si) occur independently. This means the higher the concentration of SiO_2 in a

sample, the lesser Fe_2O_3 concentration in a sample. The occurrence of mica and chlorite in the set of analysed samples is reflected in the noticeable positive correlation between MgO and Fe_2O_3 with Al_2O_3.

The overall relationship between Au and trace elements is shown in Fig. 23. A positive correlation exists between the elements such as U and Th, and transition metals (Cu, Co and Ni), which are typically associated with sulphide minerals. This relationship is attributed to the association of gold-bearing sulphide minerals with uraniferous minerals, as commonly observed in the Witwatersrand ores (Parnell and McCready, 2000; Pretorius and Wolf, 2012; Fuchs et al., 2021). Cu and Zn are chalcophile elements, while Au, Co and Ni are siderophile elements, U and Th are lithophile elements (Walters et al., 2021). Siderophile elements are high-density transition metals that have a strong affinity for metallic iron in either solid or molten form (Brenan et al., 2016). Metals and heavier non-metals that have a limited affinity for oxygen and prefer to combine with sulphur as very insoluble sulphides are known as chalcophile elements. Lithophile elements are silicate-loving and primarily comprise highly reactive metals. All of these elements have negative influence in gold glycine leaching process because they compete with gold during dissolution, and they consume a lot of leaching reagents.

The significant correlation between Co and Au (28%; Fig. 23) is attributed to the common mineral relationship between pyrite and cobaltite with gold, gold-containing minerals and gold inclusions in pyrite. The lack of correlation between Au and Zn reveals a spatial variation in the association between gold and sphalerite in the ore samples. Zn also has a negative association with Pb, indicating that galena and sphalerite occur as independent minerals. The occurrence of Cu, Ni and Pb-containing sulphides such as chalcopyrite, gersdorffite and galena in the ore samples is one factor for the strong to moderate positive correlation of these elements with Au.

The effects of transition metals as well as other elements such as U and Th on gold leaching has been reported (Tsezos et al., 1996; Rees and Van Deventer, 1999; Koç et al., 2014; Larrabure and Rodrguez-Reyes, 2021). Since minerals containing metals such as Cu, Co, Zn and Ni are thought to have detrimental impacts on gold cyanide leaching (Sayiner and Acarkan, 2014), it is anticipated that they will also affect gold glycine leaching in this study. The impact of these metals (Cu, Co, Zn, and Ni, etc.) on gold leaching recovery is mostly due to their solubility in leaching solutions, which results in a significant increase in the consumption of leaching reagents (glycine), due to the formation of metal-glycine complexes (Altinkaya et al., 2020). The type of host minerals determine the solubility of certain metals in leaching solution. Ag is one of the elements that competes with gold in the leaching process (Larrabure and Rodriguez-Reyes, 2021). As a result, various mineral impurities can be found in the leach solution after the ores have been leached. Ag and Ni dissolve as $Ag(C_2H_4NO_2)_2^-$ and $Ni(C_2H_4NO_2)_4^{2-}$ complexes in glycine leaching, which slows down the solubility of Au and affects the ability of glycine to form complexes with gold.

In mineral processing, copper minerals are divided into two categories: easily soluble copper (in cyanide/glycine solutions), which includes metallic copper, copper oxides and secondary copper sulphides; and insoluble copper (slowly dissolving in leaching solution), which mostly refers to primary copper sulphides (Koç et al., 2014). Copper can form three complexes ($Cu(C_2H_4NO_2)_2^-$, $Cu(C_2H_4NO_2)_3^{2-}$ and $Cu(C_2H_4NO_2)_4^{3-}$) in alkaline glycine solution during leaching (Hakimi and Aliabadi, 2012; Hassana et al., 2012). The $Cu(C_2H_4NO_2)_2^-$ complex forms much more quickly than the gold-glycine ($Au(C_2H_4NO_2)_2^-$) complex and uses up a lot of leaching chemicals, hence Cu is deemed the most problematic element in gold extraction (Jiang et al., 2001; Marsden and House, 2006; Lu and Xu, 2016). Both $Cu(C_2H_4NO_2)_3^{2-}$ and $Cu(C_2H_4NO_2)_4^{3-}$ complexes, on the other hand, form at a significantly slower rate than gold species and have little effect on gold dissolution (Hu, 2002; Dai and Breuer, 2009). The Cu-glycine complexes varies in response to the concentration of free glycine and the solution pH. The $Cu(C_2H_4NO_2)_2^-$ compound is formed when pH declines (Ceballos Quintana, 2014). In strong acid, Fe and Co dissolve as $Fe(C_2H_4NO_2)_6^{4-}$ and $Co(C_2H_4NO_2)_6^{3-}$ strong complexes, which have higher solubility than gold complexes (Marsden and House, 2006; Koç et al., 2014). Fe is unlikely to have a substantial impact on gold dissolution during glycine leaching because it was done in an alkaline solution where Fe has slow dissolution ability than Au (Jeon et al., 2021). Zn and Cd can produce complexes (such as $Zn(C_2H_4NO_2)^{3-}$, $Zn(C_2H_4NO_2)_4^{2-}$, and $Cd(C_2H_4NO_2)_4^{3-}$) even though they have poorer solubilities compared to gold. Furthermore, the $SC_2H_4NO_2^-$ complex generated by sulphide mineral dissolution at high glycine concentrations of 1000-2000 ppm reduces gold dissolution to some extent, although not as much as Ag and Cu.

Elements such as Cu, Co, Zn and Ni, among others, do not only compete with gold in terms of solubility and glycine consumption, but they also seep into activated carbon, causing considerable complications during purification. For example, if the gold ore contains a substantial amount of Ni that dissolves and adsorbs on activated carbon, Ni will accompany the gold to the smelting stage and raise the smelting temperature of the metal mixture due to Ni's higher melting point of 1455°C than Au's of 1063°C (Jiang et al., 2001; Sayiner and Acarkan, 2014).

The presence of chalcophile, siderophile and lithophile elements that compete with gold to form complexes with glycine during leaching process poses negative effects on gold recovery. These elements (e.g., Cu, Co, Ni, Zn, etc.) consume leaching reagents (i.e., glycine and oxygen) leading to low gold recoveries and makes the leaching process more complex and expensive since more reagents will be used in order to recover an acceptable amount of gold from the ore.

6.3 Gold extraction using glycine leaching

In leaching, comminution is crucial because finely-milled minerals react faster than coarsely crushed ore, such that their dissolution is driven by diffusion through the particle matrix (Liddell, 2005; Ghorbani et al., 2011; Nwaila et al., 2020). The greatest feasible grade for a given downstream process

recovery is determined by gold liberation (Carrasco et al., 2016). Bottle roll experiments demonstrate that the gold is well exposed to the leaching solution, based on the remarkable gold recovery percentages from crushed and milled Elsburg reefs deposits. The targeted Elsburg reef ores are very receptive to glycine leaching because the accessible surface area of the gold grains reacts with the reagent during the leaching process. The liquid/solid interaction in low porosity rocks, such as gold ore from the Elsburg reefs (MIT and ECT beds) is mostly determined by particle size.

6.3.1 Effect of glycine concentration and time

Glycine is a leaching agent that can generate stable gold complexes in alkaline solutions. Glycine concentrations of 300 ppm, 1000 ppm and 1500 ppm were utilized, all with the same liquid–solid ratios. A line graph depicting recovery performance as a function of time and glycine concentrations is given in Fig. 25A and B. The findings suggest that glycine concentration has an impact on gold desolation. Figure 25B shows that 1500 ppm yields a maximum gold recovery of 41%, whereas lower concentrations yield only 28%. It is worth noting that leaching duration plays a crucial role in gold dissolution; the results in Fig. 25A reveal poor recoveries (maximum of 35%) due to a shorter leaching time of 35 hours, whereas Fig. 25B shows the highest recovery of 41% after 50 hours leaching time.

6.3.2 Effects of recharging and solution recycling

The method of rejuvenating the strength of filtrate by adding glycine, oxidant and lime to increase concentration free glycine, thus attaining a target pH value in a solution and re-using the solution for gold leaching is referred to as recharging and solution recycling. Experiment 2 was recharged three times; resulting in a total amount of glycine used being 1500 ppm multiplied by three (4500 ppm), yielding a gold recovery rate of 41%. Despite the fact that the total amount of glycine used in experiment 2 (Fig. 25B) is the same as that used in experiments 3 and 4 (4500 ppm; Fig. 26), gold recovery from experiment 4 was only 38%. This demonstrate that using a high glycine concentration without recharging can result in a poorer gold recovery as compared to recharging the solution in different time intervals with the same amount of glycine.

There are three significant leaching parameters for the Elsburg reefs gold ore, namely leaching duration, glycine concentration and recharge, based on the results obtained from experiments 1 and 2. The optimal leaching parameters were determined to be 1500 ppm glycine concentration, eight recharges, as well as 101 hours of leaching time. Under these ideal conditions, the maximum achievable gold recovery is 86% (Fig. 27). Figure 28 depicts the relationship between gold recoveries, pH levels, and dissolved oxygen (mg/l) at room temperature (~19.35°C) for experiments 5–1 to 5–6. The relationship between dissolved oxygen and gold cumulative recovery is clearly shown in Fig. 28 (experiments 5-6), where there is lowest dissolved oxygen (mg/l) and lowest gold recovery. This simply means dissolved oxygen

and gold dissolution are directly proportional. The model in Fig. 29, predicts that a 100% gold recovery can be achieved with a leaching duration of 220 hours.

6.3.3 Effects of temperature

In terms of gold dissolution kinetics, temperature was clearly more important than other leaching parameters such as dissolved oxygen and glycine concentration. At room temperature, gold dissolution was low (between 30 and 41% after 48 hours, Fig. 25), but at elevated temperatures (between 35°C and 40°C), an average concentration of dissolved gold of 80% was attained after 48 hours (Fig. 30). This is due to the fact that, according to the literature (Eksteen and Oraby, 2015; Hidalgo et al., 2019; Oraby et al., 2019; Altinkaya et al., 2020), the reaction rate *K* is highly connected to temperature via the Arrhenius equation:

$$K = Ae^{(-Ea/RT)} \tag{3}$$

Where *A* is pre-exponential factor, *Ea* is activation energy for dissolution, *R* is gas constant, and *T* is temperature.

6.4 Glycine leaching methods for gold

Gold can be dissolved from ore using glycine in alkaline media in two ways, as discussed below. Both methods have their advantages and disadvantages.

6.4.1 Method 1

A diluted glycine solution at room temperature can be used to extract gold from ore. Due to the obvious sluggish reaction kinetics between glycine and gold, the leaching time is considerably long. This approach yielded a maximum of 86% gold recovery after 101 hours in this study. The main advantage of this procedure is that it is cost effective since no heating energy is required. The shortcoming of this process is that it takes a long time to leach an acceptable amount of gold from the ore and thus slows down production, which may be economically problematic.

6.4.2 Method 2

This technique recovers gold from ore by leaching it in a diluted glycine solution at an elevated temperature (35 – 45°C) for a shorter time. Figure 30 (EXP_6_01) demonstrates that with 4500 ppm glycine concentration, gold recoveries of 88 to 95% can be reached within 12 hours. When the solution is recharged with 1500 ppm glycine concentration at 40°C, as outlined in Fig. 30 (EXP_6_02 to EXP_6_06), an average of ~80% gold recovery can be achieved after 48 hours. The main benefit of this procedure is that it saves time; however, the use of heat incurs additional costs.

CHAPTER 7: CONCLUSION AND RECOMMENDATIONS

This chapter concludes this study. Finally, recommendations are given on what should be done in future in order to achieve a better understanding of the influence of the mineralogical assemblage with regards to leaching, and to know how effective glycine is to gold leaching.

7.1 CONCLUSION

A detailed mineralogical and geochemical characterisation of the Elsburg reefs ore bodies (MIT and ECT beds) was carried out to gain a better understanding of gold liberation and its association with minerals and elements that are known to be problematic during hydrometallurgical gold extraction. The processing behaviour of the Elsburg reefs ore was tested and characterised using bottle roll leaching with glycine as principal leaching chemical.

The Elsburg auriferous conglomerate beds are composed of (in decreasing order of abundance): quartz, pyrite, arsenopyrite, pyrrhotite, chalcopyrite, chlorite, muscovite, biotite, rutile and zircon. Inclusion-rich porous pyrite is known for being reactive with glycine. Therefore, it is expected that these porous pyrite grains and other reactive minerals such as chalcopyrite, pyrrhotite and uraniferous minerals will compete with gold during the dissolution stage, which may lead to low gold recoveries. Sulphide minerals, such as pyrite, have been found to increase reagent consumption (e.g., glycine, cyanide, and oxygen) and promote gold passivation, leading to low gold recoveries. In addition to pyrite, the over-consumption of reagents by copper-bearing minerals such as chalcopyrite, may also compete with gold for the glycine ligands, which reduces gold recovery. Similar contradicting observations have been recorded in the literature about the cyanidation behaviour of gold associated with various types of sulphide minerals such as chalcopyrite, pyrrhotite, sphalerite, galena, pentlandite and arsenopyrite (Aghamirian and Yen, 2005; Dai and Jeffrey, 2006; Azizi et al*.,* 2010; Eksteen and Oraby, 2015; Bas, 2017; Bas et al., 2017, 2018). Due to the diverse experimental methodologies utilized by various researchers to objectify the association between galvanic contacts and gold leaching, meaningful comparisons on gold dissolving in contact with sulphide minerals are difficult to standardize. Furthermore, the results from TIMA shows that more than 85% of gold is locked in silicates (i.e., quartz) and sulphide (i.e., pyrite) minerals, making it difficult for leaching solution to be in contact with gold. These ores characteristics have a negative effect on gold dissolution.

The geochemistry of analysed ore samples shows high concentrations of siderophile (i.e., Fe, Co and Ni), chalcophile (Cu, Zn and As) and lithophile elements (Cr, Th and V). All of these elements form complexes with glycine during gold leaching. Cu is regarded as the most problematic element since it generates stable complexes with leaching reagents (glycine or cyanide) and is more soluble as compared to gold. The type of Cu is the most important influencing factor regarding the leaching of gold, as it interferes with gold dissolution significantly (Birloaga et al., 2013). Therefore, due to similar

geochemical behaviour, the presence of both chalcophile and siderophile as well as lithophile elements in higher concentrations in the Elsburg reef ores provide a key diagnostic that these metals and their host minerals will have a negative impact in gold recovery. Sequential leaching (recharging) can be used to improve gold recovery from ores containing high concentrations of elements such as easily soluble Cu (Jiang et al., 2001), but it makes the entire leaching process more complex and increases glycine consumption. For ores containing too much soluble Cu, gold leaching recovery may be poor.

Bottle roll leaching of the Elsburg reefs ore samples yields a poor gold recovery (i.e., 30%) at low glycine dosages (e.g., 300 ppm) and at an ambient temperature (~23°C). However, at higher concentrations of glycine (1500 ppm), yielded a gold recovery of up to 41% (Fig. 25). The increase in glycine was complemented by an increase in oxidant concentration (potassium permanganate). The ratio of potassium permanganate to glycine was kept at 2:1 (potassium permanganate: glycine). The results from the sequential/multi-stage (recharging and solution recycling) bottle roll leaching shows that Elsburg reefs ore responds very well to glycine leaching as approximately 86% and 95% of gold was recovered from the ore within 101 hours (Fig. 27) and 48 hours (Fig. 30), respectively. There are two pathways in which gold can be recovered from Elsburg reefs ore, namely: 1) at room temperature and leach for a longer period of time, or 2) at elevated temperature (>35°C) and leach for a shorter period of time.

Based on the mineralogical assemblage, geochemistry and experimental results attained in this study, I conclude that the mineral assemblage characteristics (i.e., poor liberation of gold and presence of sulphides such as inclusion-rich porous pyrite and chalcopyrite) and positive correlation of leaching problematic metals (Cu, Ni, Co, etc.) all have a negative influence on glycine gold leaching, as first hypothesized. Nonetheless, glycine is effective in gold leaching, depending on which ore is being processed and leaching method used.

7.2 RECOMMENDATIONS

The potential for glycine leaching to recover gold is revealed in this research report. Many factors, however, influence the overall gold recovery. To acquire a better understanding of glycine gold leaching capability and the factors that influence gold dissolution during leaching, it is necessary to investigate the following:

i. Further study of glycine leaching using ore bodies or reefs with different mineralogical assemblages and geochemistries to test/assess their response to glycine leaching and examine effectiveness of glycine compared to cyanide is warranted. For example, use Witwatersrand gold ores (multiple reefs) and Barberton greenstone gold ore to test how well they respond to glycine leaching.

ii. Analysing the leaching solution (leachate) to determine the concentration of free glycine and determine the concentrations of other metals that form complexes with glycine could also be investigated.

iii. Tracking the amount of consumed glycine in relation to gold recovery to determine the amount of required glycine per tonne.

iv. Tracking the desolation rates of other metals (i.e., Cu, Co, Zn, etc.) in glycine solutions to establish which metals are more problematic during glycine leaching would provide the much needed clarity as to optimal leaching parameters.

REFERENCES:

1. Adams, M. ed., 2005. Advances in gold ore processing. Elsevier.
2. Akcil, A., Erust, C., Gahan, C.S., Ozgun, M., Sahin, M. and Tuncuk, A., 2015. Precious metal recovery from waste printed circuit boards using cyanide and non-cyanide lixiviants–a review. Waste management, 45, pp.258-271.
3. Agangi, A., Hofmann, A. and Wohlgemuth-Ueberwasser, C.C., 2013. Pyrite zoning as a record of mineralization in the Ventersdorp Contact Reef, Witwatersrand Basin, South Africa. Economic Geology, 108(6), pp.1243-1272.
4. Agangi, A., Hofmann, A., Rollion-Bard, C., Marin-Carbonne, J., Cavalazzi, B., Large, R. and Meffre, S., 2015. Gold accumulation in the Archaean Witwatersrand Basin, South Africa—Evidence from concentrically laminated pyrite. Earth-Science Reviews, 140, pp.27-53.
5. Ahtiainen, R., 2020. Development of chloride-based processing of free-milling and refractory gold ores and concentrates.
6. Altinkaya, P., 2021. Leaching and recovery of gold from low grade raw materials in cyanide-free media.
7. Altinkaya, P., Wang, Z., Korolev, I., Hamuyuni, J., Haapalainen, M., Kolehmainen, E., Yliniemi, K. and Lundström, M., 2020. Leaching and recovery of gold from ore in cyanide-free glycine media. Minerals Engineering, 158, p.106610.
8. Aylmore, M.G., 2016. Alternative lixiviants to cyanide for leaching gold ores. In: Adams, M.D. (Ed.), Gold ore processing (Second Edition), Elsevier, Amsterdam, Chapter 27, 447–484.
9. Azcue, J.M. ed., 2012. Environmental impacts of mining activities: emphasis on mitigation and remedial measures. Springer Science & Business Media
10. Barnicoat, A.C., Henderson, I.H.C., Knipe, R.J., Yardley, B.W.D., Napier, R.W., Fox, N.P.C., Kenyon, A.K., Muntingh, D.J., Strydom, D., Winkler, K.S. and Lawrence, S.R., 1997. Hydrothermal gold mineralization in the Witwatersrand basin. Nature, 386(6627), pp.820-824.
11. Birloaga, I., De Michelis, I., Ferella, F., Buzatu, M. and Vegliò, F., 2013. Study on the influence of various factors in the hydrometallurgical processing of waste printed circuit boards for copper and gold recovery. Waste management, 33(4), pp.935-941.
12. Bogdanovskaya, V. A., Safronov, A. Y., Tarasevich, M. R., & Chernyak, A. S. (1986). Adsorption and Anodic Oxidation of Glycylglycine and Some Amino Acids on a Gold Electrode. Journal of Electroanalytical Chemistry and Interfacial Electrochemistry, 202(1–2), 147-167.
13. Bordes, R. and Holmberg, K., 2015. Amino acid-based surfactants–do they deserve more attention. Advances in Colloid and Interface Science, 222, pp.79-91.
14. Burger, A.J., and Coertze, F.J., 1975, Age determinations—April 1972 to March 1974, Technical Report: Annals of the Geological Survey of South Africa, v. 11, p. 317–321.

15. Chai, J., Zhao, C., Hu, Y. and Zhang, Z.G., 2021. Structural analysis and forecast of gold price returns. Journal of Management Science and Engineering.
16. Coetzee, L.L., Theron, S.J., Martin, G.J., Van der Merwe, J.D. and Stanek, T.A., 2011. Modern gold deportments and its application to industry. Minerals Engineering, 24(6), pp.565-575.
17. Cole, M.J. and Broadhurst, J.L., 2021. Measuring the sustainable development goals (SDGs) in mining host communities: A South African case study. The Extractive Industries and Society, 8(1), pp.233-243.
18. Ceballos Quintana, J., 2014. Bio-sorption of heavy metals from wastewater by using marine biomass wastes (Doctoral dissertation, Memorial University of Newfoundland).
19. da Costa, G., Hofmann, A. and Agangi, A., 2020. A revised classification scheme of pyrite in the Witwatersrand Basin and application to placer gold deposits. Earth-Science Reviews, 201, p.103064.
20. Davidson, C.F., 1965. NAS Symposium on the Evolution of the Earth's Atmosphere: GEOCHEMICAL ASPECTS OF ATMOSPHERIC EVOLUTION. Proceedings of the National Academy of Sciences of the United States of America, 53(6), p.1194.
21. Dirks, P.H., Charlesworth, E.G., Munyai, M.R. and Wormald, R., 2013. Stress analysis, post-orogenic extension and 3.01 Ga gold mineralisation in the Barberton Greenstone Belt, South Africa. Precambrian Research, 226, pp.157-184.
22. Durand, J.F., 2012. The impact of gold mining on the Witwatersrand on the rivers and karst system of Gauteng and North West Province, South Africa. Journal of African Earth Sciences, 68, pp.24-43.
23. Drennan, G.R., and Robb, L.J., 2006, The nature of hydrocarbons and related fluids in the Witwatersrand basin, South Africa: Their role in metal redistribution: Geological Society of America, Special Paper 405, p. 353–3
24. Drielsma, J.A., Russell-Vaccari, A.J., Drnek, T., Brady, T., Weihed, P., Mistry, M. and Simbor, L.P., 2016. Mineral resources in life cycle impact assessment—defining the path forward. The International Journal of Life Cycle Assessment, 21(1), pp.85-105.
25. Drif, B., Taha, Y., Hakkou, R. and Benzaazoua, M., 2018. Recovery of residual silver-bearing minerals from low-grade tailings by froth flotation: The case of zgounder mine, morocco. Minerals, 8(7), p.273.
26. Dry, M., 2016, May. A preliminary evaluation of alkaline glycine as an alternative to cyanide for gold extraction. In Alta Gold-PM Conference
27. Edwards, R., 2012. Ore deposit geology and its influence on mineral exploration. Springer Science & Business Media.
28. Eisler, R. and Wiemeyer, S.N., 2004. Cyanide hazards to plants and animals from gold mining and related water issues. Reviews of environmental contamination and toxicology, pp.21-54.

29. Eksteen, J.J., Oraby, E.A., Tanda, B.C., Tauetsile, P.J., Bezuidenhout, G.A., Newton, T., Trask, F. and Bryan, I., 2018. Towards industrial implementation of glycine-based leach and adsorption technologies for gold-copper ores. Canadian Metallurgical Quarterly, 57(4), pp.390-398.
30. Eugene, W.W.L. and Mujumdar, A.S., 2009. Gold extraction and recovery processes. Minerals, Metals, and Materials Technology Centre, National University of Singapore.
31. Eriksson, K.A. and McClung, W.S., 2021. Source-to-Sink Analysis of the Gold-Hosting Mesoarchean Main and Mondeor Formations (Central Rand Group) in the Area South of Johannesburg, Witwatersrand Basin, Kaapvaal Province, South Africa. The Journal of Geology, 129(6), pp.000-000.
32. Fields, G., 2012. South Deep Gold Mine Technical Short Form Report.
33. Frimmel, H.E., 2008. Earth's continental crustal gold endowment. Earth and Planetary Science Letters, 267(1-2), pp.45-55.
34. Frimmel, H.E. 2014. A Giant Mesoarchean Crustal Gold-Enrichment Episode: Possible Causes and Consequences for Exploration. Society of Economic Geologists Inc. Special Publications. 18:209–234.
35. Frimmel, H.E., 2019. The Witwatersrand Basin and its gold deposits. In The Archaean Geology of the Kaapvaal Craton, Southern Africa (pp. 255-275). Springer, Cham.
36. Frimmel, H.E. and Gartz, V.H., 1997. Witwatersrand gold particle chemistry matches model of metamorphosed, hydrothermally altered placer deposits. Mineralium Deposita, 32(6), pp.523-530.
37. Frimmel, H.E. and Minter, W.E.L., 2002. Recent developments concerning the geological history and genesis of the Witwatersrand gold deposits, South Africa. Special publication-society of economic geoscientists, 9, pp.17-46.
38. Frimmel, H.E., Groves, D.I., Kirk, J., Ruiz, J., Chesley, J. and Minter, W.E.L., 2005. The formation and preservation of the Witwatersrand goldfields, the world's largest gold province. Economic Geology, 100, pp.769-797.
39. Fuchs, S.H.J., Williams-Jones, A.E., Jackson, S.E., and Przybylowicz, W.J., 2016, Metal distribution in pyrobitumen of the Carbon Leader reef, Witwatersrand Supergroup, South Africa: Evidence for liquid hydrocarbon ore fluids: Chemical Geology, v. 426, p. 45–59
40. Gartz, V.H. and Frimmel, H.E., 1999. Complex metasomatism of an Archean placer in the Witwatersrand basin, South Africa; the Ventersdorp Contact Reef; a hydrothermal aquifer. Economic Geology, 94(5), pp.689-706.
41. Ghorbani, Y., Becker, M., Mainza, A., Franzidis, J.P. and Petersen, J., 2011. Large particle effects in chemical/biochemical heap leach processes–a review. Minerals Engineering, 24(11), pp.1172-1184.
42. Goodman, P., 2002. Current and future uses of gold in electronics. Gold bulletin, 35(1), pp.21-26.
43. Gumsley, A., Stamsnijder, J., Larsson, E., Söderlund, U., Naeraa, T., de Kock, M.O. and Ernst, R., 2018. The 2789–2782 Ma Klipriviersberg large igneous province: implications for the chrono-

stratigraphy of the Ventersdorp Supergroup and the timing of Witwatersrand gold deposition. GeoCongress 2018, p.133.

44. Grunsky, E.C. and de Caritat, P., 2020. State-of-the-art analysis of geochemical data for mineral exploration. Geochemistry: Exploration, Environment, Analysis, 20(2), pp.217-232.
45. Habashi, F. ed., 2008. Alloys: preparation, properties, applications. John Wiley & Sons.
46. Hakimi, M. and Aliabadi, T.S., 2012. Coordination chemistry of copper α-amino acid complexes. catena, 6, p.25.
47. Hartnady, C.J., 2009. South Africa's gold production and reserves. South African Journal of Science, 105(9), pp.328-329.
48. Hassana, F., Mohamedb, G.G., Al-Hossainyc, A.F. and Khidrb, M., 2012. Coordination behaviour and biological activity studies of transition metal complexes with indapamide and mixed ligands of indapamide and glycine. J. Pharm. Res, 5(7), pp.3753-3763.
49. Hatch, F.H. and Chalmers, J.A., 2013. Gold Mines of the Rand: Being a Description of the Mining Industry of Witwatersrand, South African Republic. Cambridge University Press.
50. Hayward, C.L., Reimold, W.U., Gibson, R.L. and Robb, L.J., 2005. Gold mineralization within the Witwatersrand Basin, South Africa: evidence for a modified placer origin, and the role of the Vredefort impact event. Geological Society, London, Special Publications, 248(1), pp.31-58.
51. Hoal, K.E.O. and Frenzel, M., 2022. Ores Drive Operations—Economic Geology Is the Foundation of Geometallurgy. SEG Discovery, (129), pp.30-43.
52. Holtom, P.D., Bennett, C.J., Osamura, Y., Mason, N.J. and Kaiser, R.I., 2005. A combined experimental and theoretical study on the formation of the amino acid glycine (NH2CH2COOH) and its isomer (CH3NHCOOH) in extraterrestrial ices. The Astrophysical Journal, 626(2), p.940.
53. Inoue, K., Parajuli, D., Gurung, M., Pangeni, B., Khunathai, K., Ohto, K. and Kawakita, H., 2019. Gold Recovery Process from Primary and Secondary Resources Using Bioadsorbents. In Elements of Bioeconomy. IntechOpen.
54. Insausti, M.J., Mata-Perez, F. and Alvarez-Macho, P., 1992. Permanganate oxidation of glycine: influence of amino acid on colloidal manganese dioxide. International journal of chemical kinetics, 24(5), pp.411-419.
55. Jeon, S., Bright, S., Park, I., Tabelin, C.B., Ito, M. and Hiroyoshi, N., 2021. The Effects of Coexisting Copper, Iron, Cobalt, Nickel, and Zinc Ions on Gold Recovery by Enhanced Cementation via Galvanic Interactions between Zero-Valent Aluminum and Activated Carbon in Ammonium Thiosulfate Systems. Metals, 11(9), p.1352.
56. Jiang, T., Zhang, Y.Z., Yang, Y.B. and Huang, Z.C., 2001. Influence of copper minerals on cyanide leaching of gold. Journal of Central South University of Technology, 8(1), pp.24-28.
57. Kamunda, C., Mathuthu, M. and Madhuku, M., 2016. Health risk assessment of heavy metals in soils from Witwatersrand Gold Mining Basin, South Africa. International Journal of Environmental Research and Public Health, 13(7), p.663

58. Kianinia, Y., Khalesi, M.R., Abdollahy, M., Hefter, G., Senanayake, G., Hnedkovsky, L., Khodadadi Darban, A. and Shahbazi, M., 2018. Predicting cyanide consumption in gold leaching: a kinetic and thermodynamic modeling approach. Minerals, 8(3), p.110.
59. Kinzley, J.C., 2018. Natural resources and the new frontier: constructing modern China's borderlands. University of Chicago Press.
60. Kirk, J., Ruiz, J., Chesley, J., Titley, S. and Walshe, J., 2001. A detrital model for the origin of gold and sulfides in the Witwatersrand basin based on Re-Os isotopes. Geochimica et Cosmochimica Acta, 65(13), pp.2149-2159.
61. Koç, E., Ahlatcı, F., Celep, O., Yazici, E.Y. and Deveci, H., 2014. Interference of metals with the determination of free cyanide. In Proceedings of 14th International Mineral Processing Symposium, Kusadasi, Turkey (pp. 1027-1033).
62. Koglin, N., Frimmel, H.E., Lawrie Minter, W.E. and Brätz, H., 2010. Trace-element characteristics of different pyrite types in Mesoarchaean to Palaeoproterozoic placer deposits. Mineralium Deposita, 45(3), pp.259-280.
63. Kononova, O.N., Kholmogorov, A.G., Kononov, Y.S., Pashkov, G.L., Kachin, S.V. and Zotova, S.V., 2001. Sorption recovery of gold from thiosulphate solutions after leaching of products of chemical preparation of hard concentrates. Hydrometallurgy, 59(1), pp.115-123.
64. Korobushkina, E. D., Cherniak, A. S., & Mineev, G. G. (1974). Dissolution of Gold by Microorganisms and by Products of Their Metabolism (Russian). Mikrobiologiya, 43(1), 49-54
65. Kositcin, N. and Krapež, B., 2004. Relationship between detrital zircon age-spectra and the tectonic evolution of the Late Archaean Witwatersrand Basin, South Africa. Precambrian Research, 129(1-2), pp.141-168.
66. Liddell, K.C., 2005. Shrinking core models in hydrometallurgy: What students are not being told about the pseudo-steady approximation. Hydrometallurgy, 79(1-2), pp.62-68.
67. Little, L., 2016. The development and demonstration of a practical methodology for fine particle shape characterisation in minerals processing. Doctoral Dissertation, University of Cape Town.
68. Manzi, M.S., Durrheim, R.J., Hein, K.A. and King, N., 2012. 3D edge detection seismic attributes used to map potential conduits for water and methane in deep gold mines in the Witwatersrand basin, South Africa. Geophysics, 77(5), pp.WC133-WC147
69. Manzi, M.S.D., Hein, K.A.A., Durrheim, R. and King, N., 2013. Seismic attribute analysis to enhance detection of thin gold-bearing reefs: South Deep gold mine, Witwatersrand basin, South Africa. Journal of Applied Geophysics, 98, pp.212-228.
70. Mason, S.J., Wesenberg, D.J., Hojem, A., Manno, M., Leighton, C. and Zink, B.L., 2020. Violation of the Wiedemann-Franz law through reduction of thermal conductivity in gold thin films. Physical Review Materials, 4(6), p.065003.
71. Marsden, J. and House, I., 2006. The chemistry of gold extraction. SME.

72. McCarthy, T.S., Johnson, M.R., Anhaeusser, C.R. and Thomas, R.J., 2006. The Witwatersrand Supergroup. The Geology of South Africa, pp.155-186.
73. McLennan, S.M., Nance, W.B. and Taylor, S.R., 1980. Rare earth element-thorium correlations in sedimentary rocks, and the composition of the continental crust. Geochimica et Cosmochimica Acta, 44(11), pp.1833-1839.
74. McLennan, S.M., 2001. Relationships between the trace element composition of sedimentary rocks and upper continental crust. Geochemistry, Geophysics, Geosystems, 2(4).
75. Minter, W.E.L., 1977. A sedimentological synthesis of placer gold, uranium and pyrite concentrations in Proterozoic Witwatersrand sediments. In: A. D. Miall (Ed.) Fluvial Sedimentology Can. Soc. Petrol. Geol., Mem 5, pp. 801-829.
76. Minter, W.E.L., 1978, A sedimentological synthesis of placer gold, uranium and pyrite concentrations in Proterozoic Witwatersrand sediments, in Miall, A.D., ed., Fluvial sedimentology: Calgary, Alberta, Canadian Society of Petroleum Geologists, p. 801–829.
77. Minter, W.E.L., Goedhart, M.L., Knight, J., and Frimmel, H.E., 1993, Morphology of Witwatersrand gold grains from the Basal reef: Evidence for their detrital origin: ECONOMIC GEOLOGY, v. 88, p. 237–248.
78. Mngoma, L., 2012. A gold, uranium and thorium deportment analysis of Witwatersrand ore from cooke section, Rand Uranium RANDFONTEIN (Doctoral dissertation, University of Johannesburg).
79. Muntean, J.L., Cline, J., Johnston, M.K., Ressel, M.W., Seedorff, E. and Barton, M.D., 2004. Controversies on the origin of world-class gold deposits. Part I, Carlin-type gold deposits in Nevada: Society of Economic Geologists Newsletter, 59, pp.1-18.
80. Muntean, J.L., Frimmel, H.E., Phillips, N., Law, J. and Myers, R., 2005. Controversies on the origin of world-class gold deposits, part II: Witwatersrand gold deposits. SEG Discovery, (60), pp.7-19.
81. Mutobvu, T.R., 2019. Enhance South deep variography by including flat inclined boreholes in the local direct estimation methodology (M.Sc. dissertation).
82. Neingo, P.N. & Tholana, T. 2016. Trends in productivity in the South African gold mining industry. Journal of the Southern African Institute of Mining and Metallurgy. 116(3):283–290.
83. Nwaila, G., 2014. Application of HPGR and X-Ray CT to investigate the potential of Witwatersrand gold ore for heap leaching: a process mineralogy approach (Master's thesis, University of Cape Town).
84. Nwaila, G., Becker, M., Ghorbani, Y., Petersen, J., Reid, D.L., Bam, L.C., De Beer, F.C. and Franzidis, J.P., 2013. A geometallurgical study of the Witwatersrand gold ore at Carletonville, South Africa. In Proceedings of the Second AUSIMM International Geometallurgy Conference. Brisbane: AusIMM (pp. 77-85).

85. Nwaila, G., Frimmel, H.E. and Minter, W.E., 2017. Provenance and geochemical variations in shales of the Mesoarchean Witwatersrand Supergroup. The Journal of Geology, 125(4), pp.399-422.
86. Nwaila, G.T., Ghorbani, Y., Becker, M., Frimmel, H.E., Petersen, J. and Zhang, S., 2020. Geometallurgical approach for implications of ore blending on cyanide leaching and adsorption behavior of Witwatersrand gold ores, South Africa. Natural Resources Research, 29(2), pp.1007-1030.
87. Nwaila, G.T., Bourdeau, J.E., Jinnah, Z., Frimmel, H.E., Bybee, G.M., Zhang, S.E., Manzi, M.S.D., Minter, W.E.L. and Mashaba, D., 2021. The Significance of Erosion Channels on Gold Metallogeny in the Witwatersrand Basin (South Africa): Evidence from the Carbon Leader reef in the Carletonville Gold Field. Economic Geology, 116(2), pp.265-284.
88. Nwaila, G.T., Zhang, S.E., Tolmay, L.C.K. and Frimmel, H.E., 2021. Algorithmic Optimization of an Underground Witwatersrand-Type Gold Mine Plan. Natural Resources Research, 30(2), pp.1175-1197.
89. Oraby, E.A. and Eksteen, J.J., 2015. The leaching of gold, silver and their alloys in alkaline glycine–peroxide solutions and their adsorption on carbon. Hydrometallurgy, 152, pp.199-203.
90. Oraby, E.A., Eksteen, J.J. and Tanda, B.C., 2017. Gold and copper leaching from gold-copper ores and concentrates using a synergistic lixiviant mixture of glycine and cyanide. Hydrometallurgy, 169, pp.339-345.
91. Oraby, E.A., Eksteen, J.J. and O'Connor, G.M., 2020. Gold leaching from oxide ores in alkaline glycine solutions in the presence of permanganate. Hydrometallurgy, 198, p.105527.
92. Osburn, K., Pretorius, H., Kock, D., King, N., Pillaye, R. and Hlangwane, M., 2014. Enhanced geological modelling of the Upper Elsburg reefs and VCR to optimize mechanized mine planning at South Deep Gold Mine. Journal of the Southern African Institute of Mining and Metallurgy, 114(3), pp.265-273.
93. Patil, Y. and Kulkarni, A., 2014. Environmental sensitivity and management of toxic chemical waste in mining industry with special reference to cyanide. Patil Yogesh B and Kulkarni Anil R (2008) Environmental sensitivity and management of toxic chemical waste in mining industry with special reference to cyanide. In: High Performing Organizations: Needs and Challenges, Tata McGraw Hill Publications, Part D, pp.183-196.
94. Petersen, J., 2016. Heap leaching as a key technology for recovery of values from low-grade ores–A brief overview. Hydrometallurgy, 165, pp.206-212.
95. Phillips, G.N. and Law, J.D., 2000. Witwatersrand gold fields: geology, genesis and exploration. Reviews in Economic Geology, 13, pp.439-500.
96. Phillips, G.N. and Powell, R., 2011. Origin of Witwatersrand gold: a metamorphic devolatilisation–hydrothermal replacement model. Applied Earth Science, 120(3), pp.112-129.

97. Plant, J.A., Simpson, P.R., Smith, B. and Windley, B.F., 2018. 6. Uranium Ore Deposits—Products of the Radioactive Earth. Uranium, pp.255-320
98. Poujol, M., Kiefer, R., Robb, L.J., Anhaeusser, C.R., and Armstrong, R.A., 2005, New U-Pb data on zircons from the Amalia greenstone belt Southern Africa: Insights into the Neoarchaean evolution of the Kaapvaal craton: South African Journal of Geology, v. 108, p. 317–332
99. Pratesa, Y., Wibisono, A., Putra, W.N., Sadeli, T., Zakiyuddin, A. and Harjanto, S., 2019. Effect of H_2O_2 and MnO_2 as oxidators of gold and copper leach processes from printed circuit boards. Jurnal Sains Materi Indonesia, 20(3), pp.132-136.
100. Pretorius, D.A. (1991). The sources of Witwatersrand gold and uranium: a continued difference o opinion. In: Hutchinson, R.W. and Grauch, R.I. (Eds.), Historical Perspectives of Genetic Concepts and Case Histories of Famous Discoveries. Econ. Geol. Monogr., 8,139-163
101. Reimold, W.U. and Gibson, R.L., 2006. The melt rocks of the Vredefort impact structure–Vredefort Granophyre and pseudotachylitic breccias: Implications for impact cratering and the evolution of the Witwatersrand Basin. Geochemistry, 66(1), pp.1-35.
102. Robb, L.J. and Meyer, F.M., 1991. A contribution to recent debate concerning epigenetic versus syngenetic mineralization processes in the Witwatersrand Basin. Economic Geology, 86(2), pp.396-401.
103. Robert, F., Poulsen, K.H. and Dubé, B., 1997, April. Gold deposits and their geological classification. In *Proceedings of exploration* (Vol. 97, pp. 209-220).
104. Rowe, R.R. and Zhou, X., 2007. Models and exploration methods for major gold deposit types. In *Proceedings of exploration* (Vol. 7, pp. 691-711).
105. Sabbaghizadeh, R., Sedghi, A. and Amini, E., 2021. Effect of glycine molar ratios on structural and magnetic properties of combustion synthesized W-type Barium hexaferrites nanocrystalline. Optoelectronics and Advanced Materials-Rapid Communications, 15(1-2), pp.92-98.
106. Sánchez, F. and Hartlieb, P., 2020. Innovation in the Mining Industry: Technological Trends and a Case Study of the Challenges of Disruptive Innovation. Mining, Metallurgy & Exploration, pp.1-15.
107. Sayiner, B. and Acarkan, N., 2014. Effect of silver, nickel and copper cyanides on gold adsorption on activated carbon in cyanide leach solutions. Physicochemical Problems of Mineral Processing, 50.
108. Shivambu, S., 2016. The sedimentology and depositional model of VS5 Reef at Beatrix mine and surrounding areas of the Free State Goldfield, South Africa (Doctoral dissertation, Rhodes University). .
109. Smith, A.J., Beukes, N.J. and Gutzmer, J., 2013. The composition and depositional environments of Mesoarchean iron formations of the West Rand Group of the Witwatersrand Supergroup, South Africa. Economic Geology, 108(1), pp.111-134.

110. Summary, 2020. US Geological Survey, 2020. Mineral Commodity Summaries. https://doi.org/10.3133/mcs2020

111. Taylor, R.D. and Anderson, E.D., 2018. Quartz-pebble-conglomerate gold deposits: Chapter P in Mineral deposit models for resource assessment (No. 2010-5070-P). US Geological Survey.

112. Tucker, R.F., Viljoen, R.P. and Viljoen, M.J., 2016. A review of the Witwatersrand Basin–The world's greatest goldfield. Episodes, 39(2), pp.105-133.

113. Trapp, S., Larsen, M., Pirandello, A. and Danquah-Boakye, J., 2003. Feasibility of cyanide elimination using plants. ejmp & ep (European Journal of Mineral Processing and Environmental Protection), 3(1), pp.128-137.

114. Ustunol, Z., 2015. Amino acids, peptides and proteins. Applied food protein chemistry, pp.12-15.

115. Vennemann, T.W., Kesler, S.E., Frederickson, G.C., Minter, W.E.L. and Heine, R.R., 1996. Oxygen isotope sedimentology of gold-and uranium-bearing Witwatersrand and Huronian Supergroup quartz-pebble conglomerates. Economic Geology, 91(2), pp.322-342.

116. Wang, X., Qin, W., Jiao, F., Yang, C., Cui, Y., Li, W., Zhang, Z. and Song, H., 2019. Mineralogy and pretreatment of a refractory gold deposit in Zambia. Minerals, 9(7), p.406.

117. Wani, M.Y. and Malik, M.A., 2021. Chemistry of Gold. In Gold and its Complexes in Anticancer Chemotherapy (pp. 69-79). Springer, Singapore.

118. Walraven, F., 1997. Geochronology of the Rooiberg Group, Transvaal Supergroup, South Africa. Information Circular 316. Economic Geology Research Unit, University of the Witwatersrand, Johannesburg, South Africa, 21.

119. Wills, B.A. and Finch, J., 2015. Wills' mineral processing technology: an introduction to the practical aspects of ore treatment and mineral recovery. Butterworth-Heinemann.

120. Winter, H.D.L.R., 1994. The Ventersdorp Contact Reef in relation to the Witwatersrand Basin and overlying Ventersdorp volcanic rocks. South African Journal of Geology, 97(3), pp.260-278.

121. Yannopoulos, J.C., 1991. Physical and chemical properties of gold. In The Extractive Metallurgy of Gold (pp. 11-23). Springer, Boston, MA.

122. Zhou, J., Jago, B. and Martin, C., 2004. Establishing the process mineralogy of gold ores. SGS Miner. Tech. Bull. 2004-03 1–16.

123. Zhu, Y., An, F. and Tan, J., 2011. Geochemistry of hydrothermal gold deposits: a review. Geoscience Frontiers, 2(3), pp.367-374.

APPENDICES

Appendix I: Photographs of hand specimen's samples obtained from underground of South Deep Gold mine and the sampling locations are shown in Fig. 15

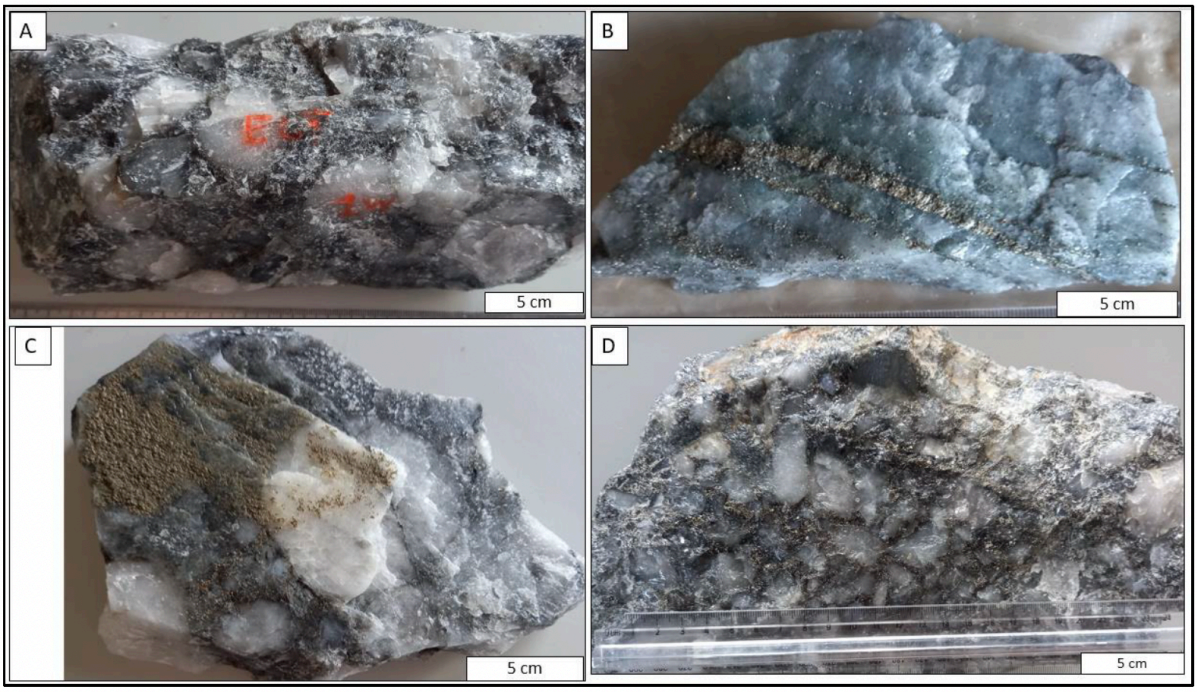

Figure 31: The Elsburg reefs samples. A: ECT metrix supported conglomerate with pebble size between 1 to 5 cm, B: MIT001 quartzite with pyrite veins, C: MIT002 Matrix supported quartz pebble conglomerate and D: MIT003 Matrix supported quartz pebble conglomerate with grain size ranging between 1 and 4 cm.

Appendix II: TIMA BSE images from ECT (A, B and C) and MIT (D, E and F) thin sections.

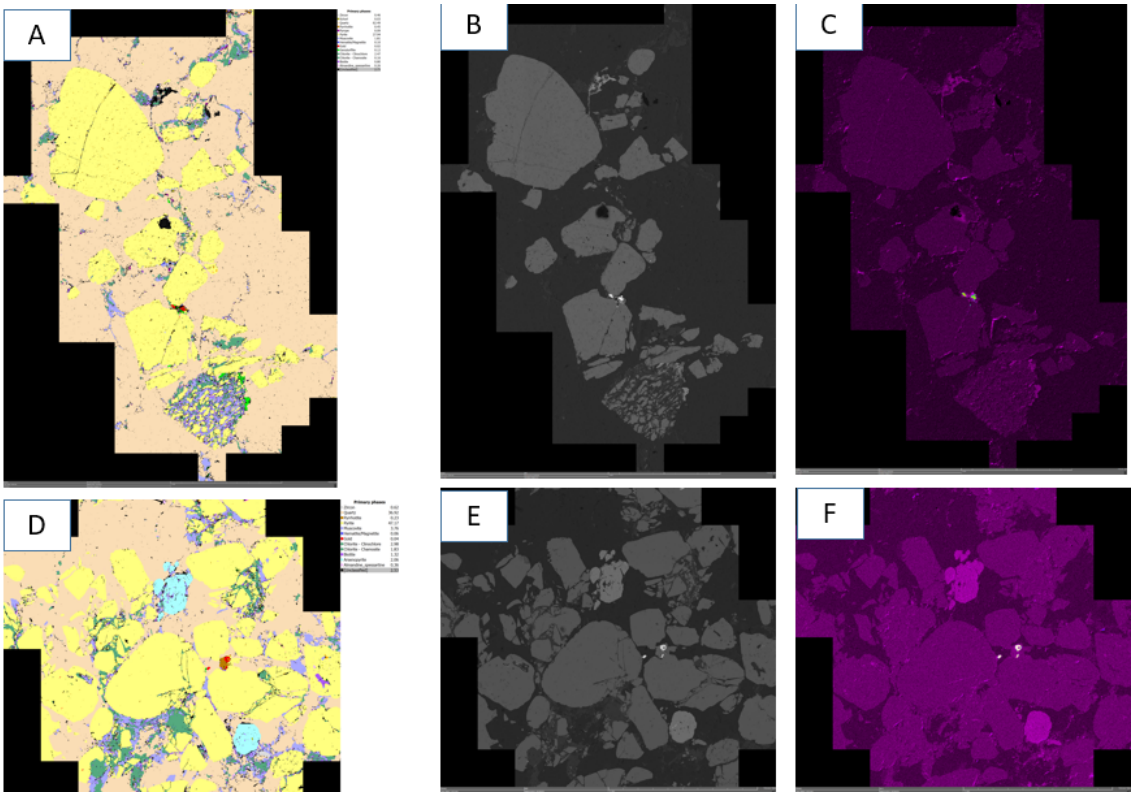

Figure 32: Small selected portions from ECT and MIT f thin sections.

Appendix III: Chemical assay of different Elsburg reefs samples using XRF (Wt.%).

wt.%	MIT01	MIT02	MIT03	MIT04	MIT05	MIT06	ECT01	ECT02	ECT03	ECT04
SiO_2	92.46	89.5	90.84	95.29	85.15	90.58	96.43	95.33	96.31	96.24
Al_2O_3	0.81	0.91	1.68	0.78	1.27	1.06	0.64	0.82	0.56	0.58
Fe_2O_3	3.99	5.62	3.78	1.53	8.18	4.83	0.98	1.72	1.71	1.56
MnO	0.01	0.01	0.01	0.01	0.02	0.02	0.01	0.01	0.01	0.01
MgO	0.17	0.05	0.24	0.33	0.23	0.27	0.21	0.12	0.12	0.12
CaO	0.05	0.03	0.05	0.03	0.05	0.04	0.06	0.04	0.04	0.03
Na_2O	0	0.01	0.01	-0.02	-0.02	-0.01	0	0	0	0
K_2O	0.1	0.2	0.38	0.06	0.21	0.16	0.1	0.06	0.04	0.04
TiO_2	0.05	0.05	0.05	0.04	0.05	0.04	0.03	0.03	0.04	0.03
P_2O_5	0.03	0.02	0.02	0.02	0.03	0.02	0.02	0.02	0.02	0.02
Cr_2O_3	0.05	0.02	0.02	0.02	0.03	0.02	0.01	0.01	0.01	0.01
NiO	0.02	0.01	0.01	0	0.02	0.01	0	0.01	0	0
LOI	1.88	2.78	2	0.56	3.96	2.34	0.53	0.92	0.79	0.73

TOTAL	99.61	99.22	99.09	98.64	99.17	99.38	99.02	99.09	99.66	99.38

Calibration standards													
Wt.%	**NIM-P**	**NIM-D**	**W2**	**NIM-S**	**GSP2**	**BCR2**	**NIM-N**	**NIM-G**	**PCC1**	**BHVO2**	**AGV2**	**G2**	**DTS1**
SiO_2	51	38.96	52.9	63.62	67.35	54.29	53.09	76.15	44.44	50.02	60.48	69.3	40.8
Al_2O_3	4.3	0.31	15.6	17.31	15.15	13.66	16.8	12.29	0.74	13.77	17.36	15.5	0.27
Fe_2O_3	1.3	1.72	1.1	0.14	0.5	1.4	0.91	0.2	0.87	1.25	0.69	0.27	0.87
MnO	10	13.96	8.88	1.13	4.07	11.33	7.35	1.61	7.05	10.14	5.57	2.18	7.07
MgO	0.2	0.22	0.17	0.01	0.04	0.19	0.17	0.02	0.12	0.17	0.1	0.04	0.12
CaO	25	44.01	6.44	0.48	0.99	3.63	7.55	0.07	45.81	7.31	1.85	0.79	50.1
Na_2O	2.7	0.33	10.9	0.61	2.11	7.15	11.52	0.78	0.63	11.49	5.32	1.94	0.19
K_2O	0.4	0.02	2.24	0.37	2.83	3.19	2.46	3.35	0.05	2.22	4.31	4.12	0.07
TiO_2	0.1	0.01	0.65	15.35	5.46	1.78	0.25	5.03	0.01	0.52	2.93	4.47	0
P_2O_5	0.2	0.03	1.08	0.05	0.68	2.28	0.2	0.1	0.02	2.77	1.06	0.49	0.02
Cr_2O_3	0	0.01	0.13	0.12	0.29	0.36	0.02	0.01	0.01	0.27	0.49	0.14	0.01
NiO	3.5	0.43	0.02	0	0.01	0.02	0.02	0.01	0.43	0.05	0.01	0	0.6
NiO	0.1	0.27	0.01	0	0	0	0.02	0	0.33	0.02	0	0	0.32
TOTAL	100	100.3	100	99.18	99.5	99.28	100.35	99.62	100.5	100	100.2	99.2	100
LOI	-0.2	-0.51	0.19	0.42	0.87	0.1	0.04	0.73	5.09	-0.48	1.8	0.64	-0.02

Appendix IV: Trace elements analysis for different Elsburg reefs samples using XRF (ppm).

ppm	**MIT01**	**MIT02**	**MIT03**	**MIT04**	**MIT05**	**MIT06**	**ECT01**	**ECT02**	**ECT03**	**ECT04**
Sc	1.39	2.33	1.2	2.29	2.64	3.12	dl	2.22	0.02	1.2
V	4.14	9.82	18.03	5.39	5.56	6.3	6.16	10.12	6.12	2.86
Cr	244.6	133.3	118.41	104.18	237.16	145.78	48.37	79.05	74.51	63.59
Co	61.55	45.89	33.14	19.25	100.91	41.85	4.16	22.62	14.74	12.31
Ni	71.47	44.23	86.37	21.21	89.92	42.46	11.58	30.42	16.98	16.89
Cu	22.37	10.46	14.79	17.77	51.5	21.63	8.83	43.09	7.65	9.63
Zn	99.85	4.88	265.13	7.02	38.43	63	9.71	163.07	33.37	43
Ga	1.69	0.59	0.87	0.17	2.15	1.1	0.64	0.18	0.12	0.92
Rb	3.64	7.6	13.12	dl	6.06	3.82	2.95	1.79	1.04	0.8
Sr	4.16	3.88	2.78	1.13	5.05	2.73	1.99	4.51	2.87	2.75
Y	10.61	6.88	5.86	13.31	16.16	9.78	2.87	6.68	4.73	5.11
Zr	126.9	89.25	47.16	71.09	90.05	61.94	26.87	49.08	34.71	31.47
Nb	4.71	2.49	1.82	1.07	2.68	1.81	0.53	2.37	1.1	1.49
Mo	1.49	0.53	1.73	1.98	2.12	1.57	0.57	1.27	1.2	1.79
Ba	13.38	31.42	74.17	dl	5.56	9.34	4.38	9.11	5.88	3.29
Pb	116.3	17.74	21.18	21.82	390.79	147.36	11.6	138.27	56.45	59.1
Th	17.36	1.78	2.49	7.97	25.85	10.77	2.96	11.39	6.35	5.77
U	166.5	21.18	23.21	45.59	404.19	112.31	3.79	106.87	49.86	46.79

Calibration standards									
ppm	**BR**	**NIM-N**	**AGV2**	**GSP2**	**NIM-D**	**NIM-S**	**BHVO2**	**NIM-G**	**AL_2O_3**
Sc	31.23	42.8	14.76	9.74	6.24	1.23	34.86	dl	dl
V	236.7	225.29	111.33	59.76	37.95	7.3	303.3	3.46	3.44
Cr	342	25.16	11.42	17.98	2509.21	6.14	288.12	25.88	dl
Co	53.39	58.71	17.75	6.66	192.67	2.78	43.3	3.33	0.21
Ni	277.8	111.86	18.36	16.34	2166.67	3.89	125.47	1.99	0.26
Cu	77.11	15.77	53.65	45.2	7.45	19.67	136.16	13.23	3.33
Zn	155.4	61.69	86.11	115.58	91.02	6.29	102.71	49.05	1.17
Ga	17.5	16.96	20.22	22.19	0.56	12.03	20.38	29.47	0.14
Rb	48.9	1.44	67.62	247.4	dl	525.7	11.17	318.46	0.49
Sr	1392	254.04	643.27	235.51	4.39	60.19	381.6	11.35	0.59
Y	29.29	7.01	19.77	26.01	0.99	2.24	26.88	132.67	0.26
Zr	283.4	12.73	238.58	554.32	2.38	15.02	175.6	279.46	dl
Nb	103.8	0.62	14.15	26.6	2.14	1.46	19.92	52.26	0.06
Mo	3.97	0.77	2.63	2.68	0.6	0.14	4.01	3.4	dl
Ba	1243	89.64	1150.62	1349.71	dl	2574	124.21	110.78	dl
Pb	6.5	3.72	16.23	46.71	2.94	4.45	3.54	41.83	3.72
Th	7.85	dl	6.16	117.33	dl	dl	dl	51.37	dl
U	dl	dl	2.37	1.81	dl	dl	dl	19.44	dl